LBL-6205
c.1

CORRELATION OF MICROSTRUCTURE OF SINTERED MULLITE BODIES WITH THEIR STRESS-STRAIN BEHAVIOR IN COMPRESSION LOADING AT 1200°C

Michael David Sacks
(M. S. thesis)

March 1977

Prepared for the U. S. Energy Research and Development Administration under Contract W-7405-ENG-48

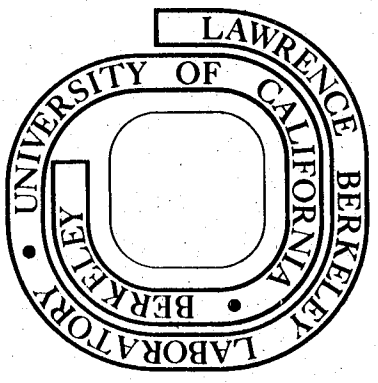

LBL-6205
c.1

CORRELATION OF MICROSTRUCTURE OF SINTERED MULLITE BODIES
WITH THEIR STRESS-STRAIN BEHAVIOR IN COMPRESSION LOADING AT 1200°C

Contents

Abstract vi

I. Part A. Introduction. 1

II. Experimental 3

A. Heat and Acid Treatment. 3

B. X-ray Diffraction. 3

C. Density and Porosity Determinations. 4

D. Optical Microscopy 4

E. Mechanical Testing 4

III. Results and Discussion 6

A. High Temperature Stress-Strain Behavior. 6

1. Comparison of As-Received and Heat Treated Samples. . . 6

2. Comparison of Acid Treated and Non-Acid Treated Samples 8

3. Comparison of Heat/Acid and Acid Treated Samples. . . . 10

B. Room Temperature Modulus of Rupture. 10

IV. Conclusion 12

Tables 13

Figures. 18

V. Part B. Introduction. 43

VI. Literature Survey. 45

A. Processing 45

B. Mechanical Properties. 47

VII. Experimental 49

A. Raw Materials. 49

B. Furnaces 49

C. Processing 50

1. Grinding. 52

(a) Alumina/Flint Grinding Media 52

(b) Alumina Grinding Media 53

2. Processing of 5 hr-Ground Mullite 54

(a) Green Density. 54

(b) Firing Time and Atmosphere 54

(c) Alumina/Silica Additions 54

D. Characterization of Fired Compacts 54

1. Mechanical Testing 55

2. Microscopy. 55

3. Density Determination 55

4. Electron Beam Microprobe Analysis 56

VIII. Results and Discussion 57

A. Sintered Kaolin Specimens. 57

B. Reaction Sintered A-14/Silica Flour Specimens of Metakaolin Composition. 58

C. Reaction Sintered ASP900 Kaolin/A-14 Alumina Specimens . 59

D. Reaction Sintered 71.8 wt% A-14 Alumina/28.2 wt% Silica Flour Samples 61

E. Results with Mullite Powder Derived from Reaction of 71.8 wt% A-14 Alumina/28.2 wt% Silica Flour Mixture. . . 64

1. Grinding with Alumina and Flint 64

2. Grinding with Alumina Only. 70

3. Results with 5 hr- Ground Mullite 73

(a) Firing Time and Firing Atmosphere. 73

(b) Green Density. 77

4. Intentional Additions of Silica and Alumina to 5 hr-Ground Mullite. 78

5. Effect of Annealing 83

IX. Summary and Conclusion 85

References 87

Acknowledgment 96

Figures. 97

CORRELATION OF MICROSTRUCTURE OF SINTERED MULLITE BODIES WITH THEIR STRESS-STRAIN BEHAVIOR IN COMPRESSION LOADING AT 1200°C

Michael David Sacks

Materials and Molecular Research Division, Lawrence Berkeley Laboratory, and Department of Materials Science and Mineral Engineering, University of California, Berkeley, California 94720

ABSTRACT

Sintered alumino-silicate bodies, containing mullite as a principle phase, were tested in compression loading at 1200°C. The observed mechanical behavior was correlated with the microstructure.

Part A is a study of seven commercial refractories. "As received" samples and specimens subjected to treatment by (1) heat, (2) aqueous hydrofluoric acid solution, and (3) heat and aqueous hydrofluoric acid solution were tested in compression at 1200°C. Room temperature modulus of rupture tests were also run on "as received" and heat treated samples. Heat treatment improved high temperature strength due to (1) the development of a more homogeneous macro- and micro-structure and/or (2) the growth of mullite crystals occurring in the glass phase. Treatment by aqueous hydrofluoric acid solution reduced the strength by leaching out glass phase (increasing porosity) and by variable attack on the refractory framework. Room temperature modulus of rupture appeared to be dependent on the surface defect structure rather than the nature, amount, and distribution of the various phases.

In Part B, mullite bodies were prepared utilizing kaolin, α-alumina, and α-quartz as raw materials. The effects of several processing variables upon high temperature mechanical behavior and sintered microstructure were studied. Chemical composition, green density, grinding

time and media, and firing time, temperature, and atmosphere were all found to be important parameters.

The presence of second phase (siliceous glass and/or corundum) appeared to be the most critical factor in determining high temperature mechanical strength. Siliceous glass phase was extremely detrimental to high temperature strength of mullite bodies because the soft, deformable glass flowed viscously at the test temperature. Ultimate engineering stresses over 100,000 psi, at 1200°C in compression loading, were obtained in samples that had only small amounts of glass phase.

Second phase also affected mechanical properties by altering the sintering behavior and, therefore, altering microstructural features such as grain size, grain morphology, total porosity, and pore size. The influence of second phase on microstructure and strength was, in turn, strongly dependent upon firing atmosphere. Both grain growth in the presence of liquid phase and boding between alumina particles and the mullite matrix were significantly affected by different firing atmospheres (air and 10^{-6} torr vacuum).

I. PART A. INTRODUCTION

The development of coal gasification processes will require large quantities of refractory materials that must be able to withstand severe erosive and corrosive conditions. Although not as stable under these conditions as desired, alumino-silicate refractories are an attractive candidate because of the abundance of necessary raw materials. In order to improve properties, such as erosion and corrosion resistance at high temperatures and/or pressures, fundamental studies of microstructure development in alumino-silicate materials are needed. The objective of such studies would be to determine the factors that control the development of stable and metastable phase compositions and the distribution of such phases.

In Part A of this thesis, seven commercial alumino-silicate refractories, ranging in overall silica content from 11 wt% to 51 wt% and containing mullite as a principal phase, were studied. These multiphase materials provided a wide range of microstructures which yielded background information on important features relative to strength and corrosive attack. In addition to information that may have direct practical importance, a study of commercial refractories may be helpful as a guide for microstructural design studies. Since erosion resistance is dependent upon the strength and toughness of the material, one objective of this study was to determine the high temperature stress-strain behavior in compression loading. Characterizations by X-ray diffraction and fluorescence analyses, density and porosity determinations, and optical microscopy were used to explain observed mechanical behavior.

In coal gasification processes, resistance to chemical attack by H_2 is critical in the development of corrosion resistance. Studies[1,2] have indicated that refractories containing a significant amount of glassy siliceous phase were excessively attacked. In order to study corrosive attack on the seven refractories, they were exposed to an aqueous HF solution and, subsequently, mechanically tested. Other studies[3,4,5] have shown improved mechanical strength for selected fireclay and high-alumina refractories by increasing firing temperatures. Therefore, stress-strain behavior was also determined for "as received" refractories which were (1) refired to 1700°C and (2) refired to 1700°C and acid treated in an aqueous HF solution.

II. EXPERIMENTAL

A. Heat and Acid Treatment

The original firing temperatures of the seven refractories varied, but all were in the range of 1400°C to 1600°C (see Table 1). Samples of each refractory were refired to 1700°C in a gas fired kiln*. The heating cycle was such that the average heating rate was ~6°/min to 1400°C, ~1°/min from 1400°C to 1600°C, and ~.4°/min from 1600°C to 1700°C. Upon reaching 1700°C, the gas/air flow was turned off and the samples were furnace cooled.

Acid treatment consisted of immersion of the samples into a hydrofluoric acid** solution which was magnetically stirred so that solution products would be removed from the immediate vicinity of the surface of the specimen. Unless noted otherwise, the acid treatment was at room temperature for 24 hours in a 15% HF solution. Several specimens were tested at room temperature for 24 hours in a 48% HF solution. Specimens which were to be mechanically tested were cut and polished to desired dimensions before the acid treatment.

B. X-ray Diffraction

X-ray diffraction† was performed on the untreated and heat treated samples. Specimens were prepared by crushing, with an alumina mortar and pestle, to a size fine enough to pass through a 325 mesh sieve. Scanning conditions were 40 KV, 20 mA, 1°/min, 1°/4°/1° entrance to

---

*Remmey No. 2320, Richard C. Remmey Son Co. Philadelphia, PA.

**Mallinckrodt Analytical Reagent, Mallinckrodt Chemical Works, St. Louis, MO.

†Norelco Diffractometer, Philips Electronic Instruments, NY.

exit collimation, time constant 3.0 and range of 1000 cps. High intensity copper K_α x-rays were used. Mullite, corundum, and α-cristobalite were the only phases detected. No quantitative measurements of peak intensities were made. The descriptive assessment of intensities (Table 2) were based on visual comparison of the heights for the strongest peak for each phase.

C. Density and Porosity Determinations

Bulk density, apparent density, and open porosity were determined by the displacement method utilizing vacuum treatment and distilled water as the soaking liquid. At least two determinations were made for each specimen. The results for untreated, heat treated, and acid treated (15% HF and 48% HF) specimens are given in Table 3.

D. Optical Microscopy

Ceramographic polishing procedures consisted of grinding on 220, 30, 15 and 6 micron metal bonded diamond wheels. This was followed by vibratory polishing* using slurries of 6, 1, and 1/4 micron diamond particles. The polished samples were observed in reflected light by interference-contrast microscopy.†

E. Mechanical Testing

Specimens for high temperature mechanical testing were of parallelpiped shape with a length to width ratio of 2:1 and dimensions of approximately .3" x .3" x .6". The specimen sides were polished on 220, 30, 15, and 6 micron metal bonded diamond wheels. The ends were

*FMC Corp., Syntron Div., Homer City, PA.

†Nomarsky Differential Interference-Constant Microscopy, Zeiss Ultraphot II, Metallograph, Carl Zeiss, W. Germany.

polished with a series of emery papers using a jig designed to keep them flat, parallel, and perpendicular to the loading axis. All stress-strain data was obtained in compression using an Instron** testing machine with a constant strain rate (based on the original sample height) of ~1.4 x 10^{-5}/sec. Specimens were heated in a furnace with $MoSi_2$ elements to 1200°C, followed by a stabilization period of ~40 minutes. The specimen temperature was taken with the thermocouple touching the Lucalox button upon which the specimen stood. A schematic diagram of the specimen arrangement in the furnace is given in Fig. 1. Reported stresses are based on the original cross-sectional area. As-received, heat treated, heat and acid treated, and acid but non-heat treated specimens were tested. The stress-strain curves are shown in Figs. 2-8.

Room temperature modulus of rupture (3 point bending) tests were also made on non-heat treated and heat treated samples. Specimens were tested with "as cut" (diamond saw blade) surfaces and dimensions were approximately 4" x .5" x .5". The crosshead speed was .05"/min. The results are tabulated in Table 4.

**Instron Engineering Corp., Quincy, MA.

III. RESULTS AND DISCUSSION

A. High Temperature Stress-Strain Behavior

1. Comparison of As-Received and Heat Treated Samples

Except in the case of #3, the ultimate engineering stress (UES) either increases (#'s 2, 4, 5, 6, 7) or remains virtually the same (#1) after heat treatment (Table 5). Specimens 4 and 5 illustrate several reasons for this increased strength. From the top micrographs of Figs. 9 and 10, it can be seen that the heat treated samples are more homogeneous on a macroscopic scale. High temperature refiring has led to further elimination of interfaces between clay binder (which develops a mullite/glass microstructure upon clay decomposition) and grog grains (which already have a well-developed mullite/glass microstructure). Continuity is facilitated by the fact that the grog and binder have similar compositions since both have clay bases. By comparing the bottom photos in Figs. 9 and 10, it can be seen that the effect of heat treatment on a microscopic level has been growth of mullite crystals. The large, acicular mullite crystals are non-deformable compared to the glassy phase which, at the test temperature of 1200°C, will deform under load relatively easily and flow viscously. The mullite needles will interact during compression deformation, thus increasing the stress required to deform the overall specimen. An increased stress for deformation would also result if the mullite needles would bond to each other forming a rigid framework.

Despite the microstructure similarities between #'s 4 and 5, they have widely different strength values. A larger amount of glass phase in #4 is indicated by the shape of the stress-strain curves (Fig. 5)

which suggest viscous flow behavior after ~2% engineering strain. An examination of Figs. 9B and 10B (bottom micrographs) also indicates that #4 does have more glass phase, or less mullite, than #5. The higher alkali content (1.92 wt% vs. 1.1 wt% - Table 1) for #4 may be responsible for some of these effects. It has been shown[6-9] that additions of Na_2O promote increased glass content and lower open porosities in alumino-silicate bodies. In addition, higher temperature firings often promote these effects.[6-9] Finally, the additional Na_2O in #4 may also contribute to its decreased strength by reducing the viscosity of the glass phase.

Improved strength upon heat treating specimens #'s 2, 6 and 7 can also be explained by increased binder/grog reaction and/or the growth of mullite crystals. The top micrographs in Figs. 11 and 12 show the former effect for specimens #6 and #7. However, continuity is achieved to a lesser degree than for #4 and #5 (Figs. 9 and 10) since grog grain and binder were not as close in composition (Table 1). Higher magnification (bottom) photos in Fig. 11 illustrate the non-uniform microstructure of specimen #6 persists even after heat treatment. The poor strength of #2 is explained by the inhomogeneous structure illustrated in Fig. 13A (top). Four principal condensed phases - α-alumina, mullite, α-cristobalite, glass - are present. The use of two types of grain and the low firing temperature (1400°C) are responsible for the as-received structure. Despite heat treatment, large "bauxite" (alumina) particles, surrounded by mullite/glass areas, persist as seen in Fig. 13 (bottom photos).

Upon heat treatment, #1 shows negligible changes in density, open porosity, x-ray diffraction pattern, and microstructure (Fig. 14).

Consequently, the strength remains virtually the same. The low strength values result from the large amount of porosity as shown in Fig. 14. Contact between particles are also weakened by the presence of pockets of glass and alumina.

Number 3 is the only specimen in which the heat treated sample had a significantly lower strength than the non-heat treated sample. The x-ray, density, and porosity determinations show almost no differences between the two samples. Figure 15 (bottom micrographs), however, indicates an increase, upon heat treatment, in the size of the pores in the critical matrix area between alumina particles. This increased defect size could weaken the refractory's framework and decrease its load-bearing capability.

2. Comparison of Acid Treated and Non-Acid Treated Samples

Acid treated specimens were always significantly weaker than their non-acid treated counterparts. The key reaction due to the treatment that was anticipated was

$$SiO_2(s) + HF(aq) = SiF_4(g)\uparrow + H_2O(aq)$$

The corresponding loss of silica is indicated in Figs. 16 and 17. The figures show that the weight loss of the samples due to acid treatment is related to their initial silica content. (It should be noted that #2 untreated, the only point deviating significantly in these plots, had such a weak structure that large particles became detached from the framework during acid treatment resulting in the high weight loss value. Number 2 untreated was the only sample which lost its integrity upon 15% HF acid treatment to a degree where the density determination and mechanical test could not be performed. All other samples changed linear

dimensions by .0015" - .5% - or less).

In Figs. 18 and 19, it is shown that, before acid treatment, there is no meaningful relationship between % open porosity and initial wt% SiO_2 content. After acid treatment, there is a direct relationship. Figures 20 and 21 show that there is a general downward trend in bulk density with increasing weight percentage SiO_2 content. This is expected since SiO_2, as glass or cristobalite, has a lower density than mullite or corundum. After acid treatment, though, this trend has been greatly accelerated. Table 3 also illustrates the expected increase in apparent density upon acid treatment and resultant silica loss. The percentage decrease in bulk density between acid and non-acid treated specimens is also shown to be directly related to initial SiO_2 content in Fig. 22. The value used in each plot for the initial wt% SiO_2 content is that determined by x-ray fluorescent analysis* (Table 1). Figure 23 shows the leaching out of glass upon acid treatment and penetration which leaves a mullite framework. The weight loss, open porosity, bulk density, and % decrease in bulk density are directly related to this process. Loss in strength after acid treatment, however, is not directly related to initial silica content as shown by comparison of Tables 1 and 5. Specimen #3 heat treated, with 11% silica, lost only 5 wt% after acid treatment, and its ultimate engineering stress (UES) after acid treatment was 57% of the heat treated specimen. Specimen #4 heat treated, with 51%

---

*Performed by Kaiser Center for Technology, Pleasanton, CA.

silica, lost 28 wt% after acid treatment and the UES after acid treatment was 65% of the heat treated specimen. The results indicate that the importance of acid corrosion in regards to strength is not simply related to the leaching of the glass phase and its consequence of reducing the load-bearing area; there appears to be some variable attack on the refractory framework as well.

3. Comparison of Heat/Acid and Acid Treated Samples

As shown in Table 5, the ratio of UES values for the acid to non-acid treated samples is generally greater for the heat treated specimens than for the non-heat treated specimens. As expected, the weight loss (Figs. 16 and 17), open porosity (Figs. 18 and 19), and percentage decrease in bulk density (Fig. 22) data show that the heat treated samples are less subject to acid attack.

A number of factors can contribute to this increased resistance. Heat treatment causes the growth and crystallization of mullite crystals. The rate of solution of mullite in HF has been shown to decrease with increasing size of crystals[10]. Heat treated specimens also have less open porosity so that less surface area is exposed to the acid attack. Finally, the more homogeneous heat treated specimens would be expected to be less subject to attack at the critical grog/binder interfaces.

B. Room Temperature Modulus of Rupture

Figures 24 and 25 show plots of room temperature modulus of rupture versus % open porosity for non-heat treated and heat treated samples, respectively. This correlation is the only one that showed a reasonable monotonic trend with the modulus of rupture. The results indicate that the strength at low temperatures of these large grain, multiphase

materials with complex microstructures appears to be more dependent on the surface defect structure rather than on the properties of the particular phases. The correlation is better for the heat treated samples. This may be due to the elimination of large defects by refiring to the same high temperature. This fact may be represented by the value for the non-heat treated specimen #2 which is the most deviant in Fig. 24 (value for 17.6 open porosity). This specimen tended to crumble after acid treatment indicating that reactions in the matrix phase had not been too extensive because of the low firing temperature (1400°C). On the same basis, the scatter in values can be attributed to variations in defects due to variations in the nature of the microstructures.

IV. CONCLUSION

Correlations were made between the microstructure of commercial alumino-silicate refractories, containing mullite as a principal phase, and (1) the high temperature (1200°C) mechanical strength in compression loading and (2) the room temperature modulus of rupture. The effect of heat treatment and hydrofluoric acid treatment on microstructure and strength were also investigated.

High temperature strength in compression loading improved upon heat treatment due to (a) the development of a more homogeneous macro- and micro-structure and/or (b) the growth of mullite crystals occurring in the glass phase. With respect to (a), homogeneity occurs more readily when the clay binder and grog are of nearly the same composition. Other important factors that should be considered are the clay binder/grog ratio and the size of the grog particles.

Treatment by aqueous hydrofluoric acid solution reduces the strength by leaching out glass phase (increasing porosity) and by variable attack on the refractory framework. Resistance to acid attack may be improved with heat treatment due to (1) growth of mullite crystals, (2) reduction in open porosity, and (3) more homogeneous samples.

Low temperature strength (modulus of rupture) seems to be more dependent on the defect structure (particularly surface defects) than on the nature, amount, and distribution of the various phases.

Table 1. Compositions of Refractory Test Specimens.

Specimen No.	Oxide Analysis*							Starting Materials		Firing Temp., °C
	Al_2O_3	SiO_2	Fe_2O_3	CaO	MgO	Alk	TiO_2	Grain	Bond	
1	71.0	21.8	1.91	0.10	0.51	1.71	4.71	fused kaolinitic bauxite	clay	~1600
2	69.7	23.4	1.64	0.12	0.29	1.58	4.36	bauxite, calcined flint clay	clay	~1400
3.	85.1	11.0	0.22	0.17	0.12	1.03	0.03	tabular alumina	reactive SiO_2	~1510
4.	43.2	51.0	0.82	0.21	0.23	1.92	2.65	calcined flint clay	clay	~1565
5.	47.4	48.2	1.07	0.08	0.15	1.11	2.87	calcined kaolin	clay	~1565
6.	58.2	35.3	1.35	0.13	0.40	1.44	3.69	calcined bauxitic kaolin	clay	~1510
7.	70.5	23.0	1.02	0.14	0.27	1.48	4.49	calcined bauxitic kaolin	clay	~1580

*X-ray fluorescence performed by Kaiser Center for Technology, Pleasanton, CA.

Table 2. X-ray Diffraction Results

Specimen No.	Treatment	Phases Detected	Intensity
1	None	mullite	strong
		α-Al_2O_3	weak
	Heat	mullite	strong
		α-Al_2O_3	weak
2	None	mullite	strong
		α-Al_2O_3	strong
		α-cristobalite	strong
	Heat	mullite	strong
		α-Al_2O_3	medium
		α-cristobalite	not detected
3	None	mullite	medium
		α-Al_2O_3	strong
	Heat	mullite	medium
		α-Al_2O_3	strong
4	None	mullite	strong
		α-Al_2O_3	weak
	Heat	mullite	strong
		α-Al_2O_3	weak
5	None	mullite	strong
		α-Al_2O_3	weak
		α-cristobalite	strong
	Heat	mullite	strong
		α-Al_2O_3	weak
		α-cristobalite	medium
6	None	mullite	strong
		α-Al_2O_3	weak
	Heat	mullite	strong
		α-Al_2O_3	weak
7	None	mullite	strong
		α-Al_2O_3	weak
	Heat	mullite	strong
		α-Al_2O_3	weak

Table 3. Physical Properties of Refractory Test Specimens As-Received and After 24 hr Acid Treatment.

Specimen No.	Treatment	% Wt. Loss	Bulk Density (g/cm^3)	Apparent Density (g/cm^3)	% Open Porosity
1	None		2.46	3.05	19.4
	Heat		2.49	3.06	18.4
	Acid*	8.0	2.33	3.16	26.1
	Heat/Acid*	7.4	2.36	3.19	26.0
2	None		2.62	3.17	17.6
	Heat*		2.44	3.10	21.2
	Acid*	30.4	nd	nd	nd
	Heat/Acid*	10.9	2.35	3.19	26.3
3	None		3.05	3.45	11.5
	Heat*		3.04	3.45	11.7
	Acid*	5.1	2.93	3.67	20.2
	Heat/Acid*	3.6	2.97	3.65	18.7
	Acid**	20.4	2.75	3.69	25.6
	Heat/Acid**	13.3	2.83	3.65	22.5
4	None		2.38	2.59	7.9
	Heat*		2.36	2.43	3.1
	Acid*	35.2	1.59	3.02	47.4
	Heat/Acid*	28.0	1.73	2.79	38.0
5	None		2.37	2.75	13.8
	Heat*		2.50	2.59	3.7
	Acid*	34.8	1.57	3.09	49.1
	Heat/Acid*	23.6	1.93	2.96	34.8
	Acid**	83.3	nd	nd	nd
	Heat/Acid**	53.3	1.19	3.15	62.2
6	None		2.51	2.92	13.8
	Heat*		2.57	2.90	11.4
	Acid*	20.9	2.00	3.16	36.5
	Heat/Acid*	15.4	2.24	3.16	29.2
7	None		2.58	2.99	13.8
	Heat*		2.58	3.00	14.0
	Acid**	7.3	2.41	3.15	23.6
	Heat/Acid**	5.6	2.47	3.16	21.8

*15% HF aqueous solution for 24 hours.

**48% HF aqueous solution for 24 hours.

nd = not determined.

Table 4. Room Temperature Modulus of Rupture.

Specimen No.	Treatment	Mean(psi)	Standard Deviation(psi)
1	None	2190	210
	Heat	2590	270
2	None	990	110
	Heat	2290	430
3	None	4050	390
	Heat	4070	350
4	None	4600	600
	Heat	6670	630
5	None	4490	380
	Heat	7050	680
6	None	3400	290
	Heat	5270	450
7	None	3480	440
	Heat	4020	450

Table 5. Ultimate Engineering Stress.

Specimen No.	Treatment	Ult. Eng. Stress (psi)	UES Acid / UES Non-Acid
1	None	4360	
			.33
	Acid*	1420	
	Heat	3930	
	Heat/Acid*	1630	.42
2	None	2130	
	Acid*	nd	
	Heat	4490	
			.68
	Heat/Acid*	3060	
3	None	10600	
			.57
	Acid*	6080	
	Heat	8000	
			.57
4	None	3310	
			.36
	Acid*	1190	
	Heat	5200	
			.65
	Heat/Acid*	3380	
5	None	6820	
			.24
	Acid*	1640	
	Heat	12790	
			.44
	Heat/Acid*	5580	
6	None	3820	
			.36
	Acid*	1380	
	Heat	11180	
			.70
	Heat/Acid*	7830	
7	None	1900	
			.62
	Acid*	1181	
	Heat	6690	
			.49
	Heat/Acid*	3290	

*15% HF aqueous solution for 24 hours.

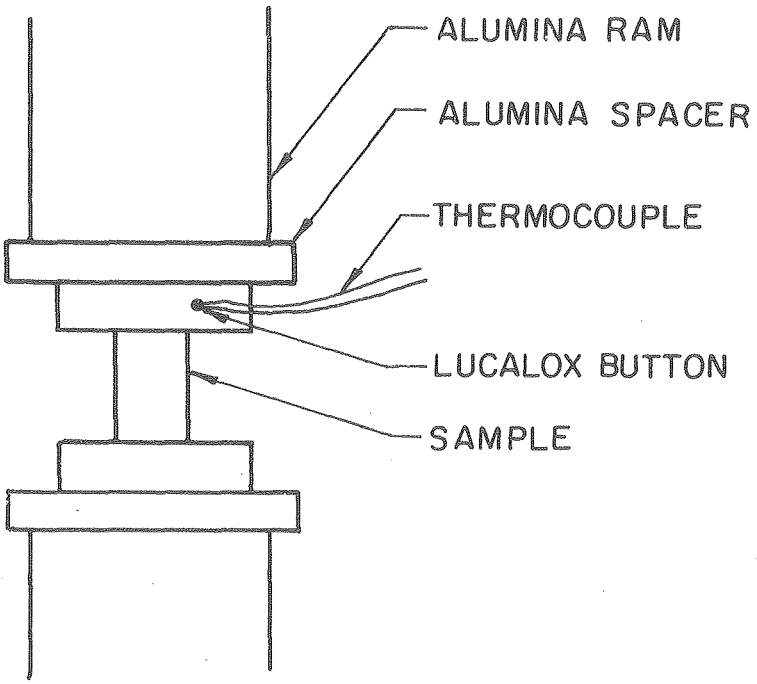

XBL 769-7506

Fig. 1. Specimen arrangement in furnace for stress-strain testing.

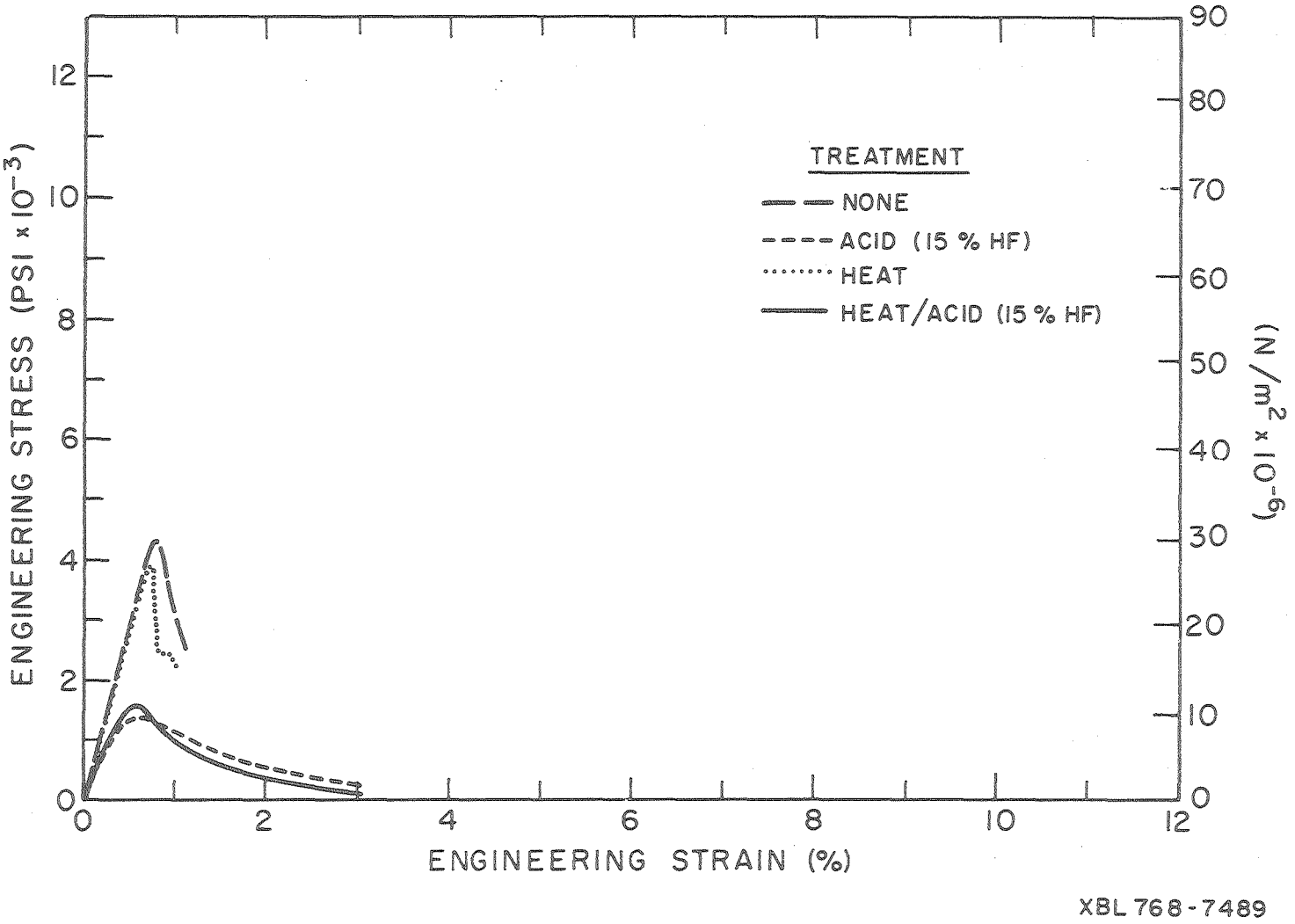

Fig. 2. Stress-strain behavior in compression at 1200°C for specimen #1 with various treatments.

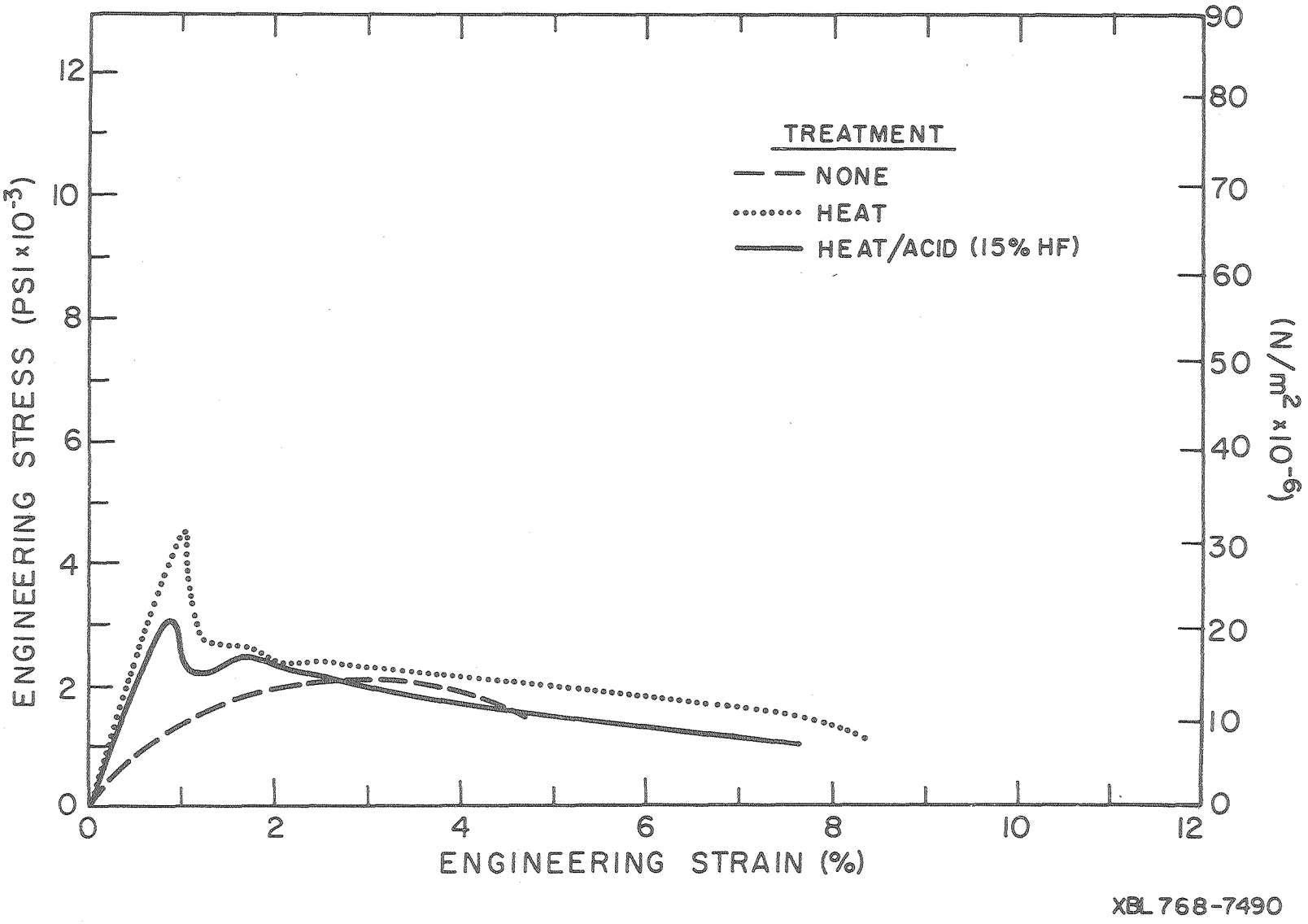

Fig. 3. Stress-strain behavior in compression at 1200°C for specimen #2 with various treatments.

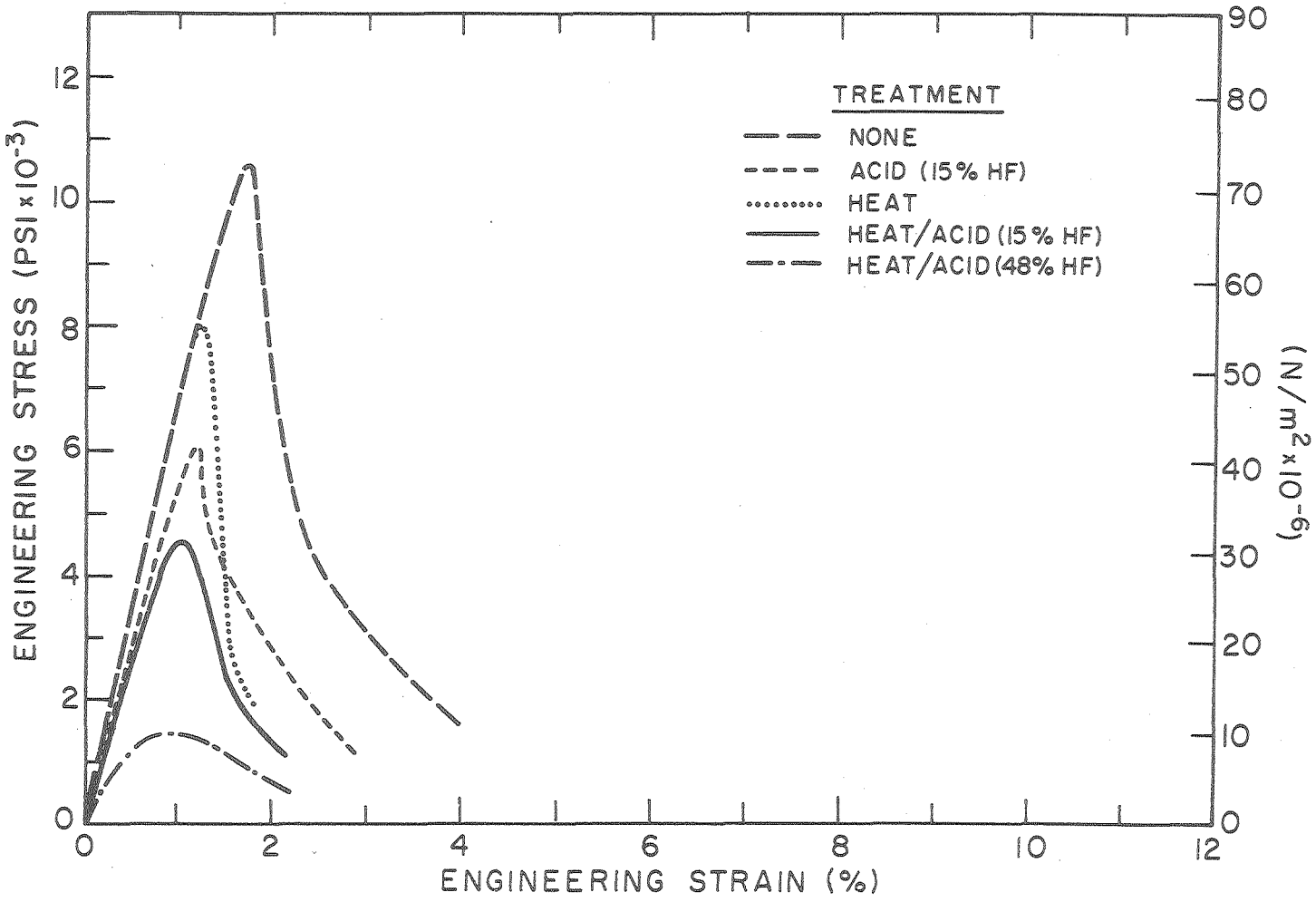

XBL768-7485

Fig. 4. Stress-strain behavior in compression at 1200°C for specimen #3 with various treatments.

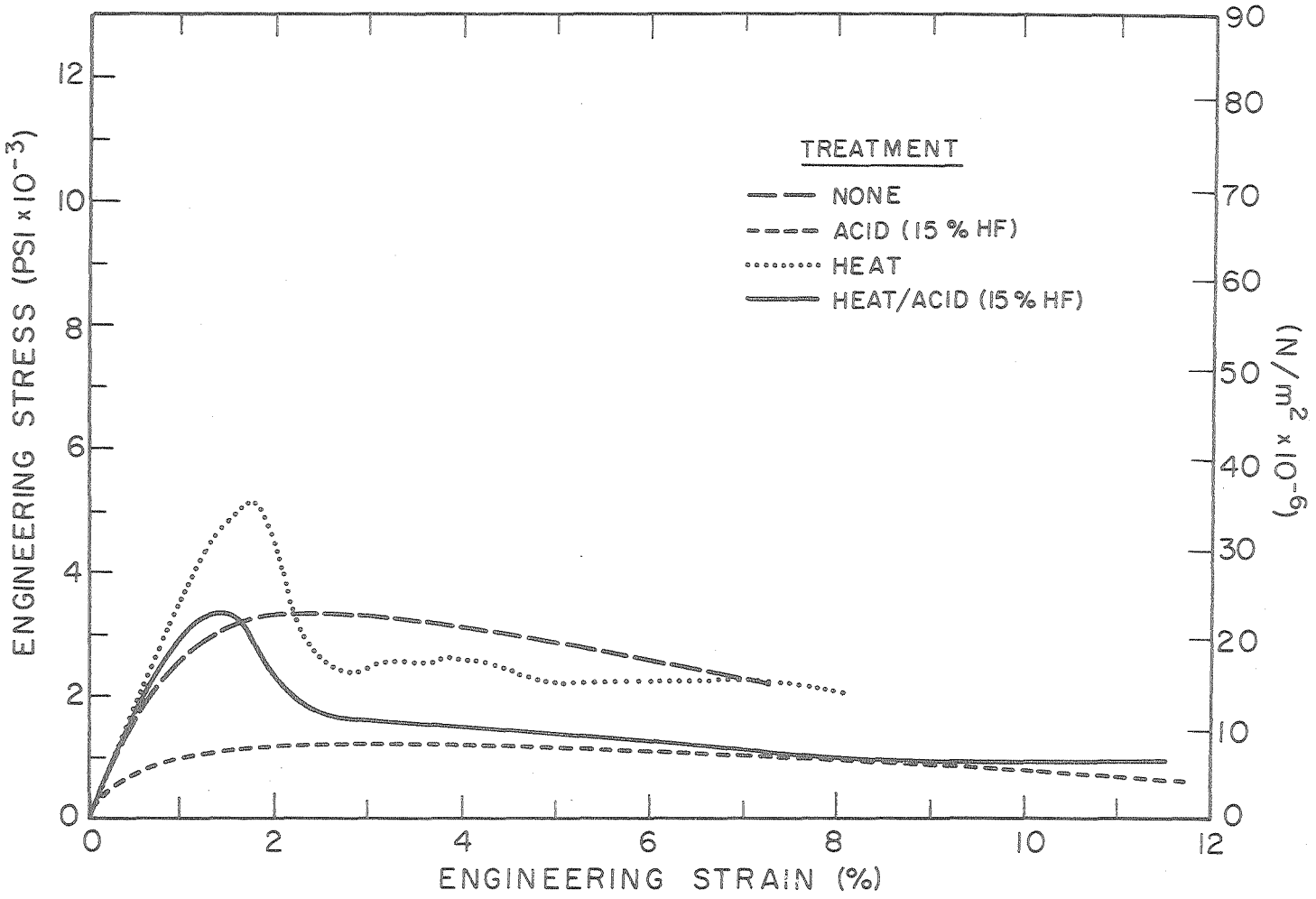

XBL 768-7486

Fig. 5. Stress-strain behavior in compression at 1200°C for specimen #4 with varous treatments.

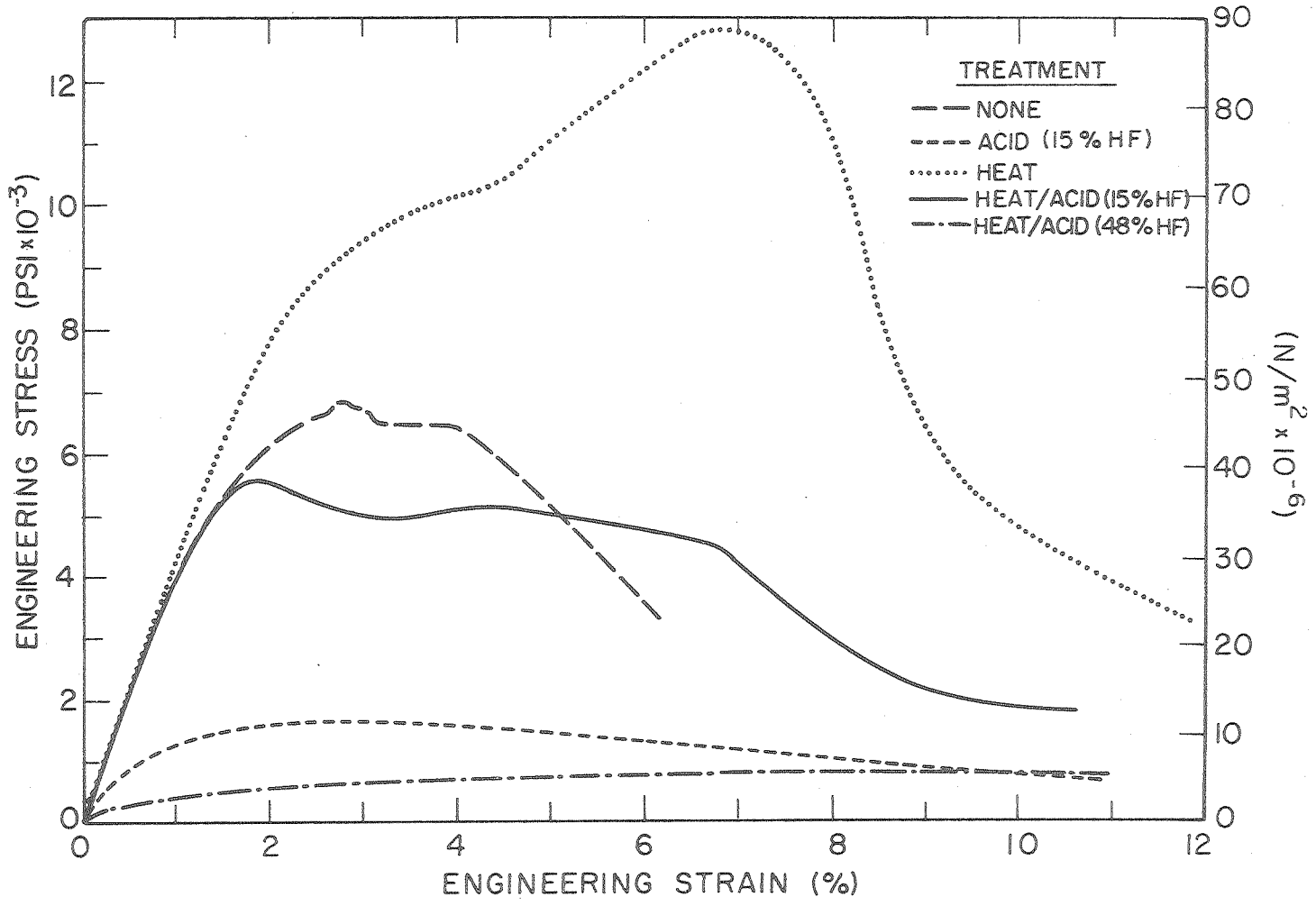

XBL768-7484

Fig. 6. Stress-strain behavior in compression at 1200°C for specimen #5 with various treatments.

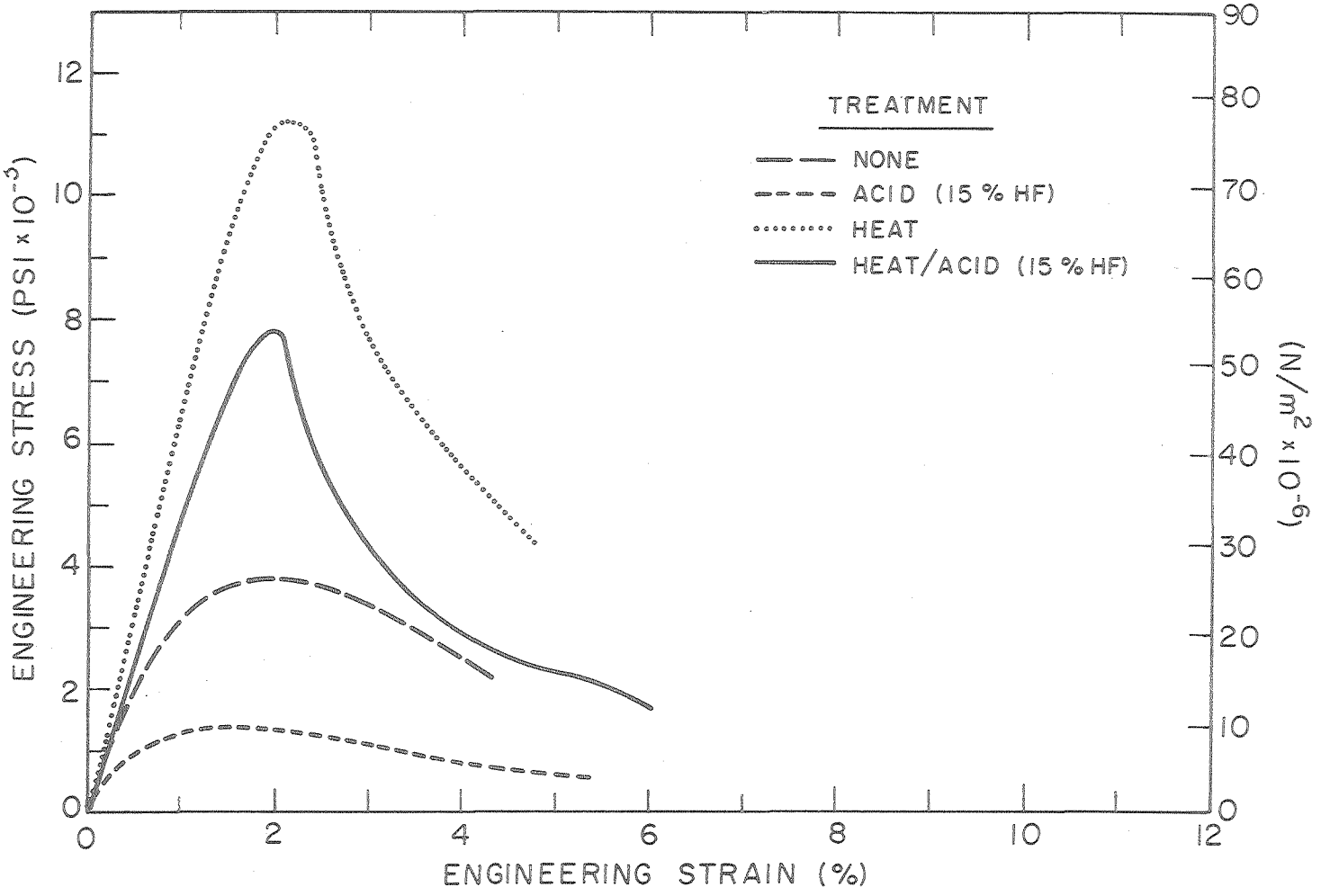

XBL 768-7487

Fig. 7. Stress-strain behavior in compression at 1200°C for specimen #6 with various treatments.

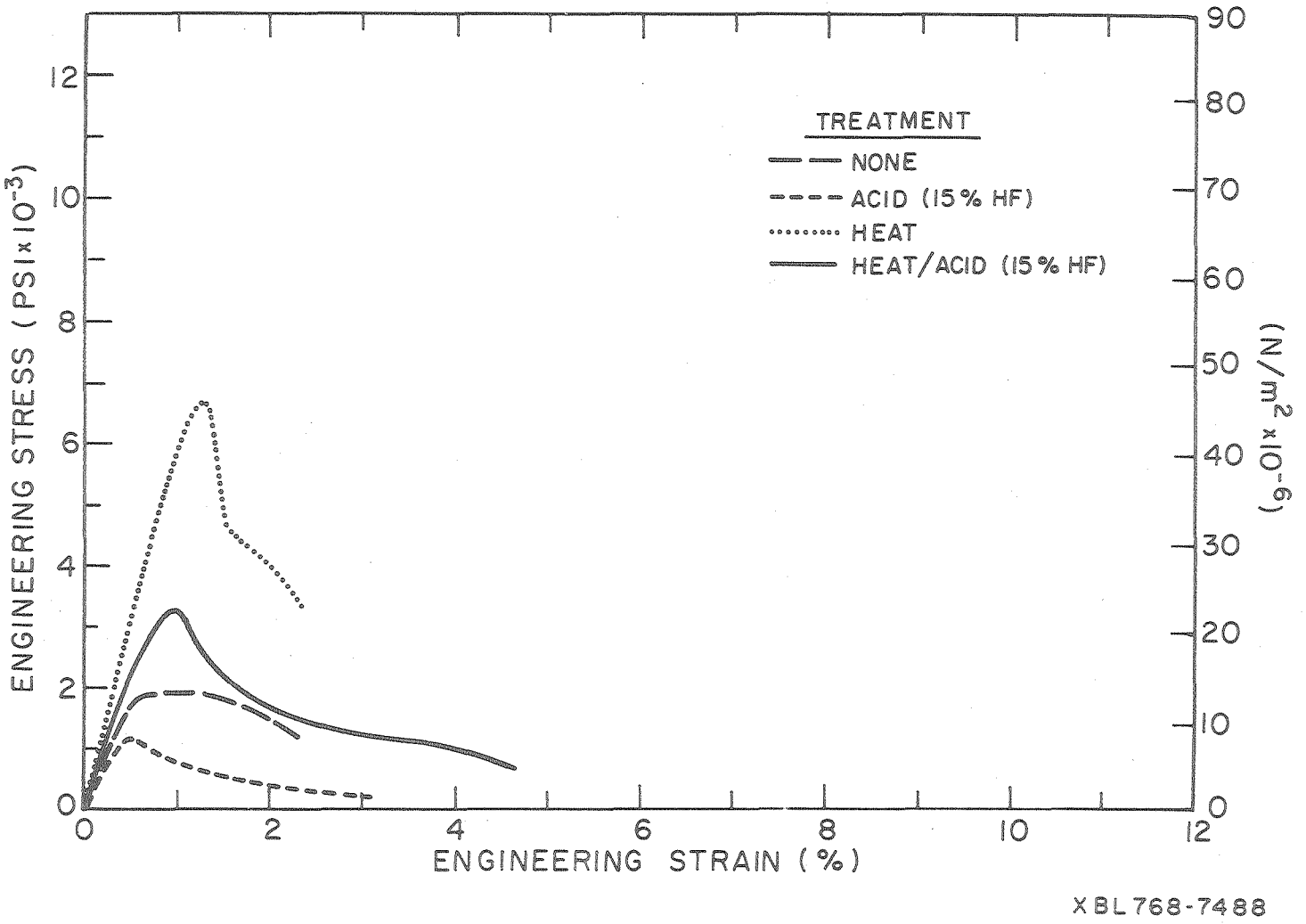

XBL768-7488

Fig. 8. Stress-strain behavior in compression at 1200°C for specimen #7 with various treatments.

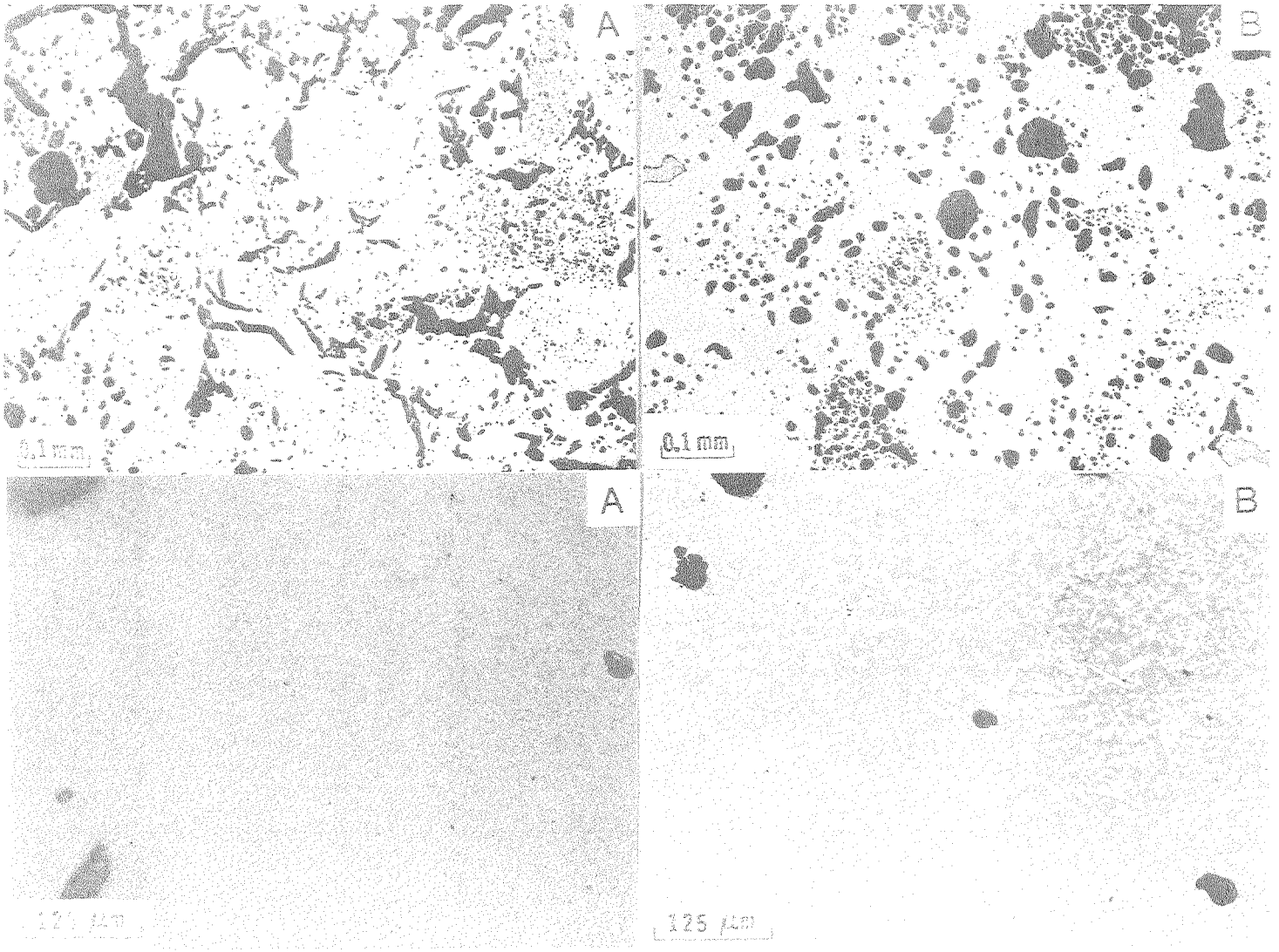

Fig. 9. Top: Specimen #4 before (A) and after (B) heat treatment.
Bottom: Specimen #4 before (A) and after (B) heat treatment.

XBB7610-9114

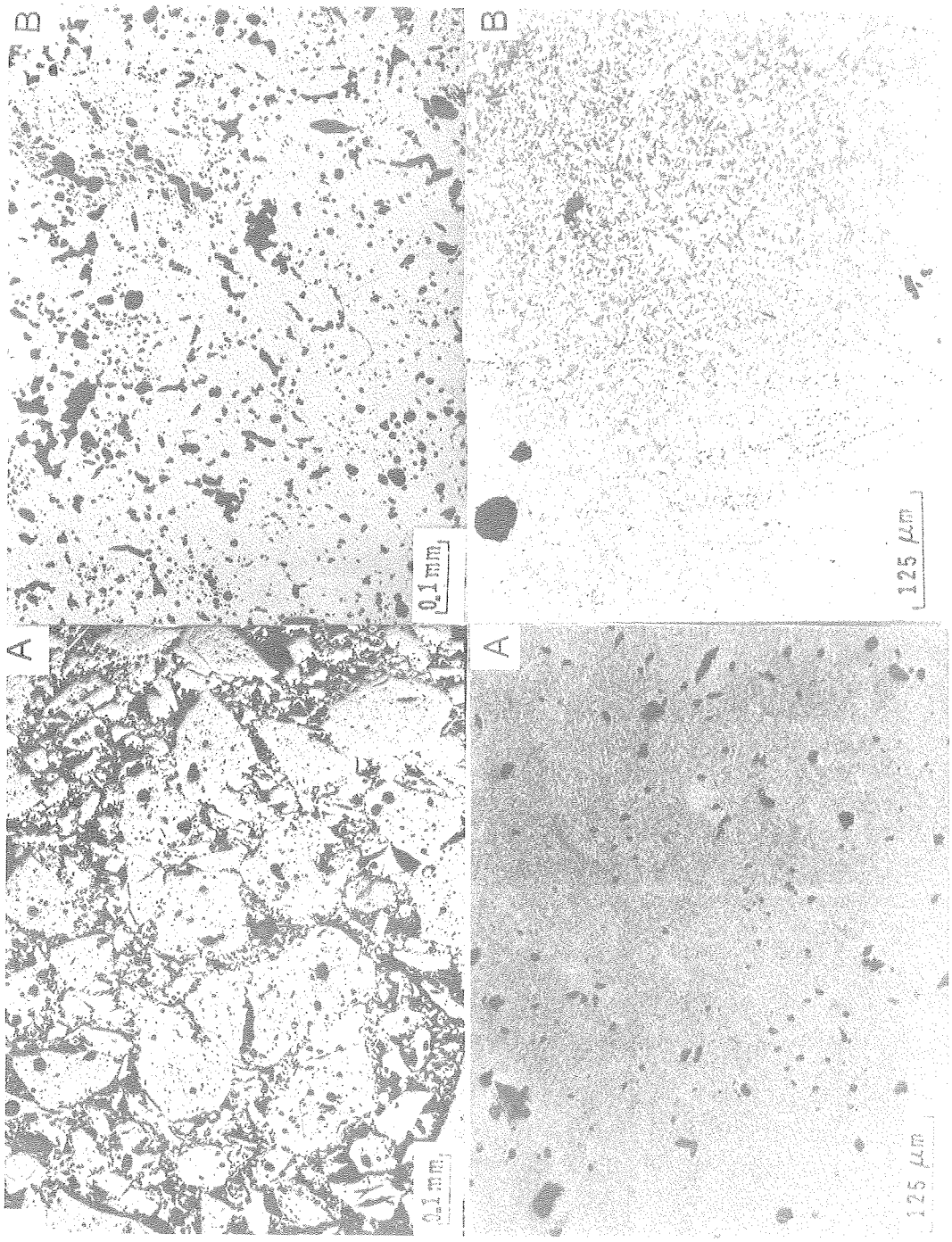

Fig. 10. Top: Specimen #5 before (A) and after (B) heat treatment.
Bottom: Specimen #5 before (A) and after (B) heat treatment.

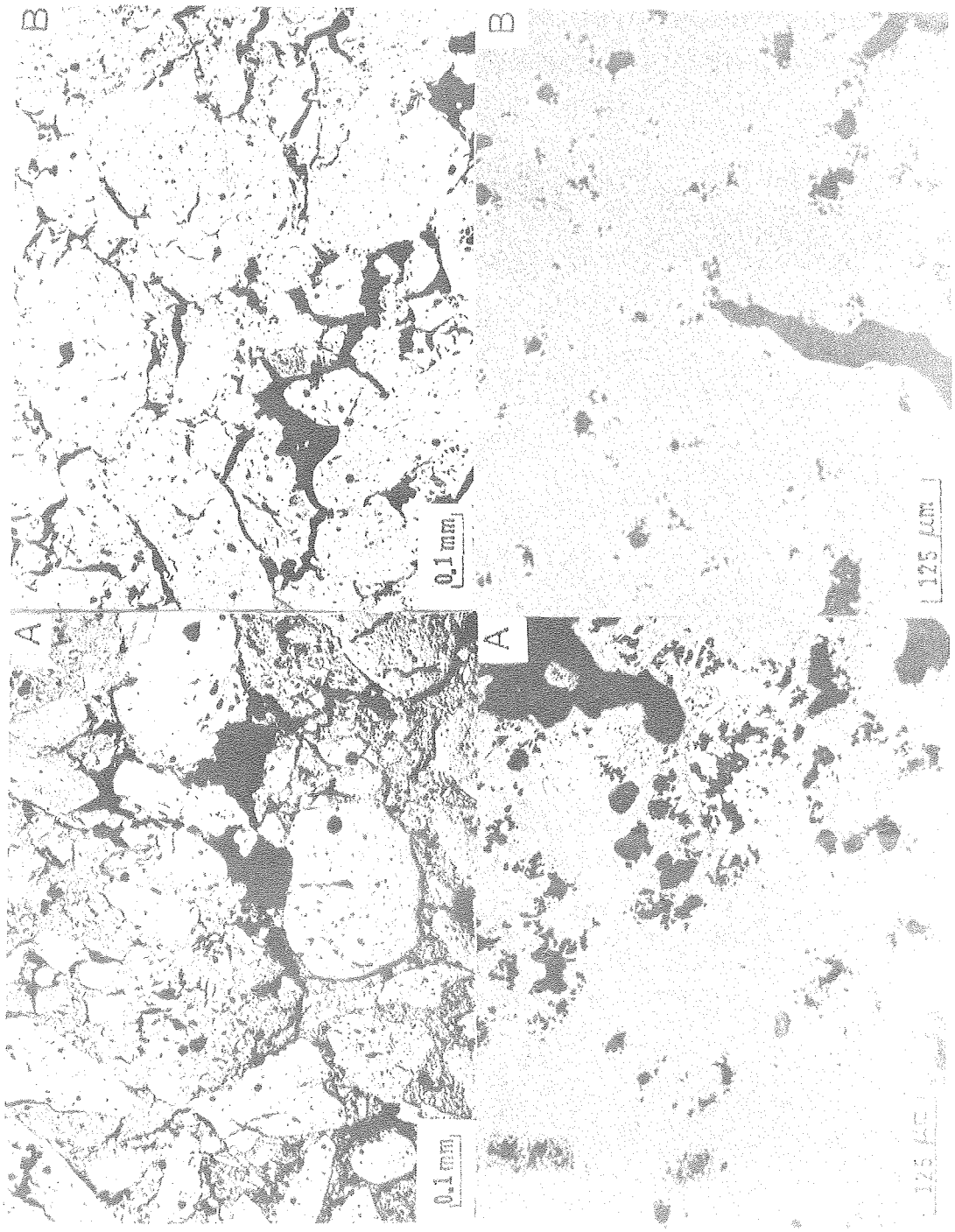

Fig. 11. Top: Specimen #6 before (A) and after (B) heat treatment.
Bottom: Two areas of specimen #6 after heat treatment.

XBB7610-9118

XBB7610-9119

Fig. 12. Top: Specimen #7 before (A) and after (B) heat treatment.
Bottom: Specimen #7 before (A) and after (B) heat treatment.

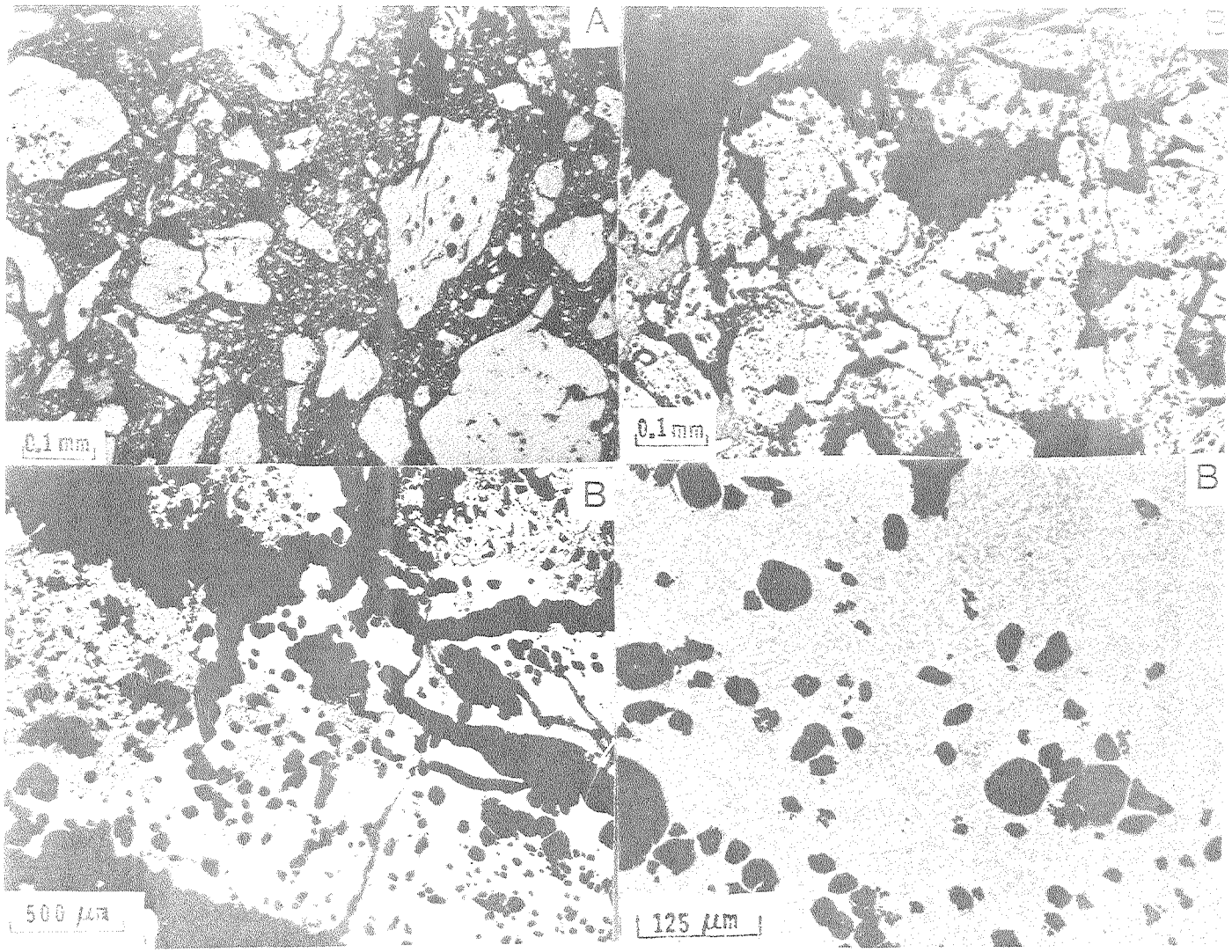

Fig. 13. Top: Specimen #2 before (A) and after (B) heat treatment. Bottom: Two areas of Specimen #2 after heat treatment. XBB7610-9117

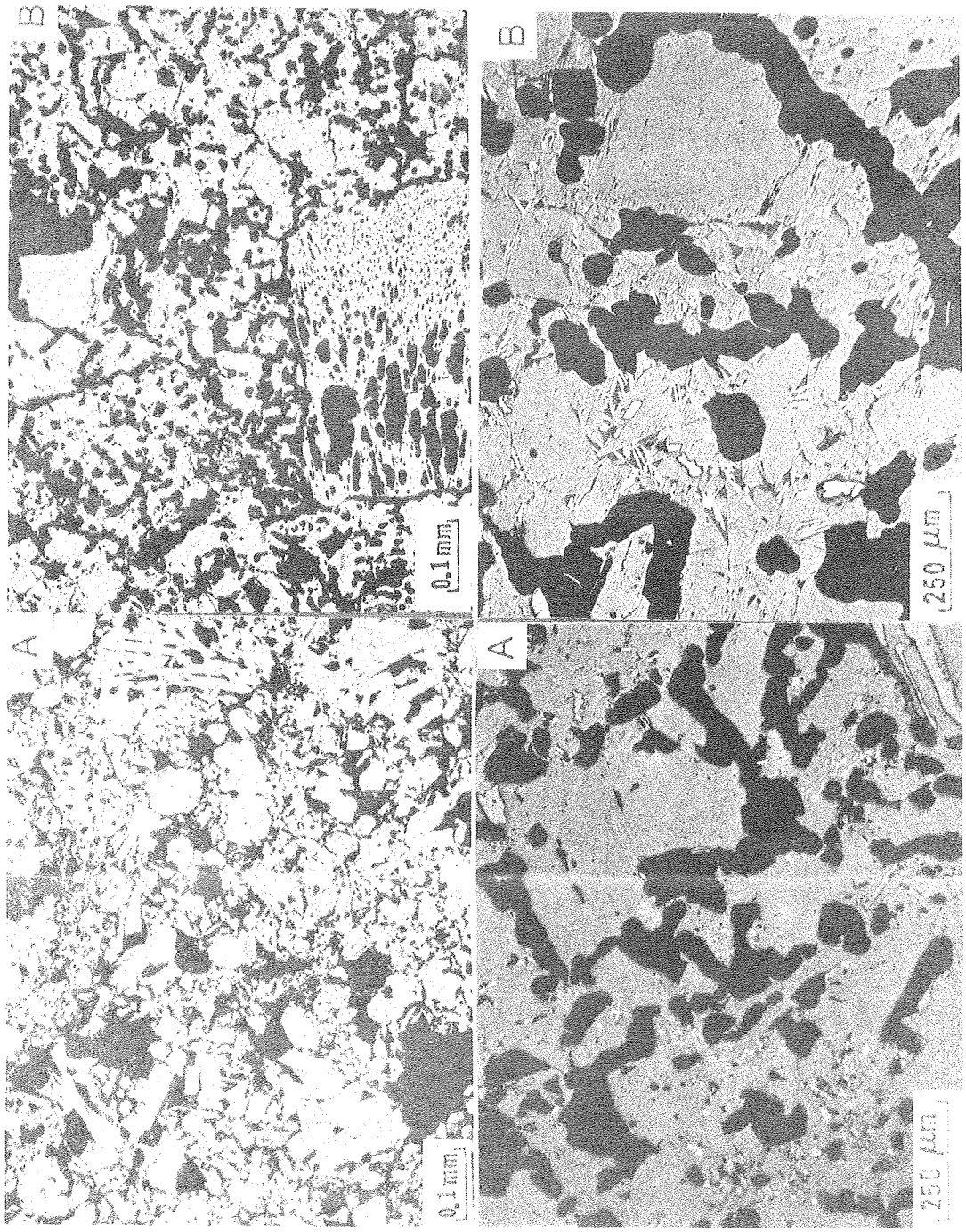

Fig. 14. Top: Specimen #1 before (A) and after (B) heat treatment.
Bottom: Specimen #1 before (A) and after (B) heat treatment.

XBB7610-9116

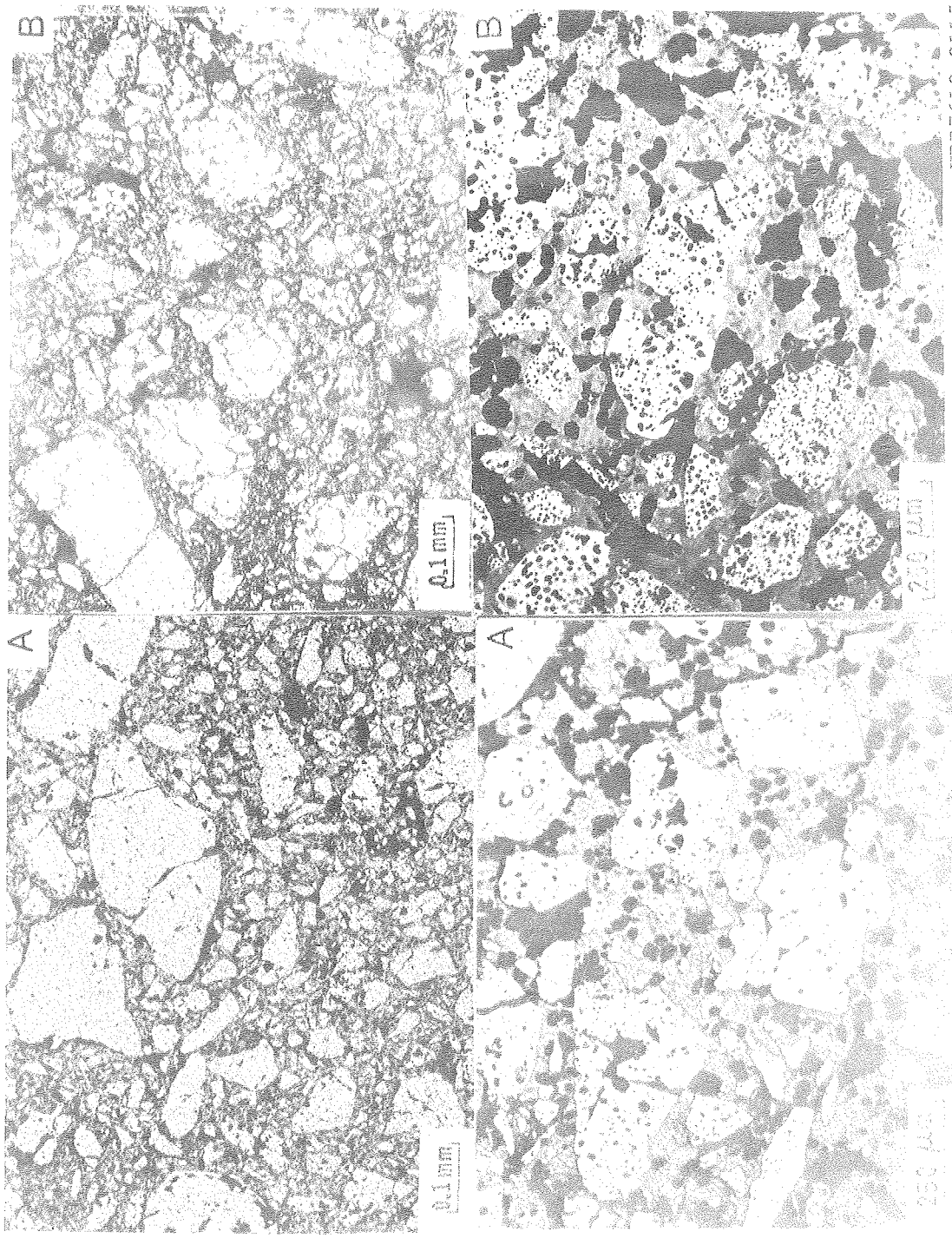

Fig. 15. Top: Specimen #3 before (A) and after (B) heat treatment.
Bottom: Specimen #3 before (A) and after (B) heat treatment.

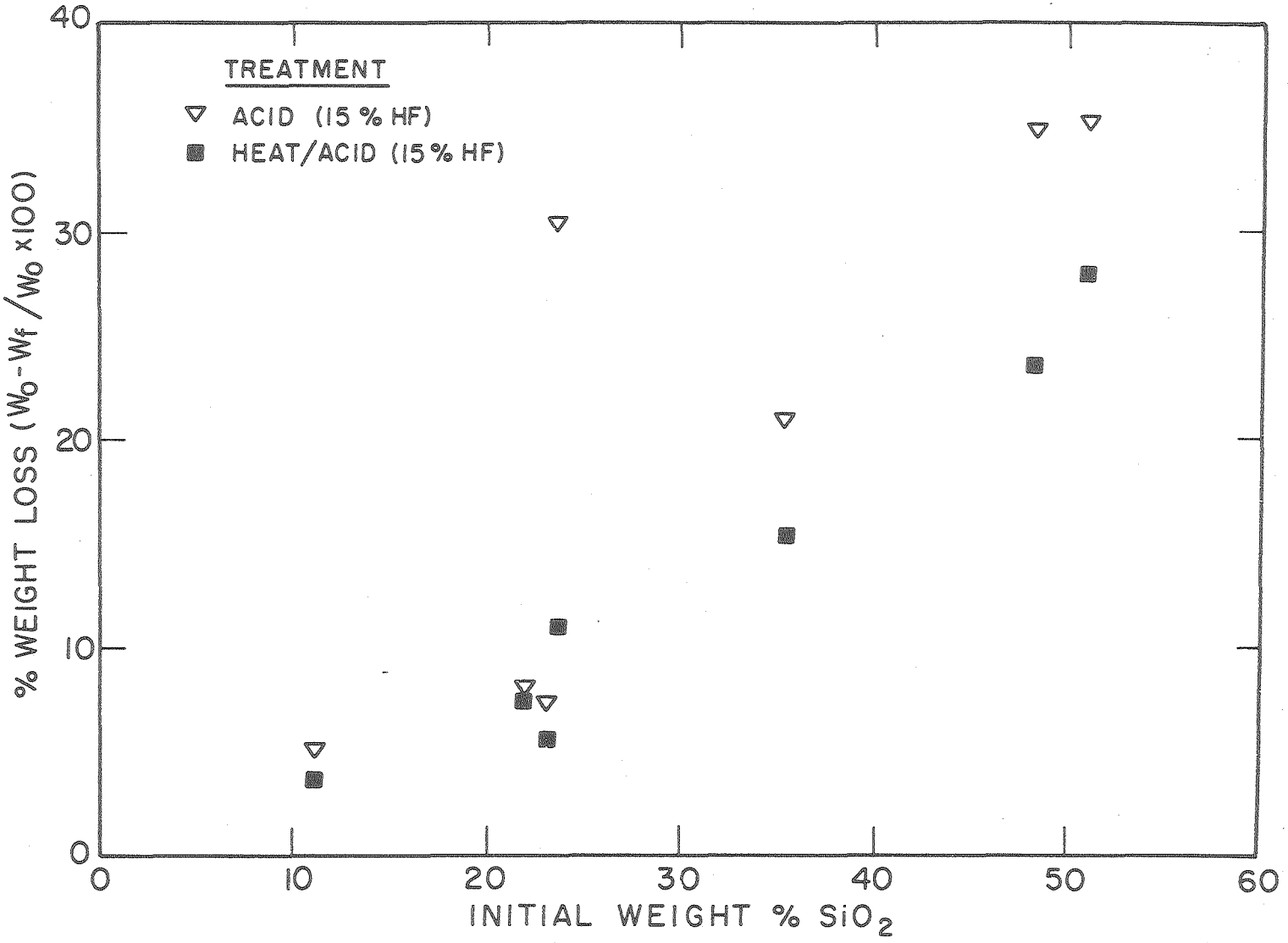

Fig. 16. Correlation of % weight loss with initial weight % SiO_2 after exposure to 15% HF aqueous solution for 24 hrs for as-received and heat treated specimens.

XBL769-7509

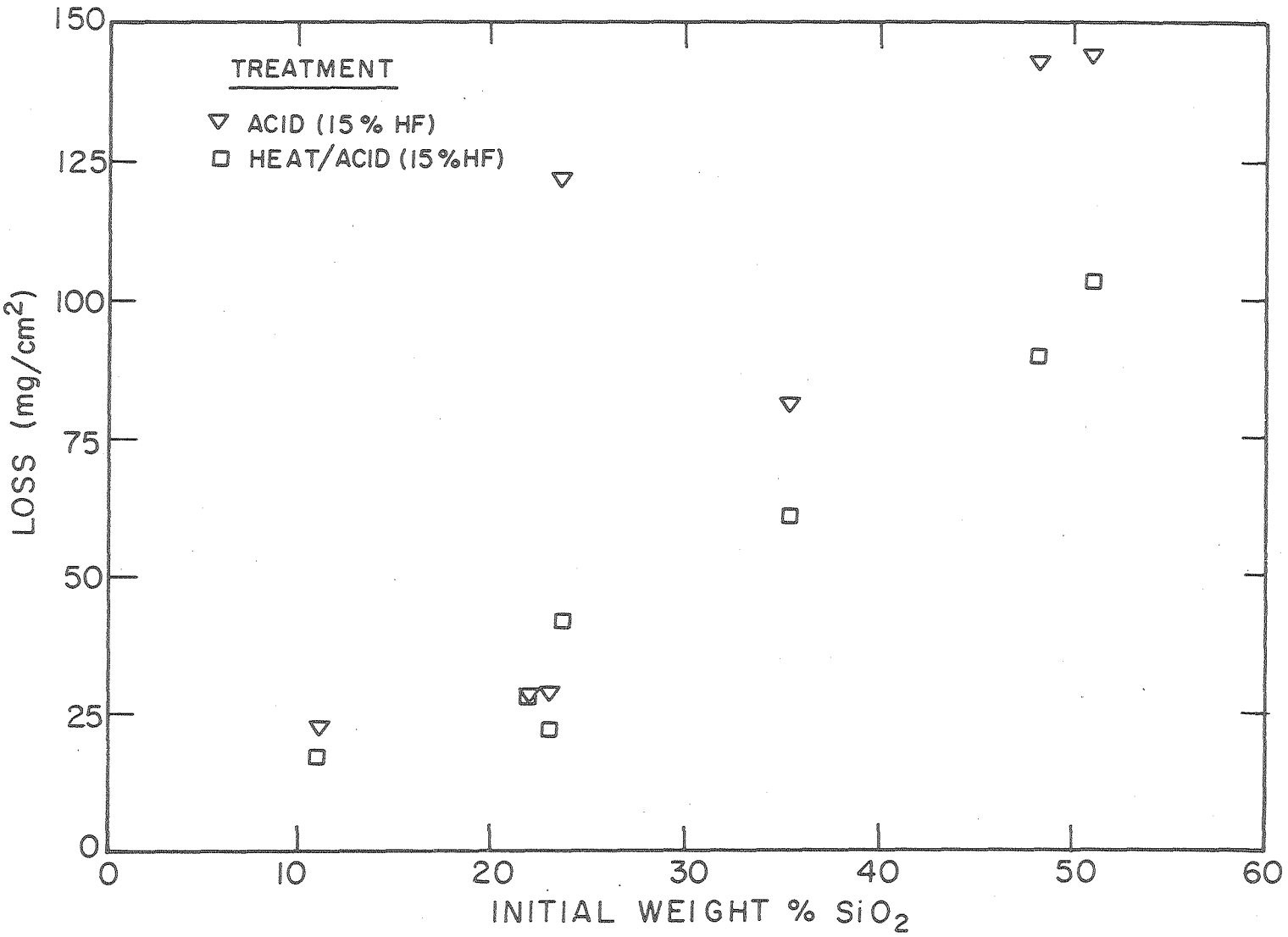

Fig. 17. Correlations of loss in mg/cm^2 with initial weight % SiO_2 after exposure to 15% HF aqueous solution for 24 hrs for as-received and heat treated specimens.

XBL 769-7515

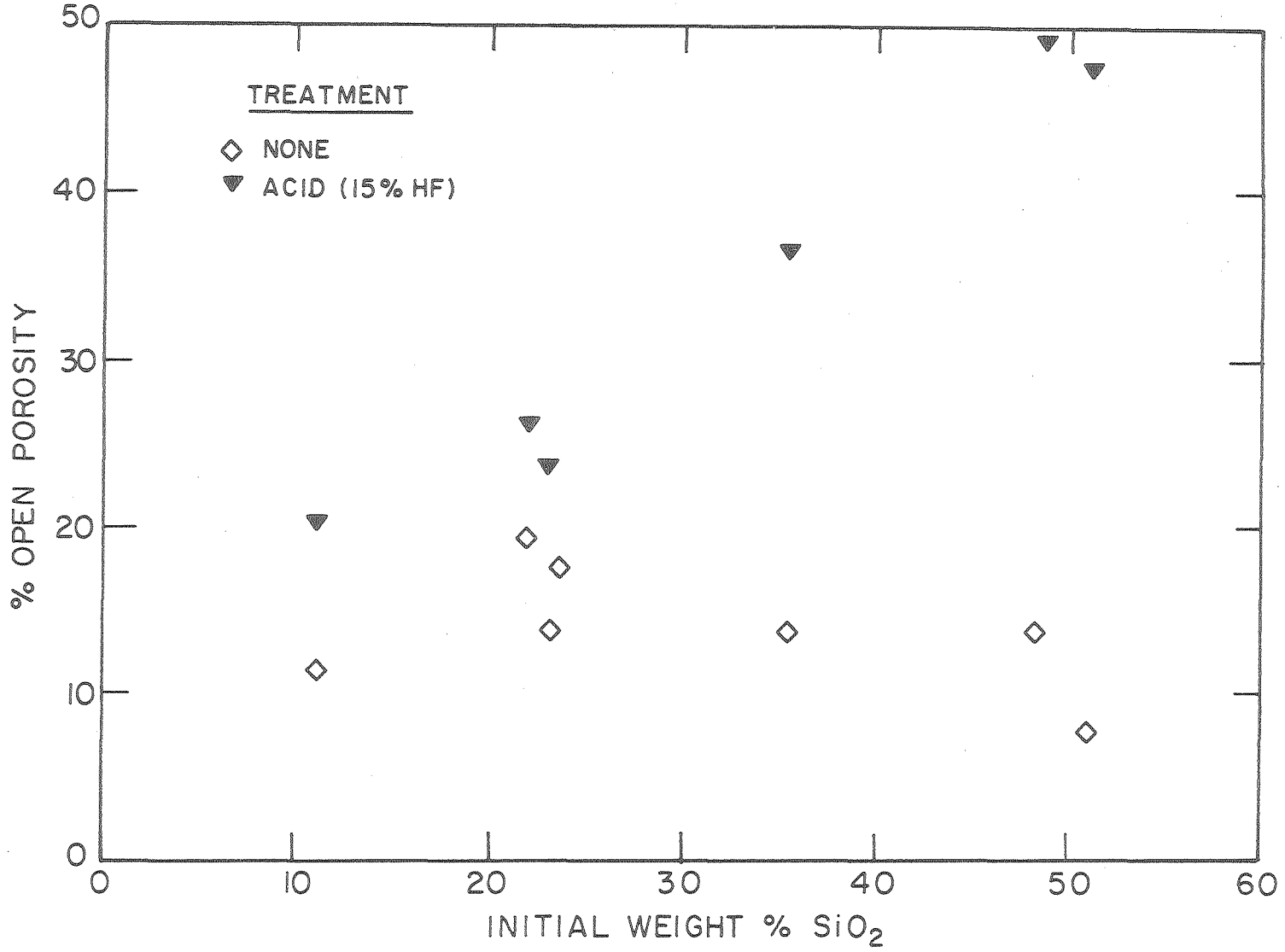

Fig. 18. Correlation of % open pores with initial weight SiO_2 for specimens as-received and after exposure to 15% HF aqueous solution for 24 hrs.

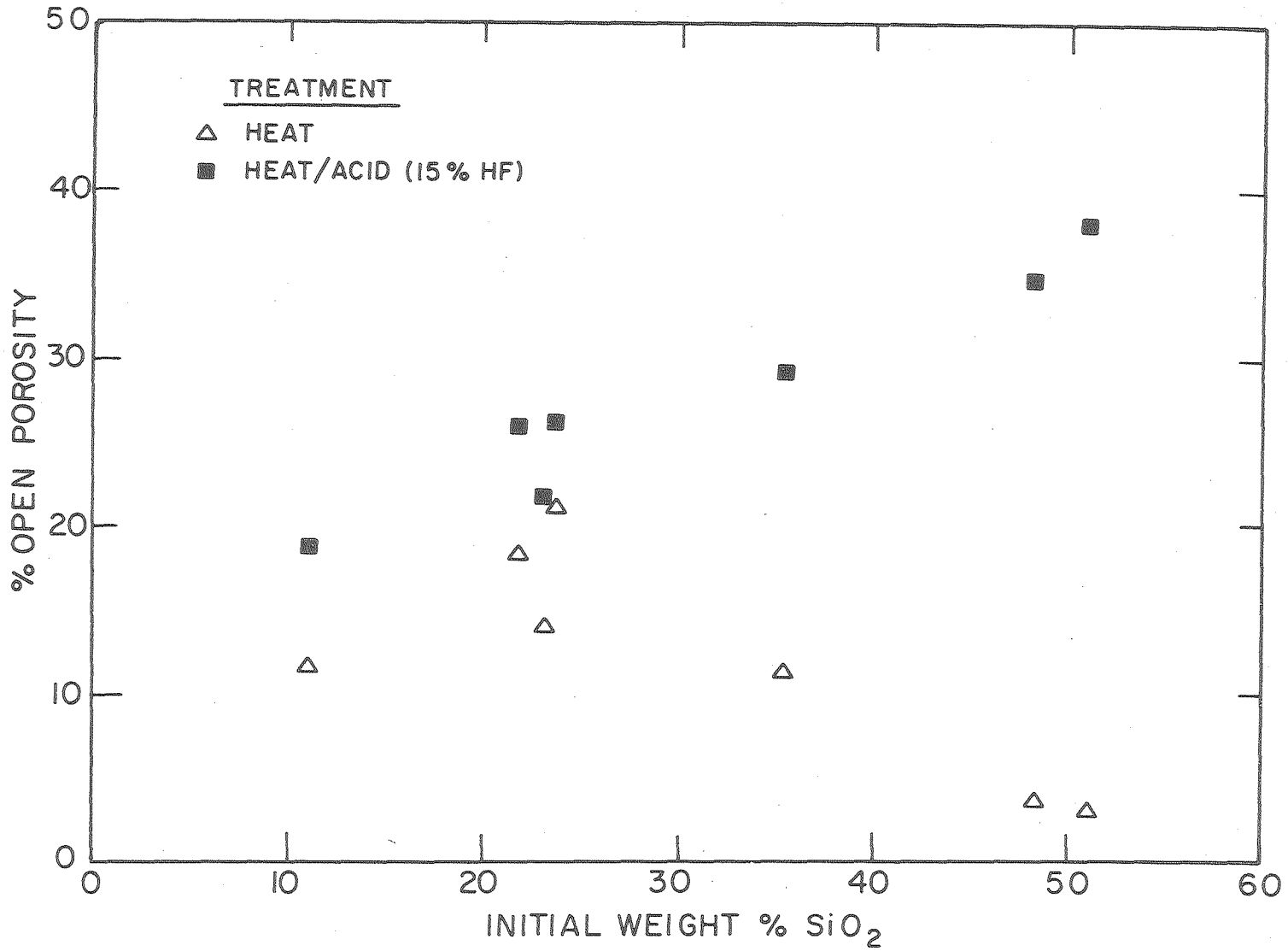

Fig. 19. Correlation of % open pores with initial weight % SiO_2 for heat treated specimens and for specimens heat treated and exposed to 15% HF aqueous solution for 24 hrs.

XBL 769-7511

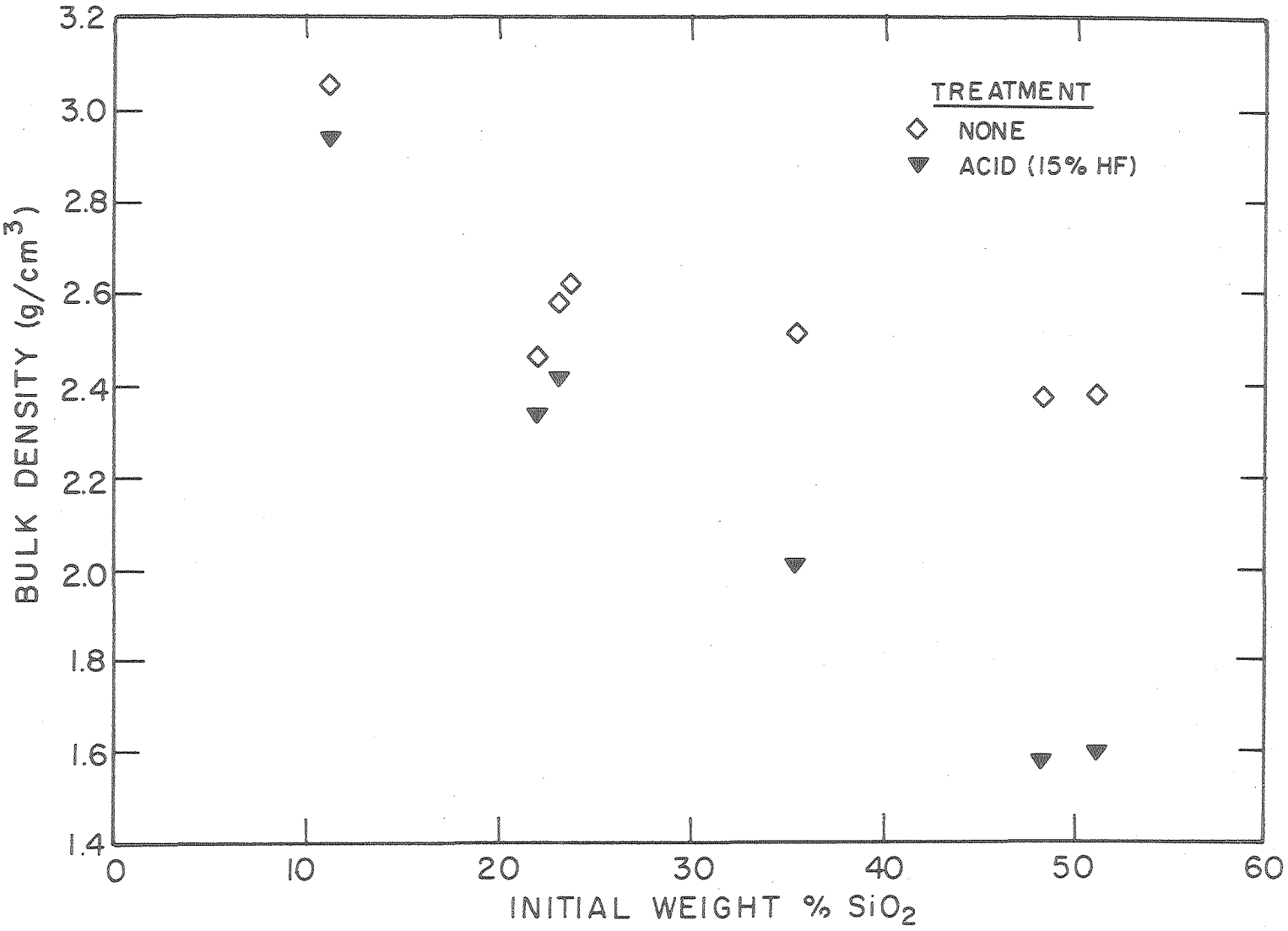

Fig. 20. Correlation of bulk density with initial weight % SiO_2 for specimens as-received and after exposure to 15% HF aqueous solution for 24 hrs.

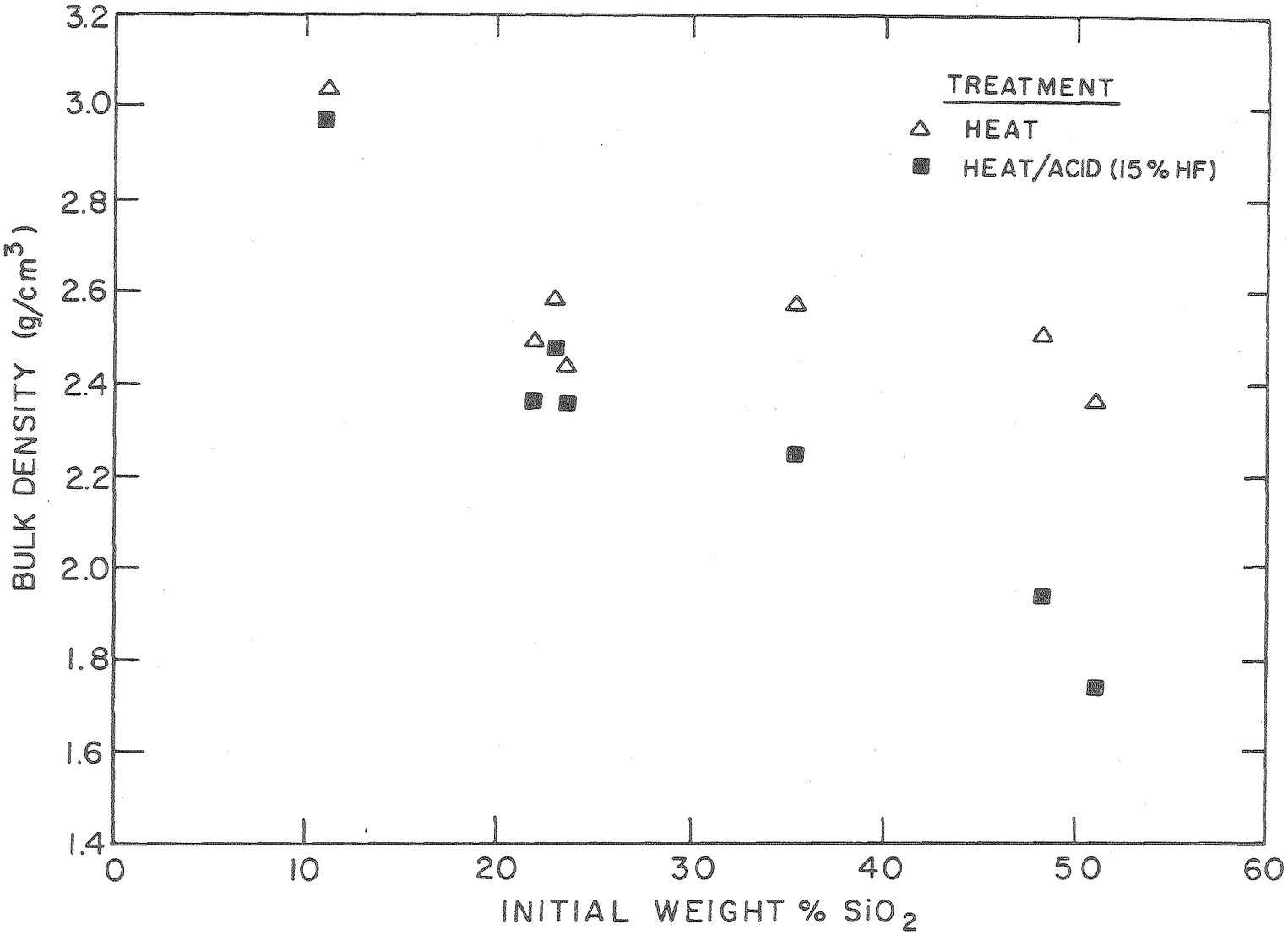

Fig. 21. Correlation of bulk density with initial weight % SiO_2 for heat treated specimens and for specimens heat treated and exposed to 15% HF aqueous solution for 24 hrs.

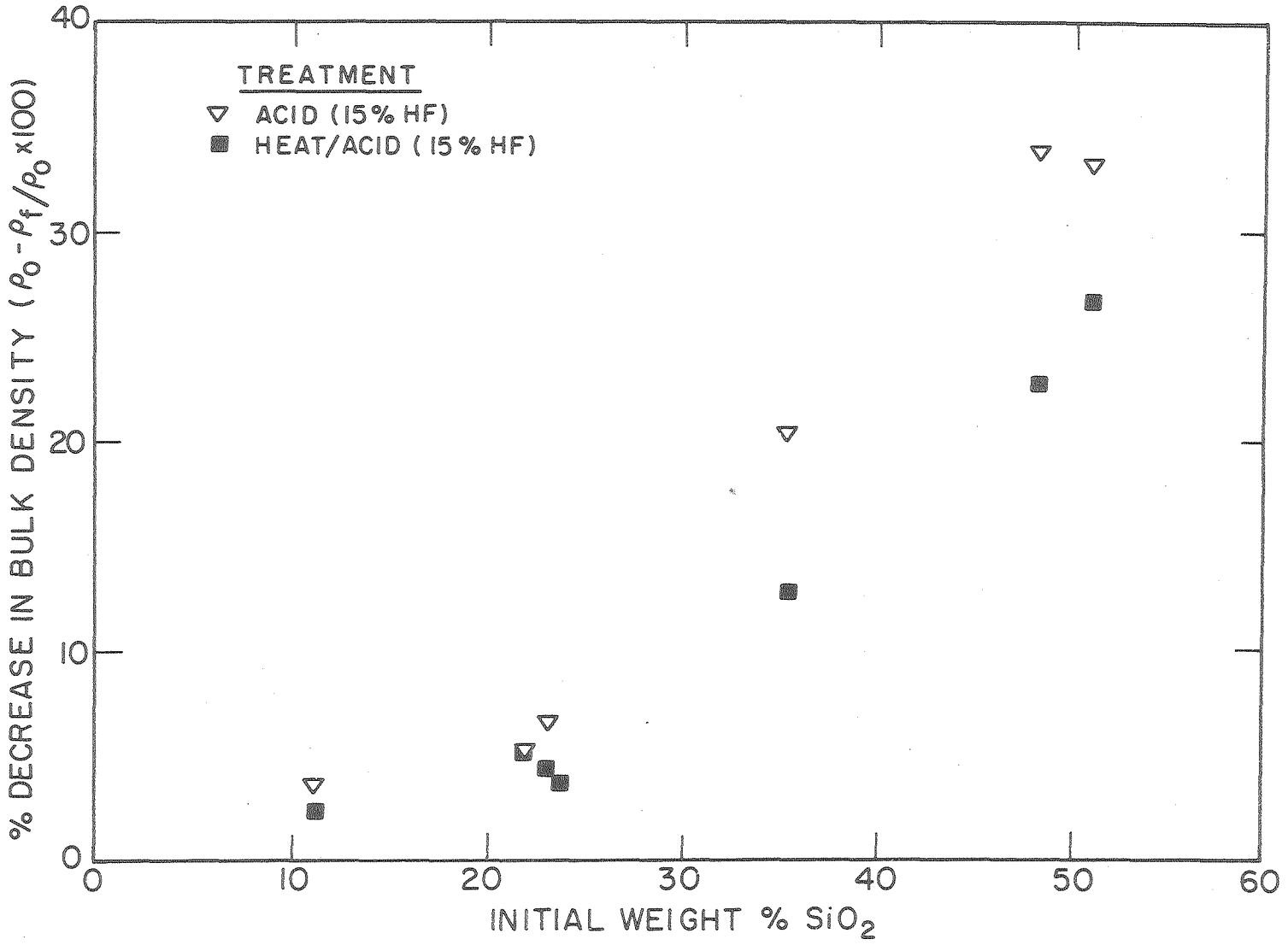

Fig. 22. Correlation of % decrease in bulk density with initial weight % SiO_2 after exposure to 15% HF aqueous solution for 24 hrs for as-received and heat-treated specimens.

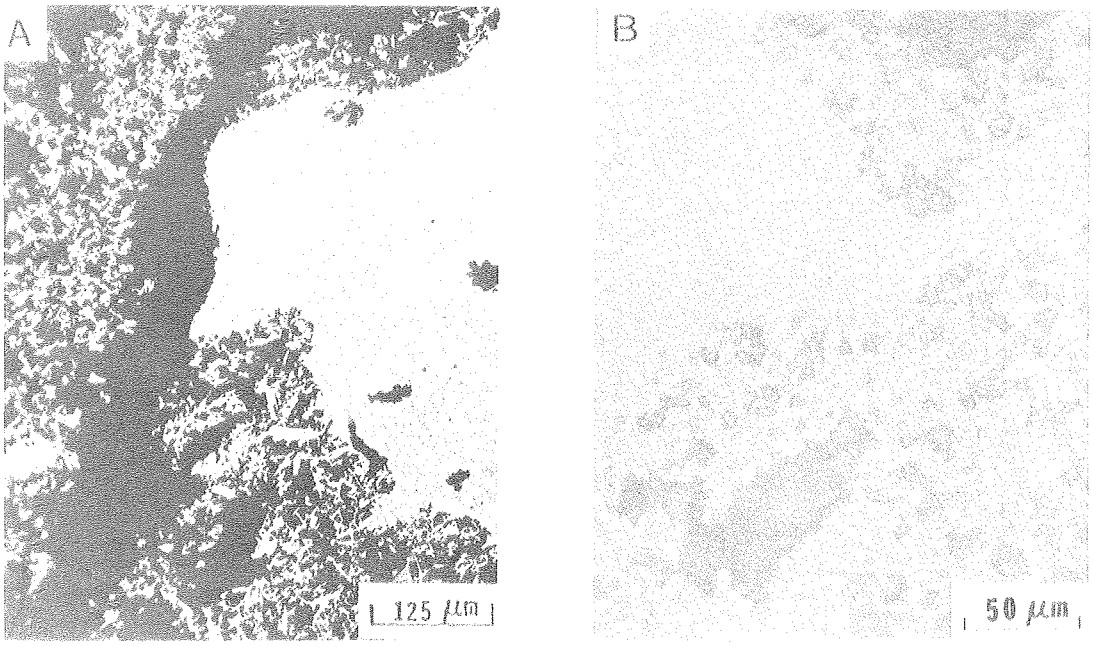

XBB7610-9620

$$SiO_2(s) + HF(aq) = SiF_4(g) \uparrow + H_2O(aq)$$

Fig. 23. Specimen #5 after exposure to 15% HF aqueous solution for 24 hrs.

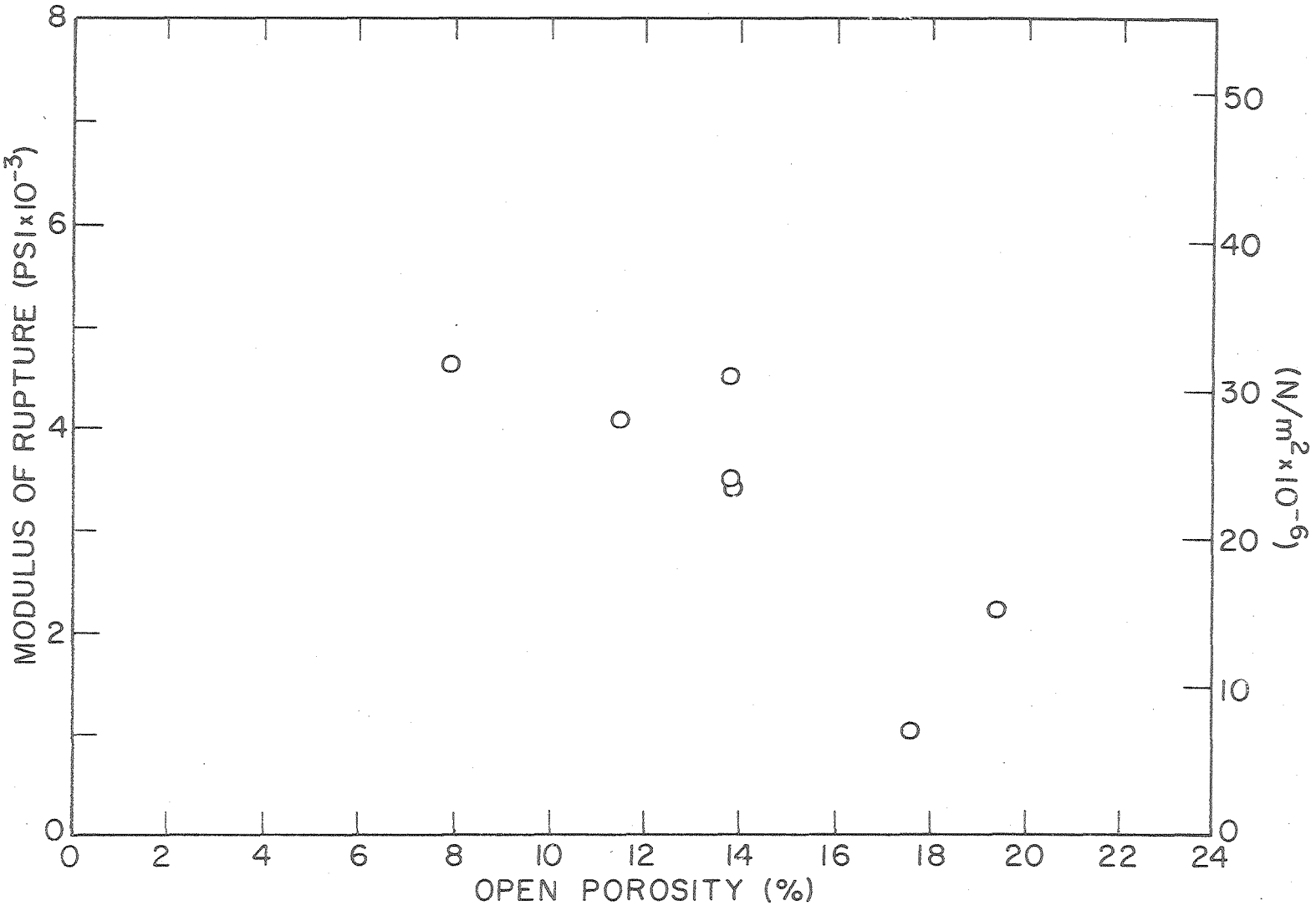

Fig. 24. Correlation of room temperature modulus of rupture with % open pores for as-received specimens.

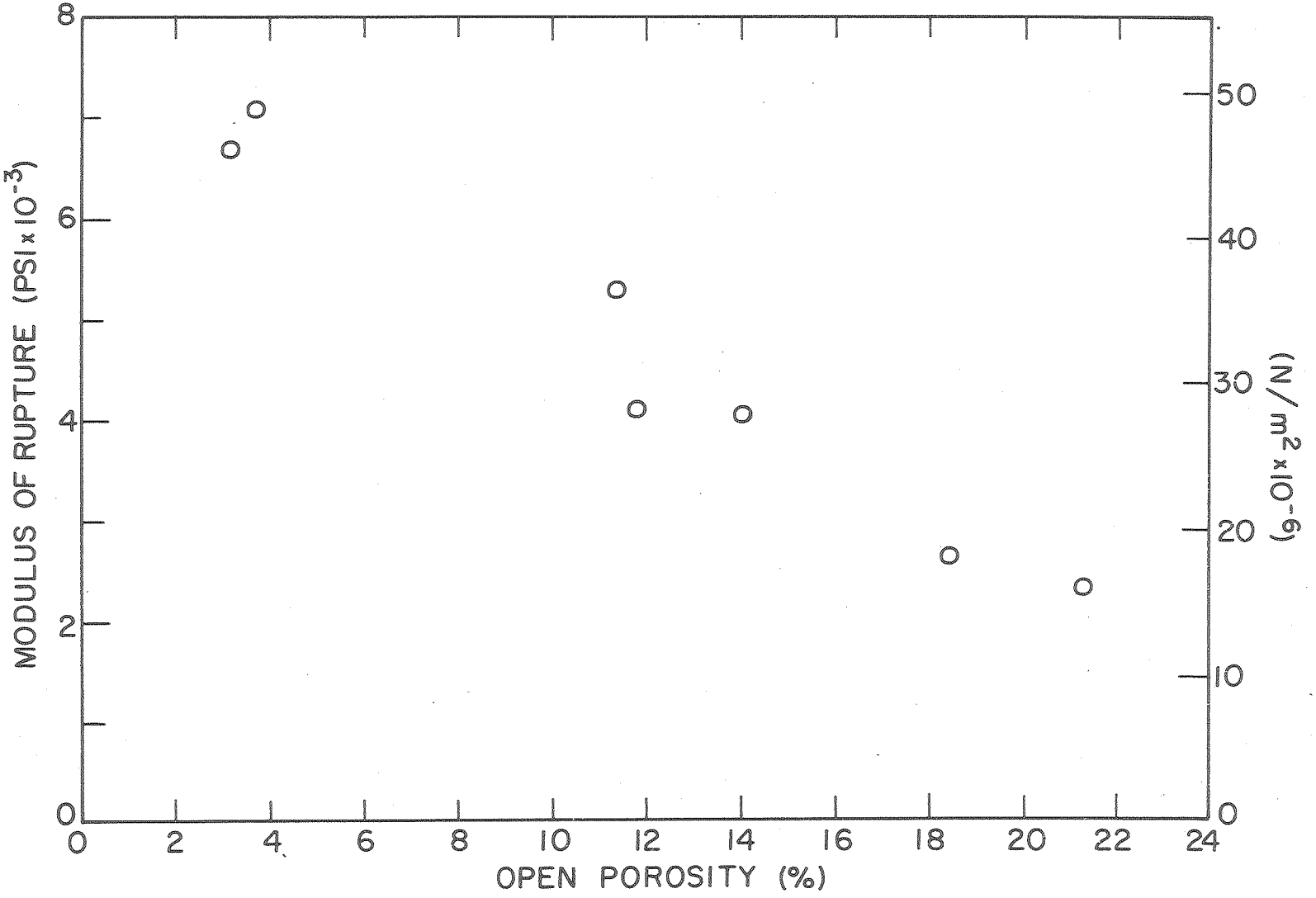

XBL768-7482

Fig. 25. Correlation of room temperature modulus of rupture with % open pores for heat-treated specimens.

V. PART B. INTRODUCTION

The Al_2O_3-SiO_2 system is probably the most important in ceramic technology due to the abundance and widespread use of alumina, silica and aluminosilicate minerals. Mullite, the only intermediate compound stable at high temperatures and normal pressures, is a commonly occurring phase in refractories, whitewares, and porcelains. Refractories containing a high percentage of mullite are useful at high temperatures because of mullite's refractoriness,[11-13] volume stability,[11] high mechanical strength,[11,14-20] low thermal expansion,[11,19] and its resistance to spalling,[11,21,22] creep,[11,23-27] abrasion,[11,28] and corrosion by acid slags.[29]

Despite technological importance, limited information is available on the correlation of major processing variables with the final microstructure of fired bodies containing mullite as a principal phase. Correlations of these microstructures with physical properties, such as strength, are also limited. Recent studies,[30-33] with single crystal and high purity, high density polycrystalline mullite, have shown that only a fraction of mullite's potential capabilities, in regards to mechanical strength, creep resistance, and acid corrosion resistance, are achieved in normal processing.

In Part B of this thesis, several important processing parameters were varied in the sintering of mullite bodies in order to investigate their effect on the final microstructure and the high temperature (1200°C) stress-strain behavior (in compression loading) of the fired compact. Correlations between microstructure and stress-strain behavior were made. However, because of the complexities involved, results were

sometimes difficult to interpret in an unambiguous fashion. The nature of the starting powders, pressing conditions, impurities, intentional additions, and the sintering time, temperature, and atmosphere may all have profound influence upon sintering kinetics and the properties of the fired compact.

VI. LITERATURE SURVEY

A. Processing

The production of mullite bodies depends on the alumina/silica ratio, the degree of mixing achieved, the firing time and temperature, and the presence of fluxes. Mullite is usually prepared by thermally decomposing naturally occurring aluminosilicates such as clay and sillimanite minerals. These materials may be mixed with some form of alumina in order to avoid excessive amounts of siliceous phase.[34-37] Mechanical mixtures of various kinds of Al_2O_3 and SiO_2 are commonly sintered in high temperature kilns in order to achieve more complete reactions and higher purity. Mechanical mixtures of α-quartz, silicic acid, β-cristobalite, or fused silica with α-alumina, diaspore ($HAlO_2$), gibbsite ($Al(OH)_3$) or AlF_3 have been reported.[36,38-43] These raw materials may also be electrofused and cast. The effect of various mineralizing agents on the formation of mullite has been studied extensively.[6-9,44-55] A detailed discussion of the commercial methods of mullite preparation is given by Grofcsik.[51]

In recent years, increasing interest has developed in the preparation and use of highly pure and highly reactive ceramic oxide powders. In the methods of synthetic mullite preparation described previously, alumina and silica are not mixed on a molecular scale and, consequently, long diffusion paths and long diffusion times result in incomplete reaction despite high firing temperatures. In addition, high temperatures result in a large-grained material. In order to achieve better composition control, complete reaction, and a fine-grained powder, a number of chemical preparation techniques have been

utilized to form mullite. McAtee and Milligan[56] formed mullite at temperatures above 1100°C using a coprecipitated mixture prepared from aluminum nitrate with ammonium hydroxide, sodium metasilicate and an excess of HCl. Grofcsik and Vago[57] formed mullite at 950°C by treating a mixture coprecipitated from ethyl orthosilicate and aluminum sulfate solution by ammonium hydroxide. Roy[58] improved this method of precipitation of SiO_2 by addition of HCl to the ethyl orthosilicate. Other coprecipitated gel processes involve the use of aluminum and silicon chlorides[59,60] and ethylates.[61] Bidet and Jouenne[62] prepared a water suspension of amorphous alumina and silica gels which yielded mullite at 960°C. Ghate[63] synthesized mullite by controlled gelling of a mixture of colloidal water suspensions of γ-alumina and amorphous silica which was subsequently fired above 1400°C. Mazdiyasni and Brown[31] prepared mullite by hydrolytic decomposition of mixed metal alkoxides. Williams et al.[64] have formed mullite by reactively sputtering aluminum and silicon. Thermal decomposition of methylsiloxaluminum compounds has also been used to prepare mullite.[65]

While the above methods have the potential advantages of achieving complete reaction and yielding a powder of high purity and fine particle size, several disadvantages may exist depending on which method is used: (1) large quantities of organic materials may have to be handled for small yields of mullite, (2) special handling is required with toxic chemicals such as $SiCl_4$, methanol, and NO_2 fumes which are evolved during firing, (3) raw materials must be carefully standardized in order to achieve close composition control resulting in time consuming and uneconomical procedures, and (4) high purity chemical materials are expensive.

B. Mechanical Properties

Although there is an abundance of information on the mechanical properties of refractories containing mullite as a principal phase, studies on high purity, high density mullite are limited in number and scope.

Fenstermacher and Hummel[66] sintered ball milled mixtures of relatively pure alumina (KC-14, Kaiser Aluminum and Chemical, Inc.) and silica (Potter's flint, Pennsylvania Pulverizing Co.) with 1 wt% MgO additions. Compositions of $2Al_2O_3 \cdot SiO_2$ and $3Al_2O_3 \cdot 2SiO_2$ were sintered at 1650°C and 1710°C, respectively in a gas fired kiln (firing time unspecified). The apparent porosities were 7.1% and 10.9% for 3:2 and 2:1 compositions, respectively. X-ray diffraction and petrographic examination indicated the presence of "free" corundum in the 2:1 mixture. The room temperature modulus of rupture was determined to be ~15000 psi for both bodies. In the temperature range 800°C to 1000°C, the strength increased to about 17000 psi. The strength decreased after 1000°C, but more significantly for the 3:2 mixture.

Penty[30] vacuum hot pressed to near theoretical density and approximately one micron grain size high purity mullite powder formed by Ghate's gel technique. The elastic modulus was determined by the composite oscillator technique and a value of $E_o \cong 32.5 \times 10^6$ was determined. Four-point bending tests determined a creep activation energy of 167 kcal/mole and found the stress exponent to vary from 1.1 at 1460°C to 1.4 at 1512°C. The room temperature strength, in four point bending, of mullite of ~1μ grain size and near theoretical density was in the range 32000 to 38000 psi. This was increased to 50000 psi with

gas flame polishing. At 1200°C, a strength of 35000 psi was maintained.

Mazdiyasni's alkoxy derived mullite powder, vacuum hot pressed to near theoretical density with a grain size of ~5μ, yielded similar results.[31,32] E_o was determined to be 32.0 x 10^6 psi and the activation energy for creep was determined to be 164 kcal/mole. The stress exponent of 1.0 indicated the creep process was controlled by a diffusional mechanism, i.e. either Coble (grain boundary) or Nabarro-Herring (lattice). The room temperature strength in four-point bending was 39000 psi. Dokko and Pask[33] studied the stress-strain and creep behavior of Mazdiyasni's mullite specimens in compression loading at 1400°C and 1500°C. The activation energy for creep was determined to be ~170 kcal/mole. A stress exponent of 1.0 and a grain size dependence of 2.0 indicated that the Nabarro-Herring diffusional mechanism was operative. In addition, intrusion and extrusion of grains on the surface of both stress-strain and creep specimens indicated the occurrence of grain boundary sliding. This was not taken as an indication of glass phase on the grain boundaries, but as an accomodation mechanism which accompanies diffusional deformation processes. These investigators also studied a mullite single crystal which showed no detectable plastic strain under a stress of 70000 psi at 1400°C for 200 hrs. On the basis of the high strength of the single crystal and the diffusion mechanism for creep of the polycrystalline mullite, they concluded that dislocations, if present, were not mobile under these conditions.

VII. EXPERIMENTAL

A. Raw Materials

The raw materials used in this study were Alcoa A-14* (α-alumina), Ottawa silica flour† (α-quartz), and Englehard ASP 900 kaolin.** The manufacturer's typical chemical analysis is given in Table 1.

Table 1. Chemical Analysis of Raw Materials

Wt% of Constituent	A-14	Silica Flour	ASP 900
Al_2O_3	99.6	.06	37.29
SiO_2	.12	99.8	45.34
Fe_2O_3	.03	.02	.61
Na_2O	.04		.35
TiO_2		.013	1.54
CaO		.01	.25
MgO		.01	.22
LOI	.2	.09	13.38

B. Furnaces

Compacts were sintered in three different types of furnaces: (1) a gas-fired kiln described in Part A, (2) two electrically heated ($MoSi_2$ elements) quench-type furnaces, and (3) an electrically heated

*Alcoa Aluminum Co. of America, Bauxite, AR.

†Ottawa Silica Co., Ottawa, IL.

**Englehard Minerals and Chemical Corp., Edison NJ.

furnace* with tantalum elements. The gas-fired Remmey furnace was fired to 1700°C under the schedule described in Part A and to 1725°C by an additional 3-1/2 hours of firing upon reaching 1700°C. Unless noted otherwise, in furnaces (2) and (3), samples were brought to temperature relatively fast (~90 minutes), held at temperature for various times, and cooled in ~90 minutes. The lower temperature $MoSi_2$ element (1700°C Kanthal† Super) furnace is shown in Fig. 1. The higher temperature $MoSi_2$ element (1800°C Kanthal Super 33) furnace was similar but Pt6%Rh-Pt30%Rh thermocouples were used. The Brew furnace temperature was controlled through a W5%Re-W26%Re thermocouple. For furnaces (2) and (3), the temperature was monitored and controlled by a Speedomax-H Recorder Series 60 Controller.** A Trendtrak Programable Controller** was also used with the Brew furnace. The atmosphere was air for the quench-type furnaces and a vacuum of $\sim 10^{-6}$ torr for the tantalum heating element furnace.

C. Processing

Powders were milled for 10 hours in a porcelain ball mill with high density, cylindrical alumina grinding media and isopropyl alcohol as the liquid media. This was done in order to: (1) break-up agglomerates and (2) achieve intimate particle mixing when two powders were used. The powders milled were: (1) 100% ASP 900 kaolin, (2) 71.8 wt% A-14 alumina/28.2 wt% silica flour mixture, (3) 45.9 wt% A-14 alumina/54.1 wt% silica

---

*Richard D. Brew and Co., Concord, NH.
†Kanthal Corp., Bethel, CT.
**Leeds and Northrup Co., Philadelphia, PA.

flour mixture, (4) 55.9 wt% ASP 900 kaolin/44.1 wt% A-14 alumina mixture and (5) 46.6 wt% ASP 900 kaolin/53.4 wt% A-14 alumina mixture. Mixtures (2) and (4) are of the composition of stoichiometric mullite ($3Al_2O_3 \cdot 2SiO_2$) and mixture (3) has the composition of metakaolin ($Al_2O_3 \cdot 2SiO_2$). After milling, the slurries were magnetically stirred while being dried at ~90°C. After screening through a 100 mesh sieve, the powders were mixed with a polyvinyl alcohol (PVA) solution for 3 hours in a plastic container with teflon cylinders. Approximately 3/4 wt% PVA was used. The mixtures were dried, screened, and compacted in a 1-1/2" steel die under a uniaxial pressure of ~7000 psi.

Compacts were pre-fired to 1000°C in a Hevi-Duty furnace.* Firing schedules for each powder mixture are described below:

(1) 100% kaolin compacts were fired with the Remmey 1700°C and 1725°C schedules. A 1725°C sample was also refired to ~1715°C for 150 hours in the quench-type furnace. Another compact was fired to ~1600°C in the quench-type furnace at an average rate of ~3°/min.

(2) 45.9 wt% alumina/54.1 wt% silica compacts were fired with the Remmey 1700°C and 1725°C schedules.

(3) 71.8 wt% alumina/28.2 wt% silica compacts were also fired with the Remmey 1700°C and 1725°C schedules. A 1725°C sample was refired at 1725°C for 12 hours in the Brew furnace. A portion of this refired sample was annealed at ~1600°C for 100 hours in the quench-type furnace.

(4) 55.9 wt% kaolin/44.1 wt% alumina compacts were fired with the Remmey 1725°C schedule and at ~1725°C for 12 hours in the Brew furnace.

---

*Hevi-Duty Heating Equipment Co., Watertown, WI.

(5) 46.6 wt% kaolin/53.4 wt% alumina compact was fired at ~1725°C for 12 hours in the Brew furnace.

The rest of the processing involved the use of a mullite powder formed from the reaction of A-14 alumina and silica flour. The 71.8 wt% A-14 alumina/28.2 wt% silica flour mixture was poured loosely into a platinum crucible and heated to ~1570°C for 48 hours. A sample was easily detached from the sintered, but porous, mass and was then ground, screened through a 325 mesh sieve, and x-rayed. If any small α-alumina peaks remained in the diffraction pattern, the material was refired until no such peaks were detected. The sintered mass was then broken up into small chunks with an alumina mortar and pestle. This was followed by ~10 minutes of grinding in a mechanically operated alumina mortar and pestle.* This powder was used to study the effects of several processing variables on the final sintered microstructure and the stress-strain behavior.

(1) Grinding

A Sweco** vibratory mill was used for additional grinding. In contrast to milling in the porcelain ball mill described earlier, Sweco grinding was intended to accomplish comminution rather than the mixing and/or the breaking of weakly agglomerated materials. Isopropyl alcohol was used as the liquid media. Two different charges of grinding media were used.

(a) Alumina/Flint Grinding Media

The mullite powder was ground for 8, 24, 72 and 144 hours with a

*Pulverisette, Alfred Fritsch Co., Germany.
**Sweco, Inc., Los Angeles, CA.

combination of high density alumina cylinders and flint pebbles. The mullite/alcohol slurry was dried, screened through a 100 mesh sieve, and calcined at 800°C for 1 hour. The powder particle size, morphology, and surface area were characterized by the Fisher Sub Sieve Sizer* (Fig. 2), scanning electron microscopy† (Fig. 3), and the Strohlein Area Meter** (Fig. 4). The Strohlein is a one point BET method with nitrogen as the adsorption gas. The powders were then compacted in a one inch diameter steel die under a uniaxial pressure of ~15000 psi. The variation in green bulk density with grinding time is given in Fig. 5. Large pores, due to inhomogeneous packing of the powder particles, are seen in Fig. 3. The compacts were fired under three conditions: (1) at ~1570°C for 24 hours in the quench-type furnace, (2) to ~1725°C in the Remmey gas-fired furnace, and (3) at ~1725°C for 12 hrs in the Brew furnace under a 10^{-6} torr vacuum.

(b) Alumina Grinding Media

The mullite powder was ground for 5, 8, 24, 72 and 144 hours with high density alumina cylinders. The powders were dried, screened, calcined, and compacted as described above. The powder particle size, morphology, surface area, and inhomogeneous packing of powders, were characterized in the same way (Figs. 6-8). Figure 9 shows the green density versus grinding time relationship. The powders were fired under condition (3) described above.

*Fisher Scientific Co., Pittsburg, PA.
†AMR 1000, Advanced Metals Research Co., Bedford, MA.
**Strohlein & Co., Düsseldorf, W. Germany.

(2) Processing of 5 hr Ground Mullite

(a) Green Density

Mullite powder, ground for 5 hours in the Sweco mill with alumina cylinders as described in Section 1 (b), was compacted under uniaxial pressures varying from 100 psi to 30000 psi. The compacts were fired in the quench-type furnace at 1710°C for 4 and 8 hours.

(b) Firing Time and Atmosphere

5 hr- ground mullite was compacted under 15000 psi and fired in: (1) the quench-type furnace at ~1710°C for 4, 8, 12, 24, and 100 hours and (2) the Brew furnace at ~1710°C for 4, 8, and 100 hrs under a 10^{-6} torr vacuum.

(c) Alumina/Silica Additions

Silica flour, screened through a 325 mesh sieve, was added to 5 hr ground mullite powder in two different proportions: .15/1.00 and .30/1.00. Each mixture was placed in a plastic container with teflon cylinders and isopropyl alcohol and mixed for 3 hrs. The slurry was then dried, screened, and calcined as described previously. The powders were compacted under 15000 psi and fired for 8 hrs at ~1710°C in the quench-type furnace. The same processing was followed with A-14 alumina additions. In addition, the compacts with A-14 alumina additions were fired for 8 hrs at ~1710°C in the Brew furnace under an ~10^{-6} torr vacuum.

D. Characterization of Fired Compacts

Due to mullite decomposition under low partial pressures of oxygen, vacuum (~10^{-6} torr) fired specimens developed a porous Al_2O_3 surface layer. This layer was ground off before the fired compact was characterized.

(1) Mechanical Testing

High temperature (1200°C) stress-strain testing under compression loading was described in Part A (Commercial Refractories). The specimen dimensions were reduced to .1" x .1" x .3" and the strain rate was slightly lower (~1.0×10^{-5}/sec). All other testing conditions were identical.

(2) Microscopy

Ceramographic polishing procedures have already been described in Part A. Samples were observed by scanning electron microscopy and in reflected light by interference-contrast microscopy. A light etch with diluted hydrofluoric acid solution and/or a thin (~200Å) gold coating was sometimes needed to bring out features viewed in the optical microscope. Polished samples viewed by SEM were thermally etched (~20 min at 1550°C in air) in order to make the grain boundaries visible. Both polished and fracture surface samples were coated with a thin (~200Å) gold layer. An EDAX* (Energy Dispersive Analysis by X-rays) attachment was available for semi-quantitative determination of phase compositions.

(3) Density Determination

Bulk density, apparent density, and open porosity were determined by the displacement method utilizing vacuum treatment and distilled water as the soaking liquid. A minimum of two determinations were made for each sample.

*North American Philips Corp., Curryview, IL.

(4) Electron Beam Microprobe Analysis

Weight percentage profiles of Al_2O_3 and SiO_2 in various microstructures were determined by electron beam microprobe analysis.** A description of the microprobe, operating conditions, specimen preparation, and computer analysis of the data are given by Draper[67] of this laboratory.

**Model 400-5, Materials Analysis Co., Palo Alto, CA.

VIII. RESULTS AND DISCUSSION

A. Sintered Kaolin Specimens

The stress-strain curves for sintered kaolin specimens at 1200°C are shown in Fig. 10. Despite a downward trend in bulk density values, the ultimate engineering stress (UES) increases with increasing heat treatment (See Table 2).

Table 2. Physical Properties of Kaolin Specimens.

Heat Treatment	Bulk Density(g/cm^3)	Open Porosity(%)	UES(psi)
1600°C	2.62	.3	7900
1700°C	2.55	.4	10300
1725°C	2.51	3.5	11000
1725°C + 150 hr refire at 1715°C	not determined	not determined	17700

The observed mechanical properties may be explained by viewing the photomicrographs in Fig. 11 and by recalling the behavior of the commercial refractory specimens Nos. 4 and 5 in Part A. The micrographs show: (1) a large amount glass phase (gray color) which accounts for the low UES values and for the viscous flow region of the stress-strain curves and (2) an increase in the size of the mullite crystals (white color) upon increasing heat treatment which accounts for the increasing strength values. As noted in Part A, larger mullite needles interact more strongly during compression deformation, thus increasing the stress required to deform the overall specimen.

B. Reaction Sintered A-14/Silica Flour Specimens of Metakaolin Composition.

Figure 12 shows the stress-strain curves for specimens of reaction sintered 45.9 wt% A-14/54.1 wt% silica flour compacts. As in the case of the kaolin specimens, the strength increases upon additional heat treatment, despite a bulk density decrease (Table 3 and Figs. 13A and B) due to mullite crystal growth (Figs. 13C and D). The change in morphology, from globular to acicular, also contributes to interaction among the mullite crystals.

Table 3. Physical Properties of A-14/Silica Flour (45.9 wt%/54.1 wt%) Specimens.

Heat Treatment	Bulk Density(g/cm^3)	Open Porosity(%)	UES(psi)
1700°C	2.55	0	5600
1725°C	2.18	.2	8000

The large spherical closed pores in the low magnification micrographs of Fig. 13 may be caused by entrapment of gases. The presence of a significant amount of a viscous glass phase, in combination with the fast heating rate used, may lead to a rapid closing of open pores (Table 3) and, consequently, pockets of entrapped air. In accordance with this explanation, increased pore size upon increased firing temperature would be due to increased entrapped gas pressures built up at higher temperatures.

C. Reaction Sintered ASP900 Kaolin/A-14 Alumina Specimens.

The stress-strain curves for reaction sintered kaolin/alumina specimens are given in Fig. 14. Bulk density, open porosity, and UES values are given in Table 4 and micrographs are shown in Fig. 15.

Table 4. Physical Properties of ASP900 Kaolin/A-14 Alumina Specimens.

Composition	Heat Treatment	Bulk Density (g/cm^3)	Open Porosity	UES (psi)
55.9 wt%/44.1 wt%	1725°C(Remmey)	3.01	.8	43600
55.9 wt%/44.1 wt%	1725°C for 12 hrs (Brew)	3.00	1.6	41800
46.6 wt%/53.4 wt%	1725°C for 12 hrs (Brew)	3.05	1.4	44800

The strength of the Remmey fired specimen is considerably greater than that of the kaolin (Section A) and the A-14/silica flour (Section B) specimens fired under identical conditions. This is explained by the much smaller amount of glass present in this sample. However, the presence of a small α-Al_2O_3 peak in the x-ray diffraction pattern is indicative of incomplete reaction and the presence of glass phase. The high impurity content of the ASP900 kaolin (Table 1) shifts the composition away from the stoichiometric values listed. The consequence of impurities such as Na_2O, Fe_2O_3, K_2O, etc., is the formation of a significant amount of glass phase.

Glass phase (dark gray color) is seen directly in the large-grained vacuum fired specimen of "stoichiometric" mullite composition. Figures 16A and 15D are micrographs before and after thermal etching. These

glass pockets limit the strength by reducing the total area of strong mullite grain to grain contacts and increase the possibility of grain boundary sliding. The catastropic failure of the vacuum fired specimen with 20% excess alumina at ~2.1% engineering strain is an indication of less glass phase being present. It should also be noted that the intergranular pockets, from which glass has been etched out (Figs. 15D and 15F) are much smaller in Fig. 15F. These observations are explained by increased mullite formation due to the presence of excess alumina which can react with siliceous phase. While a decrease in glass phase would be expected to increase the strength, the presence of excess alumina may be detrimental to mechanical properties. The strength and elastic properties of composite materials have been postulated to be a function of: (1) the elastic properties of the components,[68-70] (2) the thermal expansion coefficients of the components,[68,69,71,72] (3) the degree of interfacial bonding between components,[73] (4) the volume fraction and the particle size of the dispersed phase.[68,70,74]

The theory concerning stresses established about a particle in an isotropic matrix due to differences in coefficients of expansion has been worked out by Weyl[72] and Selsing.[71] As in the case of alumina in a mullite matrix, when the coefficient of expansion, α, for the particle (αp) is greater than α for the matrix (αm), circumferential cracking around the particles has been observed. Figure 16B shows such an effect. Clearly, interfacial bonding between the components is nonexistant at room temperature. EDAX spectra for the mullite matrix and alumina particle are shown overlapped in Fig. 16C. The peaks farthest to the right are due to the gold coating on the sample. The middle peak (Si) is only

larger than background for the mullite matrix (lined spectra). The Al peak (far left) is largest for the alumina particle (dotted spectra). The effect of the thermal expansion coefficient differences is to introduce cracks larger than inherent Griffith flaws. It would be expected that the reduction in strength as a result of this situation would be more severe at room temperature where the mullite/alumina composite behaves more like an ideal brittle material. However, some reduction is not unlikely at 1200°C where the behavior is semi-brittle.

In addition to thermal expansion effects, stress magnification occurs near the alumina particles in the presence of an applied stress due to differences in elastic properties of mullite and alumina. A weakening effect is generally not observed until second phase particles reach a certain critical size (the Griffith flaw will lie in the area of stress magnification only when large particles are present). Once again, this effect of strength reduction should be more serious at low temperature where the mechanical behavior is more ideally brittle.

Another important factor[70] that may limit the strength of the vacuum fired specimens is the large, non-uniformly distributed pores (Figs. 15C and 15E). This will result in areas where the stress concentration field is very large and, consequently, flaws located near pores will be entirely within this field.

D. Reaction Sintered 71.8 wt% A-14 Alumina/28.2 wt% Silica Flour Samples

Compacts formed from the 71.8 wt% alumina/28.2 wt% silica mixture were reaction sintered with the Remmey (air) 1700°C and 1725°C schedules. A portion of the 1725°C samples was refired in the Brew (vacuum) furnace

at 1725°C for 12 hrs. Stress-strain curves for these samples are presented in Fig. 17 and microstructural features are shown in Fig. 18. Bulk density, open porosity, and UES values are given in Table 5.

Table 5. Physical Properties of 71.8 wt% A-14 Alumina/28.2 wt% Silica Flour Samples.

Heat Treatment	Bulk Density (g/cm^3)	Open Porosity (%)	UES(psi)
1700°C(Remmey)	2.22	18.1	25400
1725°C(Remmey)	2.60	16.6	70100
1725°C(Remmey) + 1725°C, 12 hrs (Brew)	3.09	.5	92200

The increasing strength with increasing heat treatment is largely attributed to the decreasing amounts of porosity. The effect of increasing grain size can not be determined at this point, although grain growth has forced glass phase, present in small amounts due to incomplete reaction, into angular pockets (Fig. 19B). This isolation of glass in pockets is expected to be beneficial for high temperature mechanical strength compared to the 1700°C sample in which glass phase distribution is apparently more film-like (Fig. 19A). Figures 19C and D show the fracture mode in the latter specimen is primarily intergranular while a transgranular failure occurs in the former specimen. These observations indicate that grain boundary strengthening may be occurring due to the glass phase isolation in pockets.

A second specimen of the vacuum refired sample was cut and polished for mechanical testing and, prior to the compression test, was annealed

at 1600°C in air for 100 hours. The stress-strain curve, presented in Fig. 17, shows a significant increase in the ultimate engineering stress value (from 92200 psi to 112500 psi). Dimensional measurements of the annealed sample indicated negligible densification (less than 1/3% linear change). The microstructure for a vacuum refired sample which was subsequently annealed at 1600°C for 100 hours, polished, and thermally etched surprisingly indicates (Fig. 20B) no grain size increase from the vacuum fired sample (Fig. 20A). Therefore, the strength increase cannot be attributed to density or grain size changes. One explanation is the "healing" of surface damage introduced in the sawing, grinding, and polishing of the test specimen. This has been observed in studies on sapphire.[75,76] Another possibility is some type of strengthening at the grain boundaries.

Although it is not necessarily related to grain boundary strengthening, differences in grain boundaries before and after annealing are observed in Fig. 20. In contrast to specimens fired in air and thermally etched in air, vacuum fired specimens form ridges on the grain boundaries upon etching in air. This was also observed in the kaolin/alumina specimens (Figs. 15D and F) and will be seen in all other vacuum sintered samples discussed in this thesis. After extended annealing (as opposed to short thermal etching times), the grain boundaries have returned to the ridgeless appearance of specimens originally air fired. The ridges indicate a positive volume change at the grain boundaries. One possible explanation is the existence of multivalent impurity cations which segregate at the grain boundaries during vacuum firing.

Upon etching in air, oxidation (such as $2Fe + 1/2O_2 \rightarrow Fe_2O_3$) might result in a volume increase. However, since the amount of impurities is small (Table 1), another explanation is more likely. Earlier studies[77,78] have indicated that mullite decomposes under low partial pressures of oxygen according to: $3Al_2O_3 \cdot 2SiO_2(s) \rightarrow 3Al_2O_3(s) + 2SiO(g) + O_2(g)$. Decomposition at the surface, with resultant loss of two volatile species, should cause a significant weight loss in vacuum firing. This is confirmed in a plot of weight loss versus firing time which is given in Fig. 21 for air(quench furnace) and 10^{-6} torr vacuum (Brew furnace) 5 hr-ground mullite powder sintered samples. Figure 21A shows the existance of a porous surface layer (top half) which EDAX confirms to be alumina. (The peaks in the EDAX display (Fig. 21B) represent, from left to right, Al, Si, and Au. The dotted spectra, which contains all peaks significantly above background, is from the matrix while the lined spectra, containing only Al and Au significantly above the background, is from the porous layer). However, grain boundary ridges are observed in polished samples from the interior of the fired specimen. After the closing of pores, decomposition products can not be removed except through slow bulk diffusion. Therefore, the ridges suggest an oxygen deficiency and silicon monoxide excess at the grain boundaries. Upon annealing in air, oxidation of silicon monoxide ($2SiO+O_2 = 2SiO_2$) would result in the volume increase observed at the grain boundaries.

E. Results with Mullite Powder Derived from Reaction of 71.8 wt% A-14 Alumina/28.2 wt% Silica Flour Mixture.

1. Grinding with Alumina and Flint

Mullite, derived from the reaction of A-14 alumina and silica flour,

was wet (isopropyl alcohol) ground in a Sweco mill with alumina and flint grinding media for 8, 24, 72, and 144 hrs. The compacts were sintered: (1) in air at ~1570°C for 24 hrs in a quench-type furnace, (2) in air to ~1725°C in the Remmey furnace, and (3) in vacuum at ~1725°C for 12 hrs in the Brew furnace.

Stress-strain curves for specimens sintered under condition 1(~1570°C, 24 hrs in air) are shown in Fig. 22. Bulk density, open porosity, and UES values are given in Table 6. Micrographs illustrating porosity and grain size differences are shown in Figs. 23 and 24.

Table 6. Physical Properties of Ground Mullite Sintered at 1570°C for 24 Hours.

Grinding Time(hrs)	Bulk Density	Open Porosity(%)	UES(psi)
8	2.29	26.9	25400
24	2.59	15.9	37600
72	2.79	10.1	32800
144	3.05	.1	30800

The increasingly more gradual manner in which the stress decreases, after exceeding the UES, with increasing grinding time is indicative of increasing amounts of glass phase. This increase in glass is due to silica pick-up from ball milling with flint grinding pebbles. Since Fig. 24 shows that the grain size increases only slightly with increasing grinding time, the observed strength values apparently represent a trade off between decreasing porosity (Table 6 and Fig. 23) and increasing glass phase. The 24 hr-ground powder sinters to a higher bulk

density (2.59 g/cm^3) than the 8 hr- ground powder (2.29 g/cm^3) leading to a higher UES value (37600 psi > 25400 psi). The 72 hr- ground powder sinters to an even higher density (2.78 g/cm^3) but its UES value (32800 psi) is lower than the 24- hr ground specimen due to the larger amount of silica pick-up when grinding for 72 hrs. The enhanced sintering with increasing grinding time may be due to one or both of the following: (1) decreasing particle size (increasing surface area) and (2) increasing liquid phase.

Stress-strain curves for specimens sintered under condition 2 (to 1725°C in air) are shown in Fig. 25. Bulk density, open porosity, and UES values are given in Table 7.

Table 7. Physical Properties of Ground Mullite Sintered to 1725°C in Air.

Grinding Time(hrs)	Bulk Density (g/cm^3)	Open Porosity(%)	UES(psi)
8	3.03	.2	79600
24	3.03	.3	75400
72	3.03	.4	64700
144	2.98	.4	54600

Figure 26 shows the grain size of the various specimens increases only slightly with grinding time. In addition, Fig. 27 illustrates that the pore size and total porosity remains approximately same (although the 144 hr specimen appears to have a slightly larger pore size and total porosity than the others). Consequently, the decrease in strength with increasing grinding time must be due to the increasing glass phase (from

silica pick-up due to grinding with flint pebbles). The flow regions beginning at 3-4% engineering strain in Fig. 25 are also attributed to the presence of glass phase.

An important comparison should be made between specimens sintered from the 144 hr- ground powder under conditions 1 and 2. Starting with the same powder and sintering to approximately the same bulk density (3.05 g/cm^3 to 2.98 g/cm^3, respectively) widely different UES values (30800 psi to 54600 psi, respectively) were obtained. In explaining this strength difference, one must consider the distribution of the second phase(s). In this case, the soft (at a test temperature of 1200°C), deformable phase is of primary interest. Whether the glass phase exists as a film around the mullite crystals or is in isolated pockets within a framework formed by strong crystal-crystal (grain-grain) contacts of mullite will be critical in determining the high temperature mechanical behavior. By comparing the heavily etched micrographs in Fig. 28 for 144 hr- ground samples fired under conditions 1 and 2, it is seen that the distribution of glass phase was more "film-like" in condition 1 and more "pocket-like" in condition 2. Since there are more strong mullite grain-grain contacts in condition 2, the strength is greater. The higher firing temperature in condition 2 has promoted grain growth. As often observed with mullite, this growth is anisotropic leading to a more elongated character of the grains. This type of growth appears to have a beneficial effect on strength by forcing the glass phase into angular pockets.

Stress-strain curves for specimens sintered under condition 3 (at 1725°C, 12 hrs in vacuum) are shown in Fig. 29. Bulk density, open porosity, and UES values are given in Table 8.

Table 8. Physical Properties of Ground Mullite Sintered at 1725°C for 12 hrs. in Vacuum.

Grinding Time (hrs)	Bulk Density (g/cm^3)	Open Porosity (%)	UES (psi)
8	3.12	.3	82700
24	3.12	.4	79000
72	3.10	.6	66100
144	3.09	.5	56400

The results are very similar to those obtained under condition 2. As shown in Figs. 30 and 31, the final porosity and grain size remain approximately the same, irregardless of grinding time, which indicates, as before, that the decrease in strength upon increasing grinding is due to silica pick-up from the flint grinding pebbles. In comparison to firing condition 2, UES values for specimens fired under condition 3 are slightly higher which is apparently due to their higher bulk density (Tables 7 and 8) and lower total porosity (Figs. 27 and 30). The lower density for condition 2 might be explained by entrapped air in the pores. The large spherical pores are reminiscent of those obtained in the 45.9 wt% A-14 alumina/54.1 wt% silica flour specimens. As noted in discussing the latter specimens, the presence of glass phase and a fast heating rate could result in a rapid closing of pores and entrapment of gases.

Figure 32 consists of micrographs of fracture surfaces of compression tested samples. Figures 32A and B are the condition (1) 8 hr- and 144 hr- ground specimens, respectively, and Figs. 32C and D are the condition (3) 8 hr and 144 hr- ground specimens respectively. In all cases, fracture is intergranular. Another point of interest is grain morphology.

Despite the shorter firing time for condition (3), 12 hrs less than condition (1), the higher firing temperature (1725°C vs. 1570°C) for condition (3) provides an explanation for the development of an elongated grain character in the 8 hr ground sample. Grain boundary velocity, V, is generally represented by the equation V = MP where P is the driving force and M is the mobility. Assuming that the activation energy for movement of a random grain boundary is equal to the grain boundary self-diffusion in that substance, the mobility increases exponentially with temperature according to (Ref. 79):

$$M = M_o \exp(-Q_b/RT)$$

where Q_b is the apparent activation energy for grain growth kinetics, R and T have their usual significance, and M_o is a constant. It is also noted that the 144 hr- ground specimen for each firing schedule shows a more elongated character than the respective 8 hr- ground specimen. This may be explained as a kinetic phenomenon also. The lower green density with increasing grinding time (Figs. 3 and 5) tells us that more bridging and agglomeration effects are present in these compacts. It is supposed that these agglomerated areas sinter to high density very quickly due to: (1) the highly active nature (large surface area) of the 144 hr- ground powder and (2) the high firing temperature. Consequently, with pores eliminated in these high density areas, grain growth (which is anisotropic) can occur more readily. This would also explain why grain sizes are nearly the same despite the fact that the 144 hr ground powder had a particle size that was initially 1/3 the size of the 8 hr ground powder. However, the increasing amount of glass phase may also be responsible for the enhanced rate of development of

elongated grains when comparing 8 hr- and 144 hr- ground specimens fired under identical conditions. Several researchers attribute the formation of elongated grains in mullite to the presence of liquid.[63,80] The driving force, P, for grain boundary movement has been given[81] by:

$$P = 2\sigma\left(\frac{1}{P_1} + \frac{1}{P_2}\right)$$

where P_1 and P_2 are the two principal radii of curvature and σ is the interfacial energy of the grain boundary. It has been suggested[82] that anisotropic grain growth is due to surface energy anisotropy which is manifested in the presence of the liquid phase. Evidence which supports the importance of liquid phase are the observations of changes in grain boundary curvature (which changes the driving force). Large grains are frequently tabular when liquid phase is present.[83]

2. Grinding with Alumina Only

Mullite, derived from the reaction of A-14 alumina and silica flour, was also wet ground in a Sweco mill with alumina grinding media only for times of 5, 8, 24, 72, and 144 hours. The compacts were sintered under condition 3 (at ~1725°C for 12 hrs in vacuum). The stress-strain curves obtained from these specimens are given in Fig. 33. The values for bulk density, open porosity, and UES are listed in Table 9.

Table 9. Physical Properties of Ground Mullite Sintered at 1725°C for 12 hrs in Vacuum.

Grinding Time(hrs)	Bulk Density (g/cm^3)	Open Porosity(%)	UES(psi)
5	3.12	.6	91500
8	3.12	.8	81500
24	3.15	.9	75300
72	3.10	.8	70300
144	3.09	1.0	54400

Figures 34 and 35 show that porosity, grain size, and second phase (alumina particles - Fig. 34E) increase with increasing grinding time. The decrease in strength upon increasing grinding time can be partially attributed to the increasing porosity. In addition, the possible detrimental effect on mechanical properties of increasing amounts of second phase alumina particles (from pick-up due to alumina grinding media) has been discussed in depth in the section on kaolin/alumina samples. The effect of grain size on strength is uncertain. The absence of viscous flow regions which were seen in Figs. 22, 25, 29, is due to the small amount of glass phase present since flint grinding pebbles were not used. Angular pockets, from which glass phase has been etched (Fig. 35), indicates that a small amount of glass phase still persists.

The reasons for increasing porosity and increasing grain size with increasing grinding time are not entirely clear. In regards to porosity, as discussed earlier, large alumina particles cause circumferential cracking due to a thermal expansion coefficient which is

larger than the mullite matrix. Smaller alumina particles may be a source of pore nucleation if their radius of curvature is larger than the smallest radius formed by the geometric assembly of particles.[82] This effect of inclusions was demonstrated by Siegle and Pranatis.[84] Their work indicated that vacancies which diffused from the neck region were absorbed at the inclusions and, therefore, did not reach the boundaries at which their absorption would have caused shrinkage as is normally observed (without inclusions). Therefore, the presence of alumina particles in the vacuum-fired specimens may not only decrease the mechanical strength but also adversely affect the sintering kinetics and final sintered density.

As far as the increasing grain growth is concerned, the earlier sintering description is still valid (whereby agglomerated areas in long grinding time - high surface area - samples sinter very quickly to form high density, pore-free regions surrounded by rings of large pores). This description accounted for the fact that the grain size (Figs. 26 and 31) of the 144 hr- ground specimen is slightly larger than the 8 hr- ground specimen despite the fact that the former sample had an initial particle size of ~1/3 that of the latter sample. Due to increased grain growth rates, the process is accelerated in this series (alumina grinding media only) so that the 144 hr- ground sample has a much larger grain size than the 8 hr-ground sample (Fig. 35). In fact, exaggerated grain growth is observed in this series. This increased grain growth rate is illustrated by the larger grain size of "alumina ground" samples (Fig. 35) when compared to "alumina and flint ground"

samples (Fig. 31) of same respective grinding times. Both series were fired under identical conditions (1725°C for 12 hrs in a 10^{-6} torr vacuum). Apparently, glass phase restricts the rate of grain growth in vacuum-fired samples.

3. Results with 5 hr- Ground Mullite

Mullite, derived from the reaction of A-14 alumina and silica flour (71.8 wt%/28.2 wt%) and wet ground in the Sweco mill for 5 hours with alumina grinding media, was used to study the effect of several processing variables.

(a) Firing Time and Firing Atmosphere

The mullite powder was compacted under a pressure of 15000 psi and sintered at 1715°C in: (1) air (quench furnace) for times of 4, 8, 12, 24, and 100 hours and (2) 10^{-6} torr vacuum (Brew furnace) for times of 4, 8, and 100 hours. The stress-strain curves for condition (1) are given in Fig. 36. The bulk density, open porosity, and UES values are listed in Table 10. Two compression tests were run for each specimen in order to demonstrate the reproducibility of the results.

Table 10. Physical Properties of Air Fired 5 hr- Ground Mullite.

Firing Time(hrs)	Bulk Density (g/cm^3)	Open Porosity(%)	UES(psi)
4	2.94	.1	84800 85900
8	3.01	.1	86800 87000
12	3.04	.1	88800 91000
24	3.05	.2	81800 81000

Table 10. Physical Properties of Air Fired 5 hr- Ground Mullite (Cont.)

Firing Time(hrs)	Bulk Density (g/cm^3)	Open Porosity(%)	UES(psi)
100	3.05	~0	81700 80900

Low magnification porosity micrographs and high magnification grain size and morphology micrographs are given in Figs. 37 and 38, respectively. The increase in strength with increasing firing time for the 4, 8, and 12 hr specimens is explained by increased densification (Table 10) since other considerations, such as grain size and morphology (Fig. 38) and pore size (Fig. 37), show almost no change. The drop in strength for the 24 hr fired specimen is accompanied by slight, but significant, changes in these considerations (Figs. 37 and 38) while the density (or total porosity) shows almost no change (Table 10). Another important change for the 24 hr fired specimen is the region of the stress-strain curve after ~3.5% engineering strain which shows a viscous flow behavior at an engineering stress of 3000-4000 psi. These observations regarding the mechanical behavior (reduced strength and viscous flow region) may be explained by the increased grain size. The consequence of reducing the grain boundary area is to increase the thickness of glass phase areas (films and/or pockets) between grains. This assumes further reaction, between alumina and glass, to form mullite, is negligible. Pore size increase and grain morphology change, which are only slight after a 24 hr fire, are also assumed to have little effect. In the 100 hr fired specimen, the viscous flow region does not occur and the strength shows almost no decrease from the 24 hr fired specimen. The disappearance

of the flow region may be explained by the entrapment of glass into isolated pockets (Fig. 39A) due to the (anisotropic) exaggerated grain growth. The coinciding effects of a larger pore size, larger grain size, and relatively large isolated glass pockets makes it impossible to explain the strength value relative to the other values in this series. However, several interesting aspects of this sample are noted. Pore growth - not merely the elimination of small pores which increases the average pore size - occurs. Judging from the lack of entrapped pores within grains, grain boundaries are apparently unable to sweep past pores during sintering. Consequently, small pores coalesce during grain growth. The 100 hr specimen was also used to illustrate again the contention that the angular (often triangular) pockets between grains once contained glass phase that has been eliminated during thermal etching to bring out the grain boundaries (see Figs. 39A and B). Further evidence is provided by microprobe data (Fig. 40). With the 4 hr fired specimen, the grain size is small and, consequently, the glass pockets between grains are small. Since the electron beam of the microprobe is ~1 micron in diameter (and the volume affected is on the order of 6-7 cubic microns), it would be very unlikely that a glass pocket would be directly focused upon. Consequently, due to averaging effects, there is relatively little scatter in composition as one scans across the specimen. For the 100 hr fired specimen, the larger glass pockets result in a greater chance of more directly focusing upon a glass area. Consequently, we see occasional sharp composition shifts toward higher silica contents.

The stress-strain curves for condition 2(4, 8, and 100 hrs at ~1715°C in vacuum) are shown in Fig. 41. Bulk density, open porosity,

and UES values are presented in Table 11 and microstructures are shown in Fig. 42.

Table 11. Physical Properties of Vacuum Fired 5 hr- Ground Mullite

Firing Time(hrs)	Bulk Density (g/cm^3)	Open Porosity(%)	UES(psi)
4	3.08	.3	89800
8	3.13	.3	91600
100	3.14	~.0	92300

The most striking observation is the small change in strength with the long firing time. However, the increasing strength with increasing sintering time correlates well with the increasing bulk density. The higher densities of the vacuum fired specimens when compared with those sintered in air (Tables 10 and 11 and Figs. 37 and 42) may also be responsible for the higher strength of the former specimens. The increasing grain size with sintering time (Figs. 42B, D, and F) does not seem to have much effect on mechanical properties of vacuum fired samples. Although there is some preferential growth of elongated grains, the exaggerated growth in the 100 hr specimen primarily retains the blocky character (Fig. 42F) of the grains in the 4 hr (Fig. 42B) and 8 hr (Fig. 42D) samples. This observation supports those who contend that glass phase is necessary for growth of elongated mullite grains. In vacuum, enchanced volatilization of free silica (as glass) before the pores close would explain the reduced amount of glass phase present. The decreased glass content might be another explanation for the increased

strength of vacuum fired specimens when compared to the air fired specimen. Small amounts of glass phase are still present in these vacuum fired specimens, however, as indicated by angular pockets between grains.

(b) Green Density Effect

The mullite powder was compacted uniaxially under various pressures from 100-30000 psi and sintered in air (quench furnace) at ~1710°C for 4 and 8 hrs. Stress-strain curves are plotted in Figs. 43 and 44 for 4 and 8 hrs sintering times, respectively. Green bulk density, compaction pressure, final bulk density, final open porosity, and UES values are given in Table 12.

Table 12. Physical Properties of 5 hr- Ground Mullite Specimens Showing Effect of Green Density.

Compaction Pressure(psi)	Green Bulk Density(g/cm^3)	Final Bulk Density(g/cm^3)	Open Porosity(%)	UES(psi)
4 hr				
100	1.37	2.81	6.1	75800
2500	1.59	2.91	.9	79300
15000	1.82	2.94	.1	84800,84000
30000	1.94	2.99	.2	86600
8 hr				
100	1.38	2.83	.1	80300
500	1.53	2.93	.1	-
2500	1.61	2.95	.1	84500
5000	1.68	2.97	.1	86300
10000	1.76	2.99	.1	-
15000	1.82	3.01	.1	87000,86800
30000	1.93	3.03	.1	-

For both sintering times, the effect of increasing green density is increasing strength. Since the grain size and grain morphology (Fig. 45 for 4 hr- sintering time, Fig. 46 for 8 hr- sintering time) remain approximately constant, irregardless of green density, increased strength is due to increasing density.

4. Intentional Additions of Silica and Alumina to 5 hr- Ground Mullite

A-14 alumina and silica flour were intentional additives to 5 hr- ground mullite. Both were added in two proportions: .15/1.00 and .30/1.00 by weight. The silica-rich compacts were sintered at ~1710°C for 8 hrs in air (quench furnace) while alumina-rich compacts were sintered at ~1710°C for 8 hrs in air (quench furnace) and 10^{-6} torr vacuum (Brew furnace). While the additions did alter the green bulk density (from 1.66 g/cm^3 for 30% excess silica to 1.90 g/cm^3 for 30% excess alumina), the variation of % of theoretical density is small. Assuming pure mullite, corundum, and α-quartz and assuming theoretical densities of 3.19, 3.97, and 2.65 g/cm^3, respectively, the % of theoretical density has the range of 56.0%±1.5.

The stress-strain curves for sintered silica-rich compacts are given in Fig. 47. The undoped (100% 5 hr- ground mullite) sample, sintered under identical conditions, is included for comparison. The bulk density, open porosity, and UES values are listed in Table 13 and microstructures are shown in Fig. 48.

Table 13. Physical Properties of Sintered Compacts of 5 hr-Ground Mullite with Silica Flour Additions.

Specimen	Bulk Density(g/cm^3)	Open Porosity(%)	UES(psi)
undoped	3.01	.1	86800,87000
15% excess SiO_2	2.74	~0	51200
30% excess SiO_2	2.57	~0	27600

The change in the shape of the stress-strain curves, from catostrophic failure to an increasing flow character, is indicative of the presence of increasing amounts of glass phase. Figures 48 D and F show this second phase and the siliceous nature is confirmed by EDAX. The decreasing area of mullite-mullite grain contacts is largely responsible for the strength decrease, though the increased pore size and total porosity (particularly for the 15% excess silica specimen - Fig. 48C - compared to the undoped specimen - Fig. 48A) would also have some effect. Once again, it is postulated that the large, rounded pores occur due to entrapped air. The pores close rapidly (Table 13) due to the fast heating rate and large amount of glass phase. One other point of interest is the increasing grain size, despite identical firing conditions, with increasing glass phase. This effect for air fired compacts is the opposite of that encountered in vacuum firing where decreased amounts of glass phase seems to promote grain growth (compare Fig. 31 of Section E.1 and Fig. 35 of Section E.2). Another example supporting this idea

is the comparison of samples fired under condition 2 (to ~1725°C in air) and condition 3 (at ~1725°C for 12 hrs in vacuum) in Section E.1. Figures 26 and 31 show the air-fired samples have the same or slightly larger, grain size despite the 12 hrs at temperature (~1725°C) for the vacuum-fired samples. These samples, particularly those ground for 144 hrs, have a significant amount of glass phase from grinding with flint pebbles.

The stress-strain curves for sintered alumina-rich compacts are given in Fig. 49. The undoped (100% 5 hr- ground mullite) samples, sintered under identical air and vacuum conditions, are included for comparison. The bulk density, open porosity, and UES values are listed in Table 14.

Table 14. Physical Properties of Sintered Compacts of 5 Hour- Ground Mullite with Additions of A-14 Alumina.

Specimen	Bulk Density(g/cm^3)	Open Porosity(%)	UES(psi)
Undoped(air)	3.01	.1	86800,87000
15% excess Al_2O_3(air)	2.94	2.0	104900,100800
30% excess Al_2O_3(air)	2.84	10.6	89000,88700
Undoped(vacuum)	3.13	.3	91600
15% excess Al_2O_3(vacuum)	3.13	~0	85000,83700
30% excess Al_2O_3(vacuum)	3.17	~0	86200,85400

The air fired specimen will be discussed first. Figures 50 A, C, and E illustrate that grain size remains approximately the same despite the change in alumina content. Figures 51 A, C, and E and Table 14 show the increasing total porosity with increasing alumina content. While

the presence of excess alumina adversely affects the final density achieved, the mechanical strength increases significantly for the 15% excess Al_2O_3 sample and increases slightly for the more porous 30% excess Al_2O_3 sample. This may be explained by Fig. 52. The large glassy area in the center of Fig. 52A is an atypical feature for small-grained samples. It was included in order to further support the contention that a small, but significant, amount of glass phase is always present (due to incomplete reaction and impure starting materials) in the mullite samples discussed in this thesis. The circled areas in Fig. 52A are, however, a typical feature. Figure 52B show that the addition of 15% excess alumina has almost completely eliminated these areas of weak mullite grain-grain contacts. The 30% excess alumina accomplishes the same effect, but further reduction in density lowers the strength from the value for 15% excess alumina sample. The circled areas are too small to be analyzed by microprobe or EDAX, but it is speculated that they are glass pockets. Excess alumina can react with glass phase to produce mullite. Due to strong mullite grain-grain comtacts, a compression strength over 100,000 psi at 1200°C is achieved despite a density only ~90% of theoretical. Clearly, the presence of second phase is critical in determining the high temperature mechanical strength of mullite. Another critical point is the fact that alumina particles form good interfacial bonds with the mullite matrix in <u>air</u> firing. <u>Vacuum</u> fired specimen with excess alumina (see Figs. 16B, 35D, 50F) show circumferential cracking which is not detected in air fired samples. Perhaps, bonding in air firing is facilitated by a glass phase layer which may volatilize in vacuum firing. Further evidence

supporting the belief of stronger grain-grain contacts of the specimens with excess alumina is the fracture surfaces of compression tested specimens. The undoped sample shows primarily intergranular fracture (Fig. 53A) while the sample with excess alumina has a fracture mode which is primarily transgranular, (Fig. 53B).

The vacuum fired results are more difficult to interpret. Figures 51B, D, and F show the usual effect of increasing porosity with increasing amounts of alumina (It should be remembered that the values in Table 14 are bulk densities and the true densities are actually decreasing since the theoretical density of alumina is greater than that of mullite). If we temporarily neglect grain size effects (Figs. 50B, D, and F), based on our earlier experience of vacuum fired specimens (Section E.3.(a), Figs. 41, 42), one might expect a decreasing strength with increasing alumina content (due to the resultant increasing porosity and the poor interfacial bonding between alumina particles and the mullite matrix). However, the order of decreasing strength is: undoped, 30% excess alumina, 15% excess alumina. Apparently, either there is some grain size effect (with increasing grain size being detrimental to strength) or the excess alumina has another, as yet undetermined, effect. The large grain size of the 15% excess alumina sample is not surprising in view of the other results with vacuum fired specimens (Section E.2, Fig. 35). In contrast to air fired samples (Fig. 48), smaller amounts of glass phase in vacuum fired specimens result in the promotion of grain growth. In the 15% excess alumina sample, the absence of angular pockets between grains (Fig. 53C) indicates negligible glass phase which results in a tremendous rate of grain growth (and entrapped pores).

It is also noted that the grain morphology is primarily blocky in character which further supports the contention that glass phase promotes elongated grain growth. The reason for relatively small grain size of the 30% excess alumina specimen is not entirely clear, but is probably related to the larger amount of porosity. The dispersion of a second phase (including pores) has been observed to impede grain boundary movement. For a grain boundary to move past an inclusion, new grain boundary, equal in area to the cross-sectional area of the inclusion, must be formed. Zener[85] postulated that during normal grain growth, the average grain size, D, is given by $D \approx d/f$ where d is the inclusion diameter and f is the volume fraction of inclusions.

5. Effect of Annealing

Two other samples were subjected to the same annealing treatment as described in Section D on reaction-sintered 71.8 wt% alumina/28.2 wt% silica samples. A 5 hr- ground mullite sample, sintered at ~1710°C for 8 hrs in vacuum, showed similar behavior upon annealing (at ~1600°C for 100 hrs in air) to the latter sample. Linear dimensional change was not detected. The grain size (Figs. 54A and B) remained the same, although the grain boundary ridges disappeared after annealing. Therefore, the observed increase in UES values (Table 15) is explained by (1) "healing" of surface damage from the sawing, grinding, and polishing to prepare the test specimen and/or (2) some, as yet undetermined, grain boundary strengthening mechanism.

The other sample subjected to annealing was the 5 hr- ground mullite with 30% excess alumina sample which was originally fired at ~1710°C for 8 hrs in air. The increase in UES value is given in Table 15. A

significant 1% linear shrinkage and a grain size increase (Figs. 54C and D) complicates interpretation of the results.

Table 15. Ultimate Engineering Stress Before and After Annealing

Sample	Treatment	UES(psi)
5 hr- ground mullite	8 hrs, 1710°C in vacuum	91600
5 hr- ground mullite	8 hrs, 1710°C in vacuum & anneal	102600
5 hr- ground mullite + 30% excess Al_2O_3	8 hrs, 1710°C in air	88700,89000
5 hr- ground mullite + 30% excess Al_2O_3	8 hrs, 1710°C in air & anneal	98800

IX. SUMMARY AND CONCLUSION

The effect of selected processing variables on final microstructure and high temperature (1200°C) stress-strain behavior (in compression loading) of sintered mullite bodies was studied. Attempts to correlate the microstructure with stress-strain behavior were made.

The presence of second phase appeared to be the most critical factor in determining the high temperature mechanical strength. Naturally, this is partially a function of the difference in mechanical properties of the single phase materials. For example, siliceous glass phase is extremely detrimental to the high temperature mechanical strength of mullite bodies because the soft, deformable glass will flow viscously at the test temperature. However, second phase may also affect the mechanical properties by altering the sintering behavior and, therefore, altering microstructural features such as grain size, grain morphology, total porosity, and pore size. For example, in air firing, siliceous phase apparently promotes grain growth and, in vacuum firing, its absence appears to promote grain growth. Excess alumina also affected the nature of grains because it could react with excess siliceous glass to form mullite. Both glass and alumina phases also produced changes in the amount and size of pores in the final microstructure.

The effect of grain size and morphology on mechanical properties is closely related to the fact that not only the amount but also the distribution of second phase is an important concern regarding the high temperature strength. Apparently, grain growth is anisotropic in the presence of siliceous liquid phase which leads to the isolation of the glass into "pockets". This distribution appears to be beneficial

for the high temperature strength. Although the effect of the grain size on mechanical properties was not studied independently of the second phase, available evidence indicates that there is only a weak dependence in this system. This is possibly a reflection of the absence of mobile dislocations in mullite tested at 1200°C.

The influence of second phase on microstructure and strength is, in turn, strongly dependent on firing atmosphere. An example of this was already described concerning grain growth in the presence of siliceous liquid phase. In other cases, vacuum sintering resulted in poor bonding between alumina particles and the mullite matrix while air sintered compacts showed good bonding and improved strength. Densification kinetics and grain growth kinetics are dependent upon the sintering atmosphere since phase composition and distribution and interfacial energies are affected by the atmosphere. A literature survey did not reveal any other observations of ridges at grain boundaries such as those encountered in this study for mullite samples sintered in a vacuum atmosphere. The significance of this is that if previous investigators were not cognizant of subtle changes in the nature of the grain boundaries which may drastically affect the sintering behavior of mullite, then they may have been unaware that such changes (e.g. in composition, in valence) would make phase equilibria in the Al_2O_3-SiO_2 system very sensitive to atmosphere. A systematic study of the effect of firing atmosphere on the sintering behavior of mullite might provide valuable information in explaining the contradictory results obtained over the last half century by investigators studying the Al_2O_3-SiO_2 phase relationships.

REFERENCES

1. M. S. Crowley, "Hydrogen-Silica Reactions in Refractories," Bulletin of the American Ceramic Society, 46 [7], 679-682 (1967).

2. M. S. Crowley, "Hydrogen-Silica Reactions in Refractories," Am. Ceram. Soc. Bull., 49 [5], 527-530 (1970).

3. G. R. Eusner and W. S. Debenham, "Effect of Firing Temperature on Properties of Fireclay Brick," Am. Ceram. Soc., Bull., 35 [4], 151-154 (1956).

4. H. F. Folk and W. C. Bohling, "High Temperature Strength of High Alumina Refractories," Am. Ceram. Soc. Bull., 27 [6], 580-583 (1968).

5. K. E. Gronitzki, "High Temperature Properties of Mullite Bricks," Tonind.-Ztg. Keram Rundschau, 92 [7], 241-245 (1968).

6. H. Moore and R. Heeley, "An Experimental Investigation of Alumina-Silica Refractories of High Purity for Use in Glass-Melting, Part I," J. Soc. Glass Tech., 34, 274-304 (1950).

7. R. Heeley and H. Moore, "An Experimental Investigation of Alumina-Silica Refractories of High Purity for Use in Glass-Melting, Part II," J. Soc. Glass Tech., 36, 242-265 (1952).

8. H. Moore and M. Prasad, "The Effects of Various Mineralizing Agents in Promoting Recrystallization in Mixtures of Clay and Alumina During Firing," J. Soc. Glass Tech., 39, 314T-350T (1955).

9. G. M. Gad and L. R. Barrett, "The High-Temperature Breakdown of Mullite and other Alumino-Silicates in the Presence of Alkalis," Transactions of the British Ceramic Soc., 49, 470-491 (1950).

10. K. Konopicky, V. Hofmann and P. Kampa, "Theory of Fire-Clay Refractories: II," Ber. Duet. Keram. Ges., 33, 52-59 (1956).

11. K. K. Kappmeyer and R. H. Manning, "Evaluating High-Alumina Brick," Am. Ceram. Soc. Bull., 42, 398-403 (1963).

12. D. N. Poluboiarinov and G. G. Fol'dgandler, "Deformation of Fireclay Ware Under Load at Various Temperatures," Ogneupory, 13, 107-118 (1948).

13. D. N. Poluboiarinov, G. P. Kalliga, "Deformation Under Load at High Temperatures of Alumina-Silicate Refractories with High Content of Alumina," Ogne pory, 16, 272-280 (1951).

14. E. D. Miller and B. Davies, "Modulus of Rupture of Alumina-Silica Refractories at Elevated Temperatures," Am. Ceram. Soc. Bull, 45, 710 (1966).

15. M. Palfreyman, "Hot Strength of High-Alumina Refractories," Am. Ceram. Soc. Bull., 49, 638-642 (1970).

16. E. I. Greaves, "Modulus of Rupture of High-Alumina Refractories at Elevated Temperatures and Their Performance in Arc-Furnace Roofs," Trans. Brit. Ceram. Soc., 68, 15-20 (1969).

17. H. F. Folk and W. C. Bohling, "High Temperature Strength of High Alumina Refractories," Am. Ceram. Soc. Bull., 47, 580-583 (1968).

18. G. C. Padgett and J. F. Clements, "High Temperature Stress-Strain Behavior of Commercial Ceramics," Proc. Brit. Ceram. Soc., No. 15, 61-68, Jan. 1970.

19. T. B. Shaffer, Materials Index I, 407-408, Plenum Press, New York, 1964.

20. A. G. Crouch and K. H. Jolliffe, "The Effect of Stress Rate on the Rupture Strength of Alumina and Mullite Refractories," Proc. Brit. Ceram. Soc., No. 15, 37-46, Jan. 1970.

21. S. P. Chaudhuri and M. K. Chatterjee, "Studies on Thermal-Shock Resistance of Alumino-Silicate Refractories in Relation to Strength, Thermal Expansion and Modular of Elasticity," Trans. Indian Ceram. Soc., 27 63-68 (1968).

22. S. P. Chaudhuri and M. K. Chatterjee, "Spalling Characteristics of Alumino-Silicate Refractories in Relation to Their Chemical and Mineralogical Composition," Trans. Indian Ceram. Soc., Vol. 28, 44-51, (1969).

23. J. F. Clements and J. Vyse, "Creep Measurements on Some High-Alumina Refractories," Trans. Brit. Ceram. Soc., 65, 58-89 (1966).

24. V. L. Burdick and D. E. Day, "Creep of High-Alumina Refractories," Am. Ceram. Soc. Bull., 49, 638-642 (1970).

25. J. R. Kreglo and W. J. Smothers, "Creep Characteristics of Selected High Alumina Brick," J. Metals, 19, 20-22 (1967).

26. L. E. Mong, "Elastic Behavior and Creep of Refractory Brick Under Tensile and Compressive Loads," J. Am. Ceram. Soc., 30, 69-78 (1947).

27. Y. Letort, "The Creep of Aluminous Refractory Products at High Temperatures," Refractories, J., 30, 240-243 (1954).

28. J. Mackenzie, "The Abrasion Resistance of Refractory Bricks," Trans. Brit. Ceram. Soc., 50, 145-171 (1951).

29. T. E. Campbell, High-Temperature Technology, Wiley, N.Y., 1956.

30. R. Penty, "Pressure-Sintering Kinetics and Mechanical Properties of High-Purity, Fine-Grained Mullite," (Ph.D. Thesis), Lehigh University, 1972.

31. K. S. Mazdiyasni and L. M. Brown, "Synthesis and Mechanical Properties of Stoichiometric Aluminum Silicate (Mullite)," J. Am. Ceram.

Soc., 55, 548-552 (1972).

32. P. A. Lessing, R. S. Gordon and K. S. Mazdiyasni, "Creep of Polycrystalline Mullite," J. Am. Ceram. Soc., 58, 149 (1975).

33. J. A. Pask, R. B. Langston, P. C. Dokko and M. D. Sacks, "Structure, Strength, and Corrosive Resistance of Alumino-Silicate Materials," Department of Materials Science and Mineral Engineering, University of California, Berkeley, (1976).

34. W. H. Hawkes, "The Production of Synthetic Mullite," Trans. Brit. Ceram. Soc., 61, 689-703, (1962).

35. A. R. Rossini, S. C. Arazi, and T. G. Krenkel, "Mullitization of Mixtures of Kaolinitic Clay and Aluminum Hydroxide," Bol. Soc. Espan. Ceram., 9, 579-591 (1970).

36. N. B. Chatterjee and B. N. Panti, "Mullite Refractories from Clay-Bauxite or Quartz-Bauxite Mixes," Trans. Indian Ceram. Soc., 24, 116-121 (1965).

37. B. P. Locsei, "Possible Technical Developments in the Manufacture of Fireclay Refractory Materials: III, Mechanism of the Synthesis of Mullite in the System Kaolinite-Aluminum Fluoride," Keram. Z., 20, 362-367 (1968).

38. H. P. Rooksby and J. H. Partridge, "An X-ray Study of Natural and Artificial Mullite," J. Soc. Glass Tech., 23, 338-346 (1939).

39. P. P. Budnikov, T. N. Keshishyan and A. V. Volkova, "Kinetics of Mullite Formation from Technical Aluminum Oxide and Silica," Zh. Priklad. Khim., 35, 1171 (1962).

40. E. B. Kroll and D. N. Poluboiarinov, "Investigation of the Sintering of Mullite Ceramics Synthesized from Commercially Pure

Materials," Tr. Gos. Nauchn.-Issled. Inst. Stroit. Keram., 24, 105 (1964).

41. L. B. Pankratz, W. W. Weller and K. K. Kelly, "Low Temperature Heat Content of Mullite," U. S. Bur. of Mines Rep. Invest. 6287, 1963.

42. F. M. Wahl, R. E. Grim and R. B. Graf , "Phase Transformations in Silica-Alumina Mixtures as Examined by Continous X-ray Diffraction," Am. Mineralogist, 46, 1064 (1961).

43. B. P. Locsei, "The Kinetics of Mullite Formation in the System Aluminum Fluoride-Silica, II," Interceram, 17, 27-29, 145-148 (1968).

44. A. I. Avgustinik, M. F. Nazarenko and V. A. Sviridenko, "The Effect of Valence and Radius of the Citron of Mineralizers on the Process of Mullitization," Zh. Priklad. Khim., 27, 782 (1954).

45. A. I. Avgustinik and I. P. Adamashvilli, "Mineralizing Action of Titanium Dioxide on Mullitization of Ceramic-Stone Bodies," Izv. Vyssh. Ucheb. Zaved. Khim. Tekhnol., 13, 400-402 (1970).

46. T. C. Shutt, "Influence of Fluorides on the Formation of Mullite in Kaolin," J. Can. Ceram. Soc., 37, 33-38,(1968).

47. K. G. Skinner, W. H. Cook, R. A. Potter and H. P. Palmour, III, "Effect of TiO_2, Fe_2O_3 and Alkali on Mineralogical and Physical Properties of Mullite Type and Mullite Forming Al_2O_3-SiO_2 Mixtures: I," J. Am. Ceram. Soc., 36, 349-356 (1953).

48. P. P. Budnikov, T. N. Kreshishyan and A. V. Volkova, "Effect of Small Additions on Mullite Formations at Low Temperatures," Silikaty Okisly Khim. Vys. Temp., 233 (1963).

49. P. P. Budnikov, and K. M. Shmukler, "Effect of Mineralizers on the Process of Mullitization of Clays, Kaolins, and Synthetic Masses,"

Zh. Priklad. Khim., 19, 1029 (1946).

50. S. P. Chaudhuri, "X-ray Study of Induced Mullitization of Clay," Trans. Indian Ceram. Soc., 28, 24-30 (1969).

51. J. Grofcsik and F. Tamas, Mullite, Its Structure, Formation and Significance, Publishing House of the Hungarian Academy of Sciences, Budapest, 1961.

52. H. M. Kraner, "Considerations in the Production of Fused Mullite Refractories," J. Am. Ceram. Soc., 21, 360 (1938).

53. V. R. Palmeri, "Mullite Formation by Decomposition of Kaolinite," J. Soc. Glass Tech., 36, 25-28 (1952).

54. C. W. Parmelee and A. R. Rodrigues, "Catalytic Mullitization of Kaolinite by Metallic Oxide," J. Am. Ceram. Soc., 25, 1-10, (1942).

55. S. F. Rustambekyan and N. V. Solomin, "Investigating the Phase Composition of Fused High-Alumina (Mullite) Refractories," Ogneupory, 2, 28 (1965).

56. J. L. McAtee and W. O. Milligan, "X-ray Diffraction Examination of Synthetic Mullite," Texas J. Sci., 2, 200 (1950).

57. J. Grofcsik and E. Vago, "Modern Methods of Clay Investigation," Epitoanyag, 4, 3 (1952).

58. R. Roy, "Aids in Hydrothermal Investigation II: Methods of Making Mixtures for Both 'Dry' and 'Wet' Phase Equilibrium Studies," J. Am. Ceram. Soc., 39, 145 (1956).

59. J. D. Crofts and W. W. Marshall, "A Novel Synthesis of Alumino-Silicates and Similar Materials," Trans. Brit. Ceram. Soc., 66, 121 (1967).

60. T. D. McGee and C. D. Wirkus, "Mullitization of Alumino-Silicates Gels," ERI 87400 Preprint Project 345, Iowa State University, Ames, Iowa, 1970.

61. H. Yamada and S. Kimura, "Studies on the Nature of the Mullite from Coprecipitate of Alumina and Silica Gels," J. Ceram. Assoc. Japan, 70, 237-243 (1962).

62. J. P. Bidet and C. A. Jouenne, "Contribution a l'Etude des Reactions de la Kaolinite sous l'Effect de la Temperature," Bull. Soc. Fr. Ceram. 39, 43 (1958).

63. B. B. Ghate, "Synthesis and Pressure-Sintering Kinetics of High-Purity, Fine-Grained Mullite," (Ph.D. Thesis) Lehigh University, 1972.

64. J. C. Williams, W. R. Sinclair and S. E. Koona, "Preparation of Thin Mullite Films," J. Am. Ceram. Soc., 55, 548-552 (1972).

65. S. Otani and A. Kojima, "Thermal Transformation of SiO_2-Al_2O_3 Gels Prepared from Methysiloxyaluminum Compounds," Kogyo Kagaku Zasshi, 67, 1509-1512 (1964).

66. J. E. Fenstermacher and F. A. Hummel, "High-Temperature Mechanical Properties of Ceramic Materials: IV, Sintered Mullite Bodies," J. Am. Ceram. Soc., 44, 284-289 (1961).

67. V. F. Draper, "Mullite Phase Equilibria in the System: CaO-Al_2O_3-SiO_2," (M.S. Thesis), University of California at Berkeley, 1976.

68. W. J. Frey and J. D. Mackenzie, "Mechanical Properties of Selected Glass-Crystal Composites," J. of Materials Science, 2, 124-130 (1967).

69. R. W. Davidge and T. J. Green, "The Strength of Two-Phase Ceramic/Glass Materials," J. of Materials Science, 3, 629-634 (1968).

70. D. P. H. Hasselman and R. M. Fulrath, "Micromechanical Stress Concentrations in Two-Phase Brittle-Matrix Ceramic Composites," J. Am. Ceram. Soc., 50, 399-403 (1967).

71. J. Selsing, "Internal Stresses in Ceramics," J. Am. Ceram. Soc., 44, 449, (1961).

72. D. Weyl, "Influence of Internal Strains on Texture and Mechanical Strength of Porcelains," Ber. Deut. Keram. Ges., 36, 24 (1959).

73. M. A. Stett and R. M. Fulrath, "Mechanical Properties and Fracture Behavior of Chemically Bonded Composites," J. Am. Ceram. Soc., 53, 5-13 (1970).

74. D. P. H. Hasselman and R. M. Fulrath, "Proposed Fracture Theory of a Dispersion-Strengthened Glass Matrix," J. Am. Ceram. Soc., 49, 68-72 (1966).

75. A. H. Heuer and J. P. Roberts, "The Influence of Annealing on the Strength of Corundum Crystals," Proc. Brit. Ceram. Soc., No. 6, 17-28 (1966).

76. L. M. Davies, "The Effect of Heat Treatment on the Tensile Strength of Sapphire," Proc. Brit. Ceram. Soc., No. 6 29-36 (1966).

77. R. F. Davis, I. A. Aksay and J. A. Pask, "Decomposition of Mullite," J. Am. Ceram. Soc., 55 98-101 (1972).

78. V. Skola, "Thermal Decomposition of the Mullite Phase," Keram. Rundsch. Kunst.-Keram., 45, 188-215 (1937).

79. D. Turnbull, "Theory of Grain Boundary Migration Rates," Trans. AIME, 191, 661-665 (1951).

80. W. Von Lohre and H. Urban, "Contribution to the Morphology of Mullite," Ber. Deut. Keram. Ges., 37, 249-251 (1960).

81. J. E. Burke, "Grain Growth," Report No. 67-C-046, G. E. Research Laboratory, Schectady, NY (1967).

82. R. L. Coble and J. E. Burke, "Sintering in Ceramics," in Progress in Ceramic Science ed. by J. E. Burke, Vol. 3, 197-252, Permagom Press, Ltd., (1963).

83. H. Cahoon and C. Christensen, "Sintering and Grain Growth of Alpha-Alumina," J. Am. Ceram. Soc., 39, 337-344 (1956).

84. L. L. Siegle and A. L. Pranatis, Conference on Powder Metallurgy in Nuclear Engineering, Amer. Soc. Metals, Cleveland Ohio (1958).

85. C. Smith, "Grains, Phases and Interfaces: An Interpretation of Microstructure, Trans. AIME, 175, 15-51 (1949).

ACKNOWLEDGMENT

It is a pleasure to express my appreciation to Professor Joseph A. Pask for providing excellent guidance, encouraging my efforts, and being available for countless hours of helpful discussions.

Interaction with colleagues and friends, particularly David N. K. Wang and Victor F. Draper, greatly assisted the completion of this work. I would also like to thank Professors Richard M. Fulrath and James W. Evans for their time and effort in critically reading and commenting on the thesis.

The technical assistance of the support staff of the Materials and Molecular Research Division, Lawrence Berkeley Laboratory was greatfully appreciated. Special thanks are extended to Gay Brazil (manuscript preparation), Rich Lindberg (SEM and electron microprobe assistance), Gloria Pelatowski (technical drawings), Lee Johnson (optical microscopy assistance), Glenn Baum and Jack Wodei (equipment maintenance), and James Maccoun and Joyce Mori (laboratory assistance).

Thanks are also due Kaiser Center for Technology, Pleasanton, CA (supplying commercial refractories and performing the fluorescence analyses) and Matrecon, Inc., Oakland, CA (use of Scott Tester for MOR tests).

This work was supported by the National Science Foundation and the US Energy Research and Development Administration, Division of Physical Research.

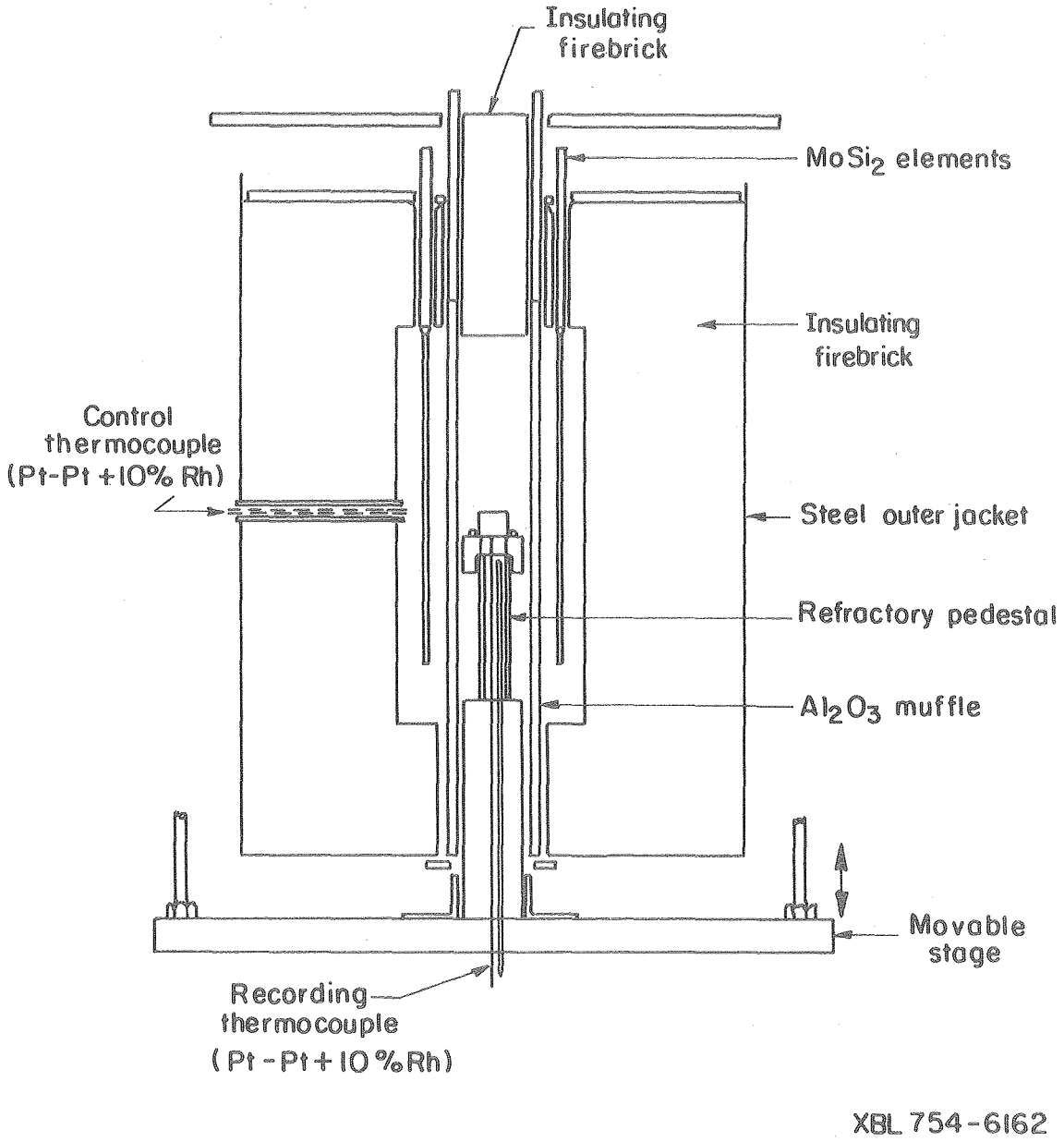

Fig. 1. Schematic diagram of quench-type furnace.

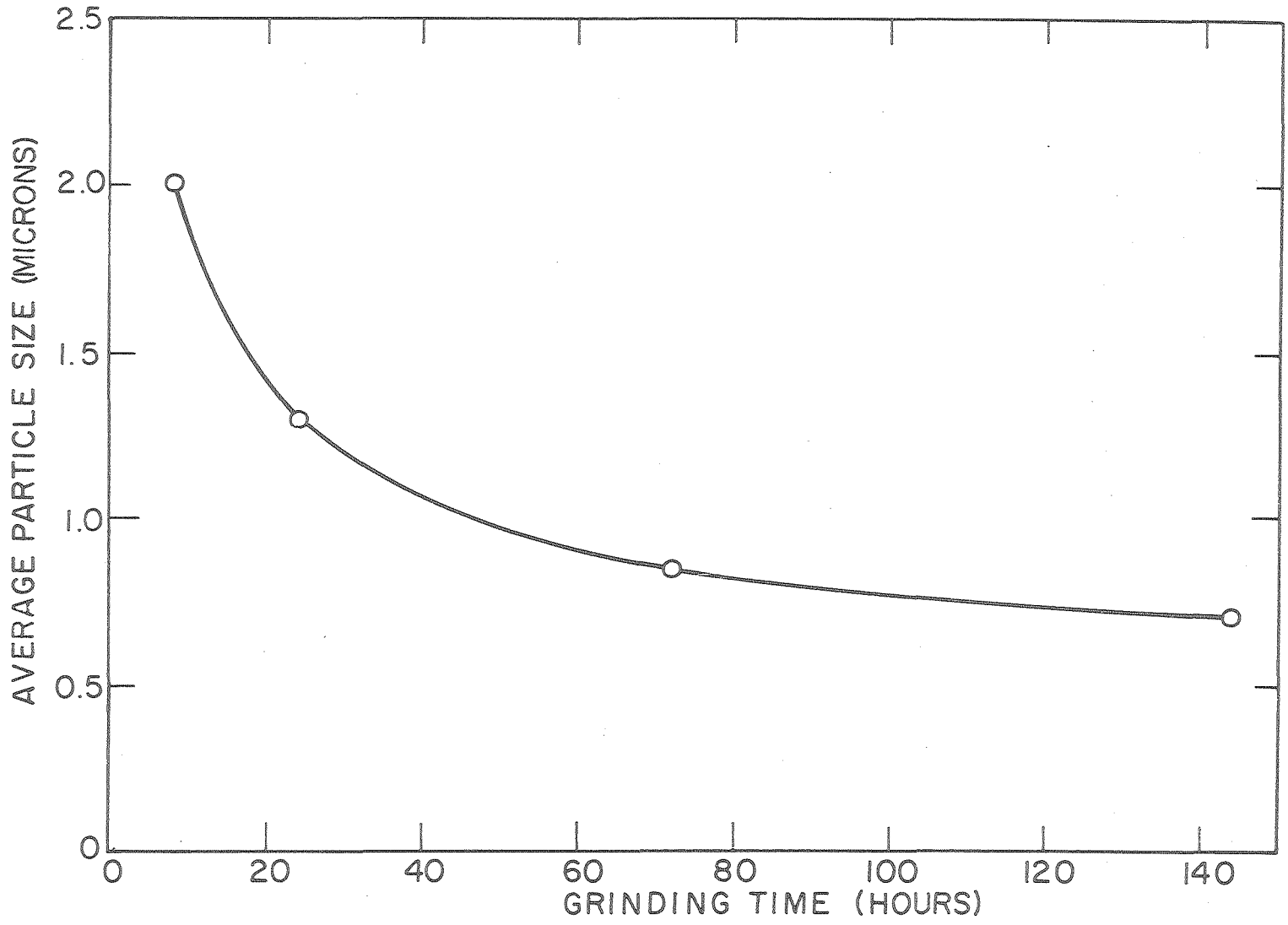

XBL 769-7562

Fig. 2. Relationship between average particle size and grinding time for mullite powders ground with alumina and flint media.

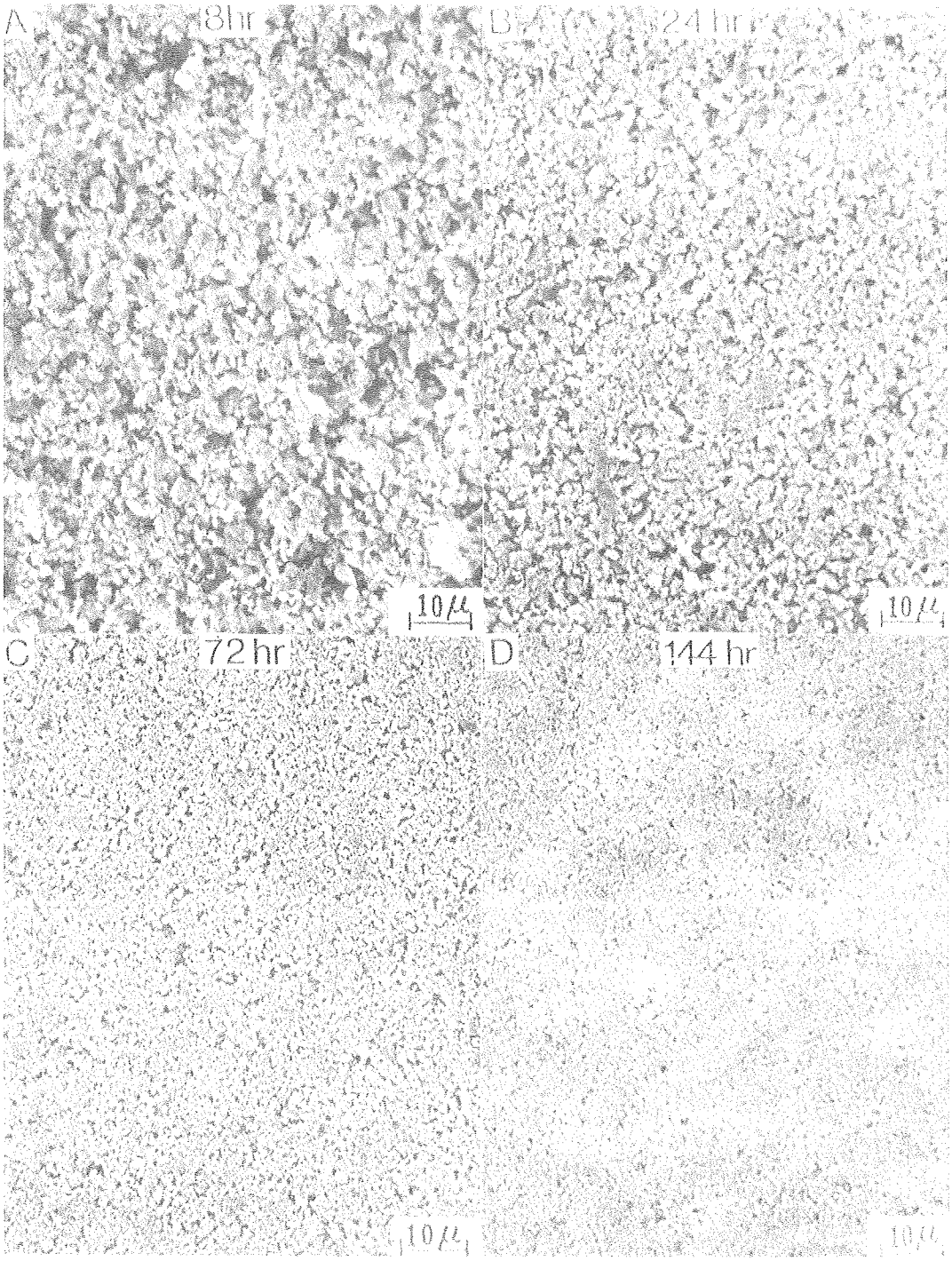

XBB760-10593

Fig. 3. Pressed surfaces of green compacts of mullite powders ground for various times with alumina and flint media.

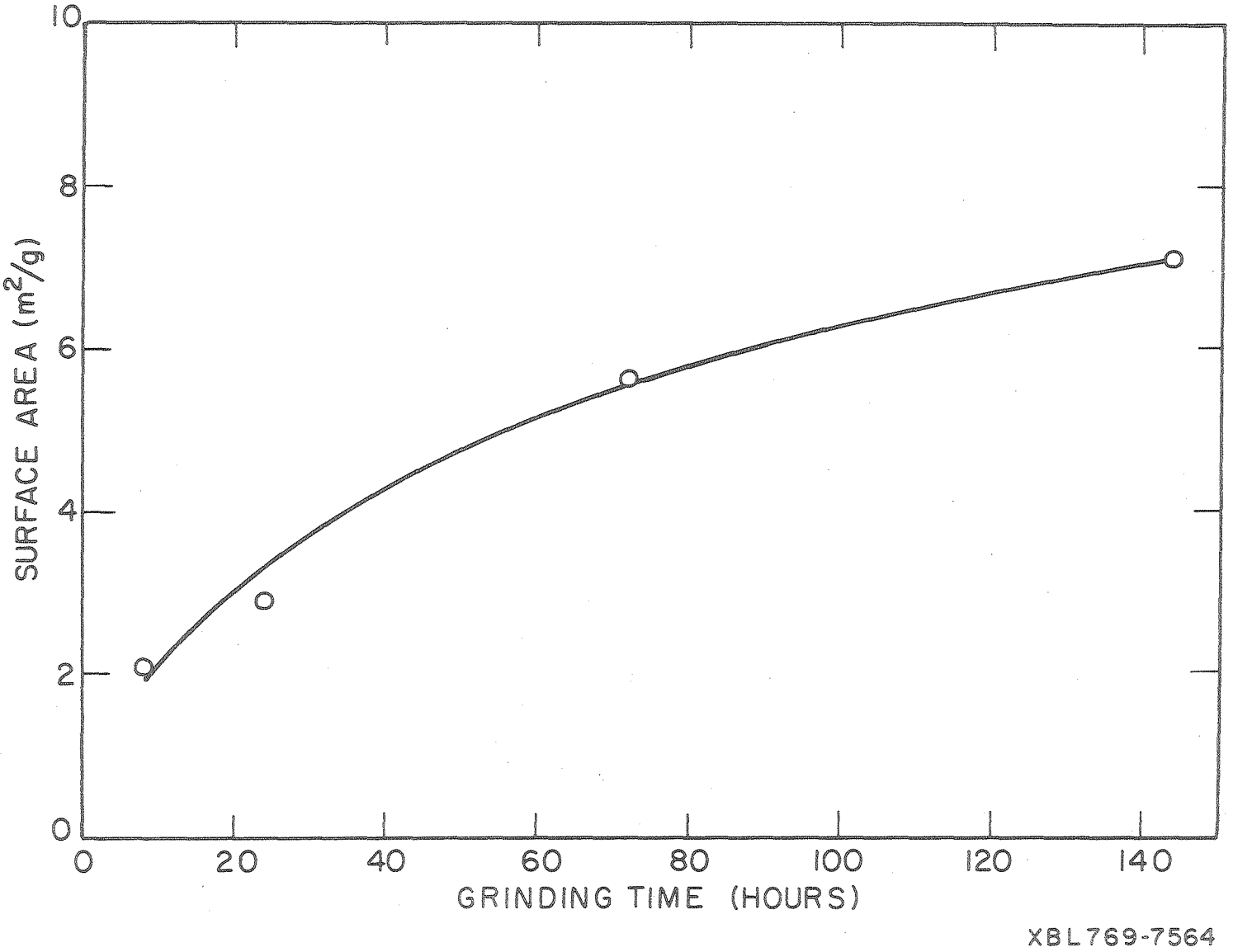

Fig. 4. Relationship between surface area and grinding time for mullite powders ground with alumina and flint media.

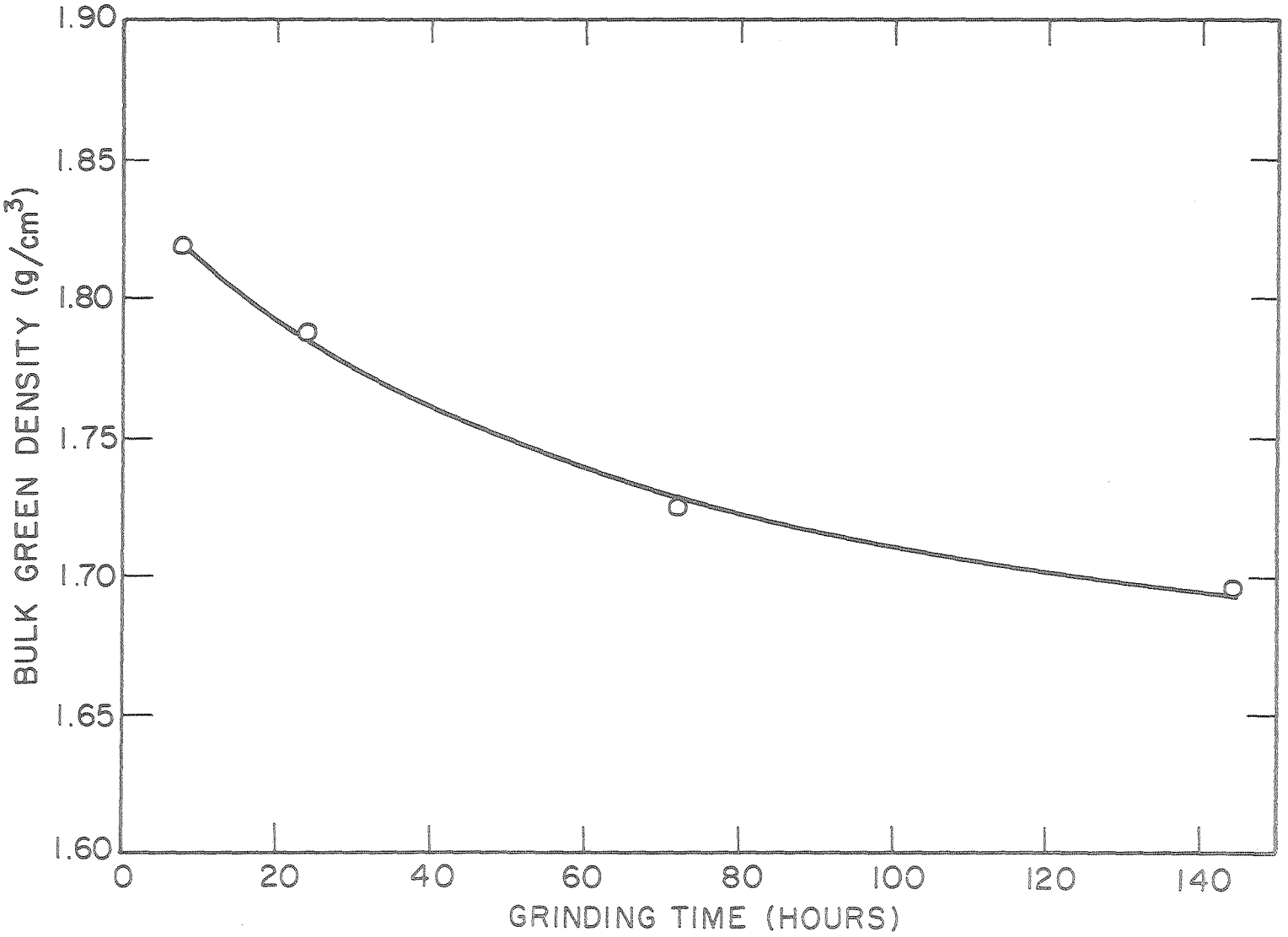

XBL 769-7567

Fig. 5. Relationship between green bulk density and grinding time for mullite powders ground with alumina and flint media and compacted uniaxially under 15000 psi.

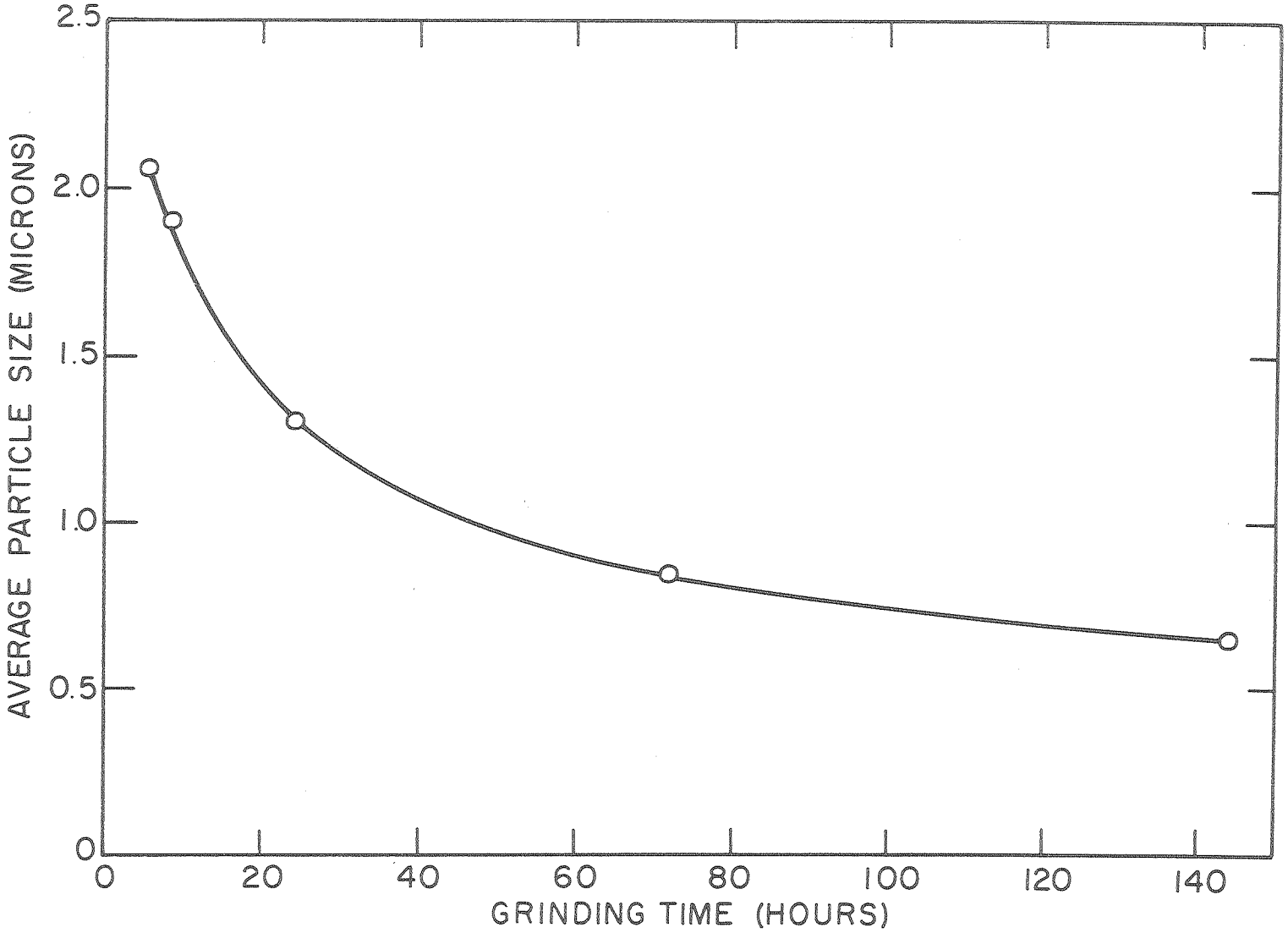

XBL 769-7563

Fig. 6. Relationship between average particle size and grinding time for mullite powders ground with alumina media only.

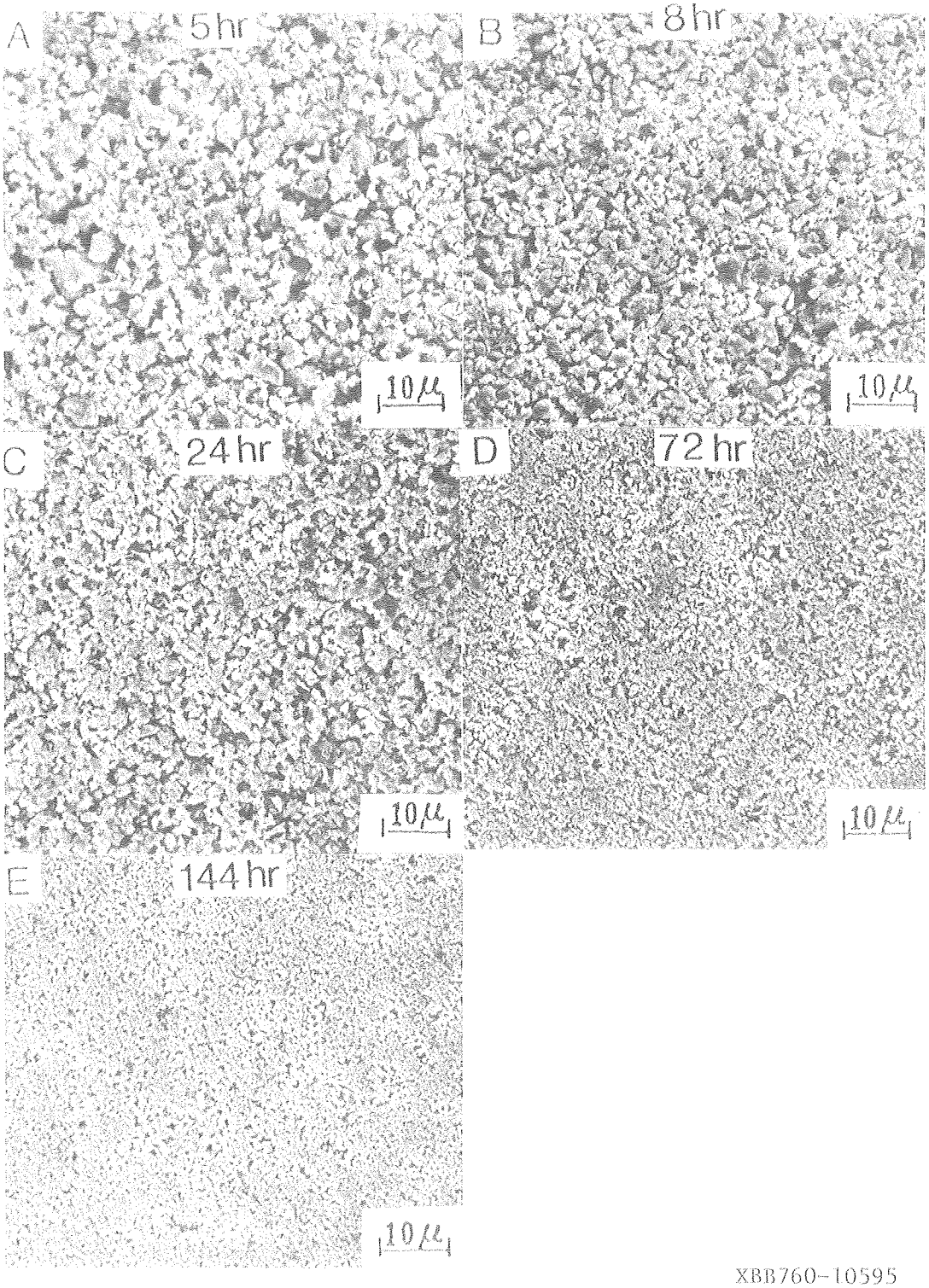

XBB760-10595

Fig. 7. Pressed surfaces of green compacts of mullite powders ground for various times with alumina media only.

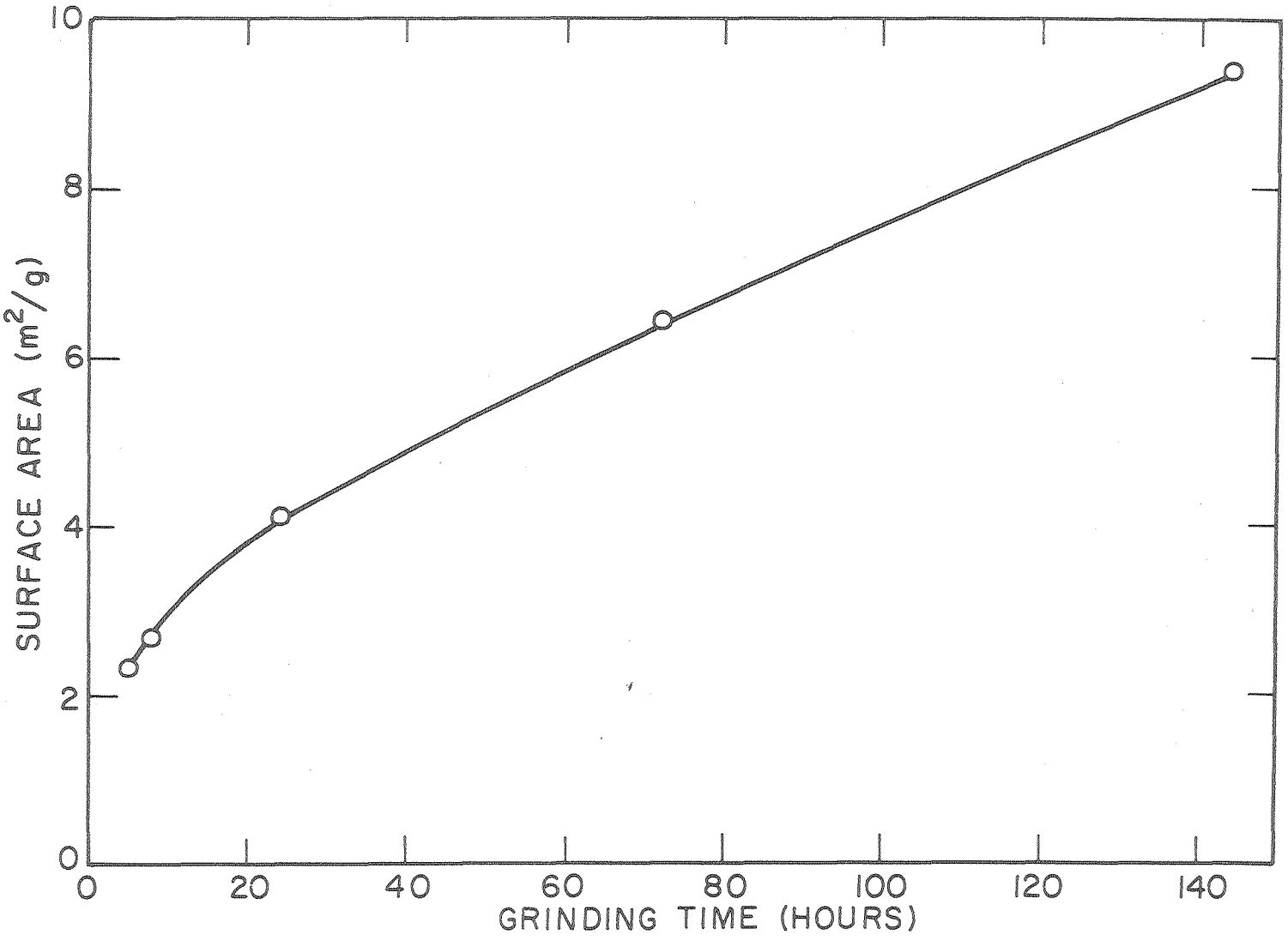

XBL 769-7565

Fig. 8. Relationship between surface area and grinding time for mullite powders ground with alumina media only.

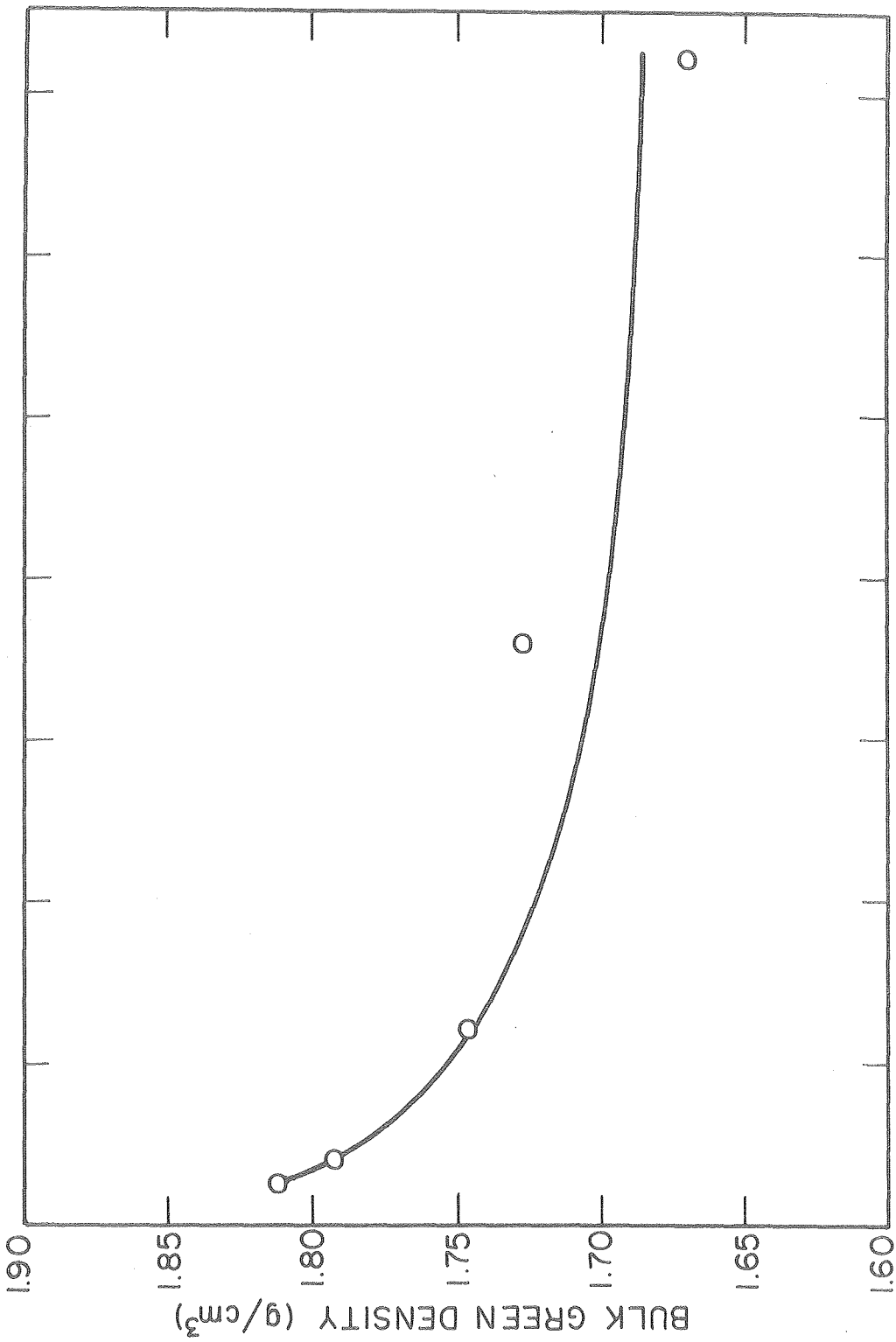

Fig. 9. Relationship between green bulk density and grinding time for mullite powders ground with alumina media only and compacted uniaxially under 15000 psi.

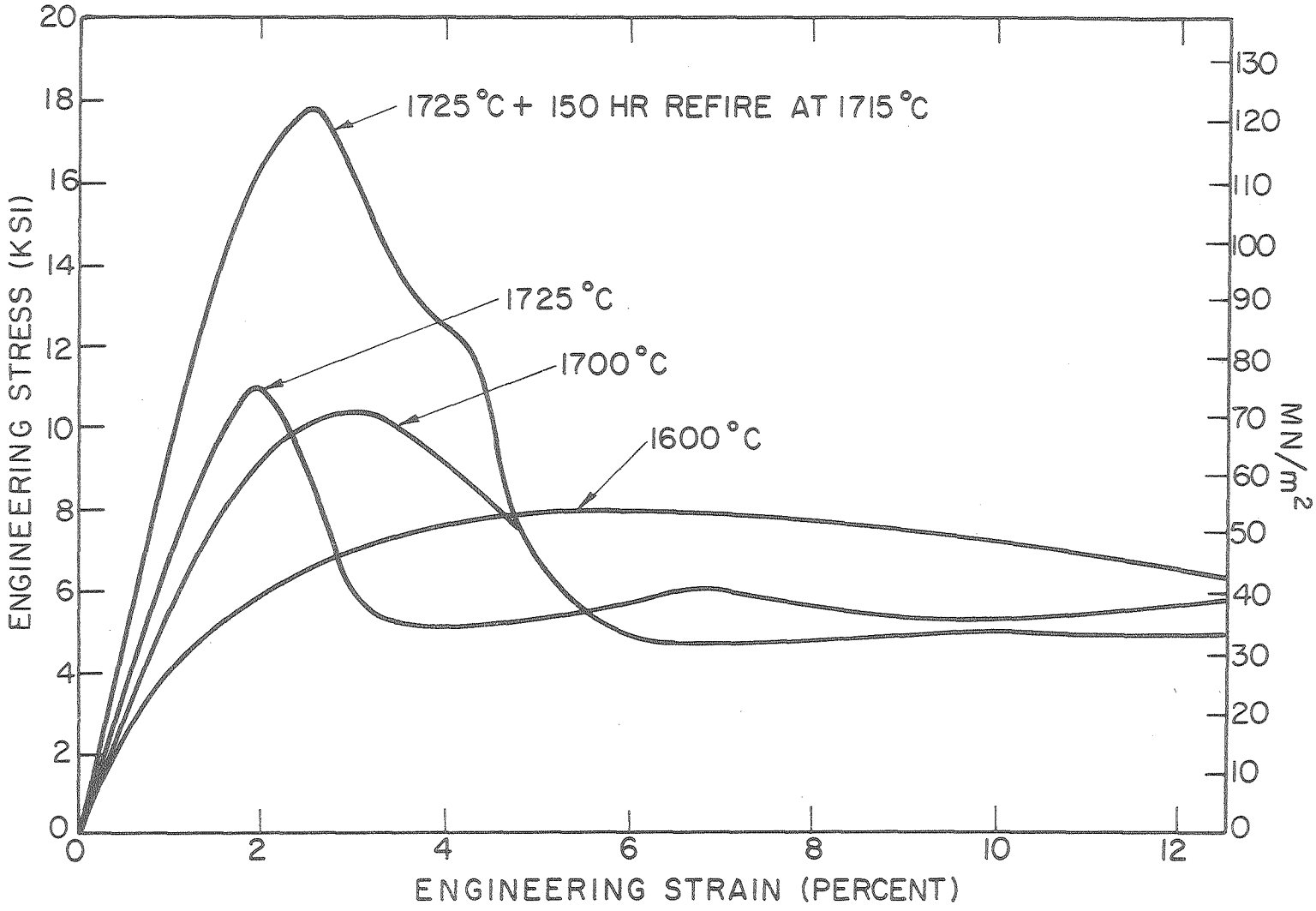

XBL 7610-7614

Fig. 10. Stress-strain behavior in compression at 1200°C for kaolin specimens fired under various conditions.

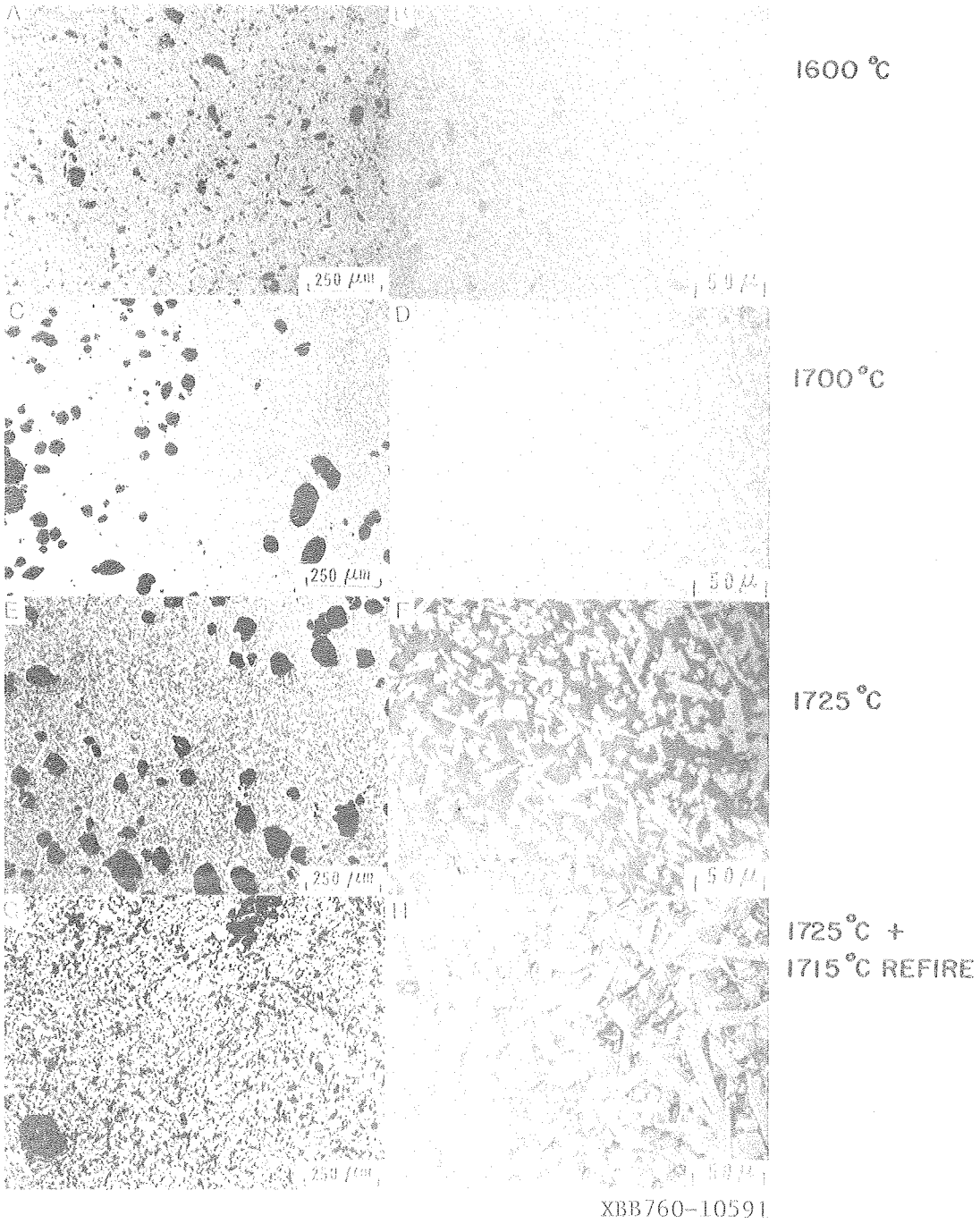

Fig. 11. Micrographs showing porosity (left side) and grain size (right side) effects with increasing heat treatment for kaolin samples.

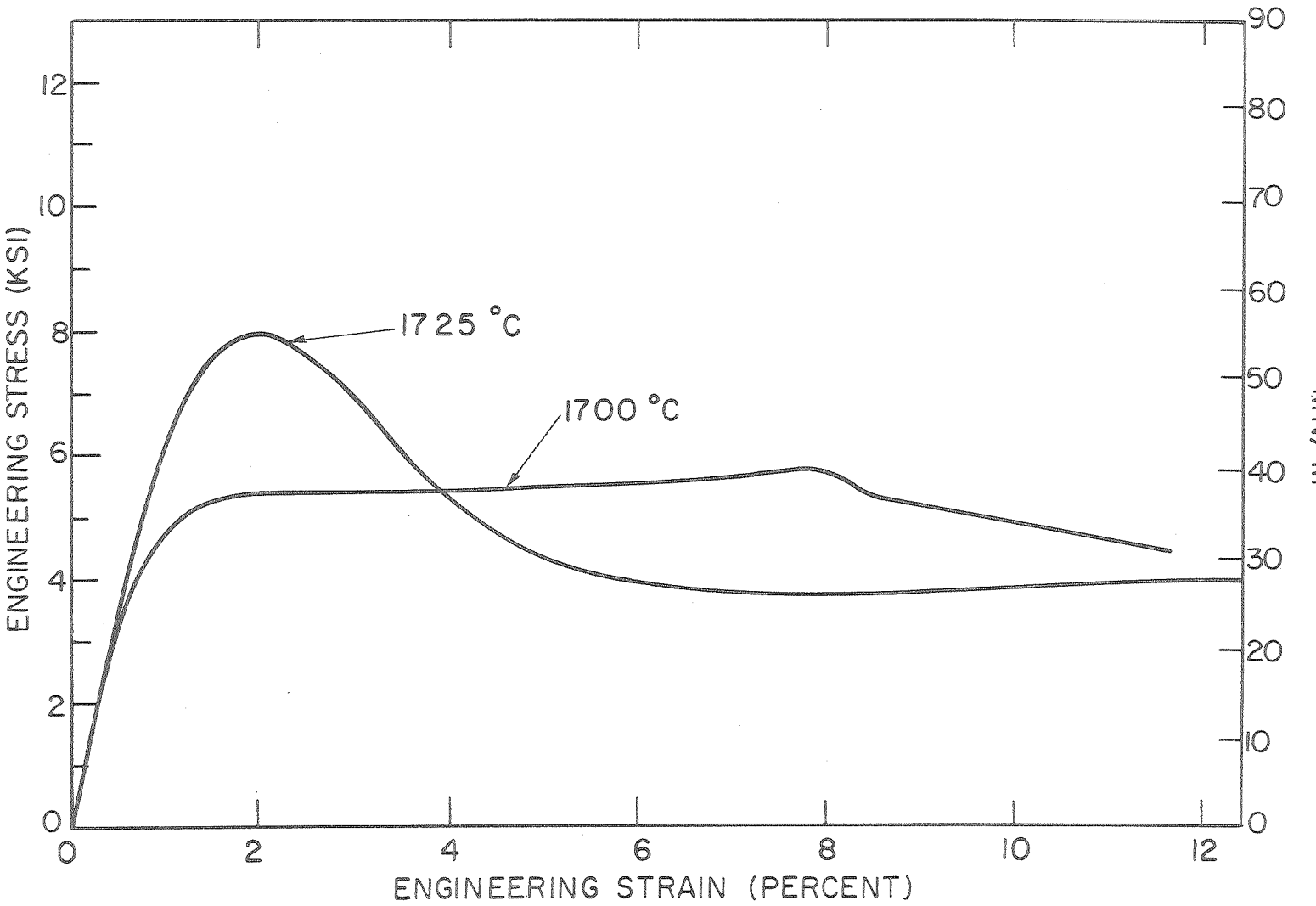

XBL 7610-7615

Fig. 12. Stress-strain behavior in compression at 1200°C for 45.9 wt% alumina/54.1 wt% silica compacts fired under different conditions.

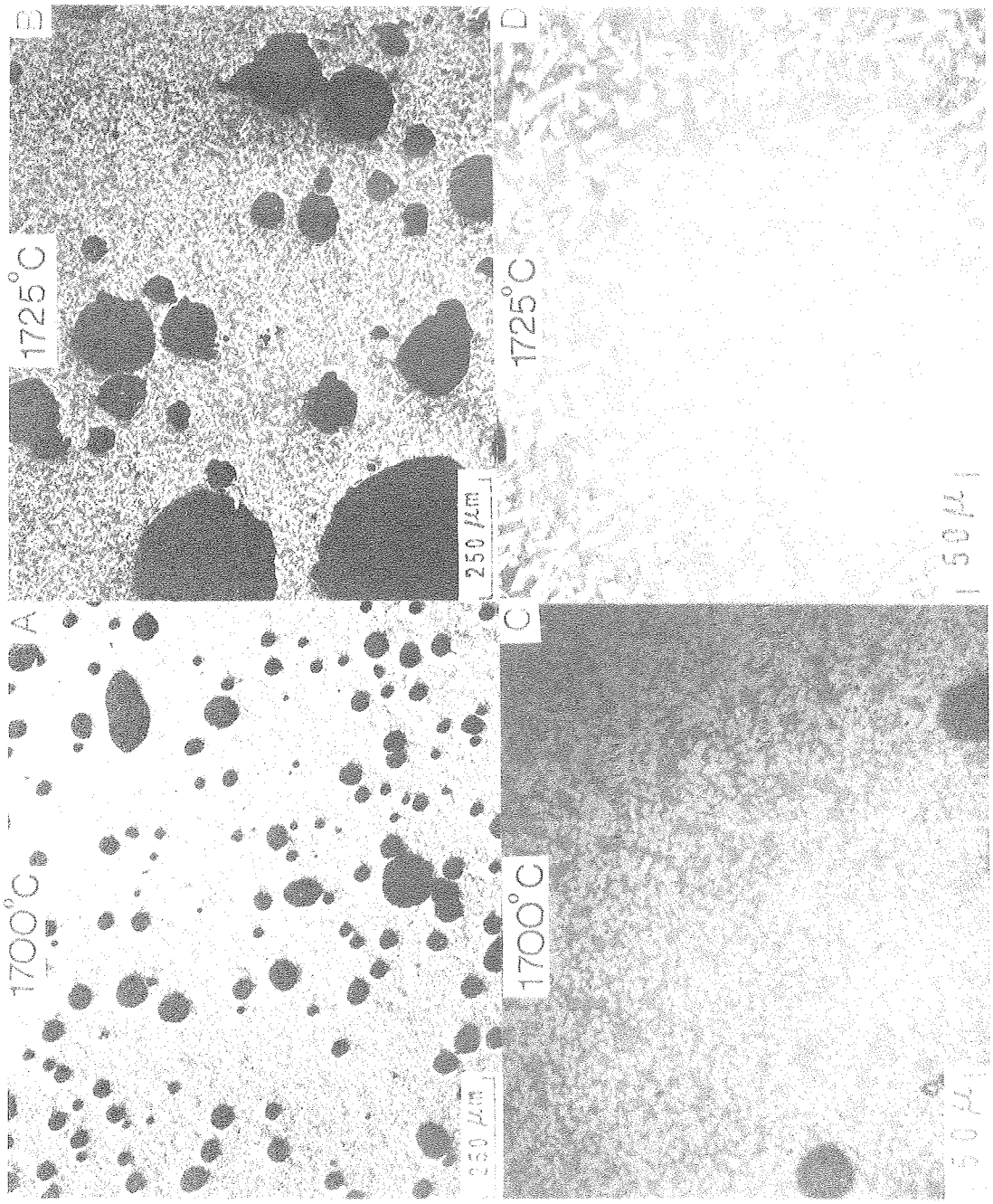

XBB760- 10574

Fig. 13. Micrographs illustrating porosity (top), grain size (bottom), and grain morphology (bottom) effects with increasing heat treatment for 45.9 wt% alumina/54.1 wt% silica samples.

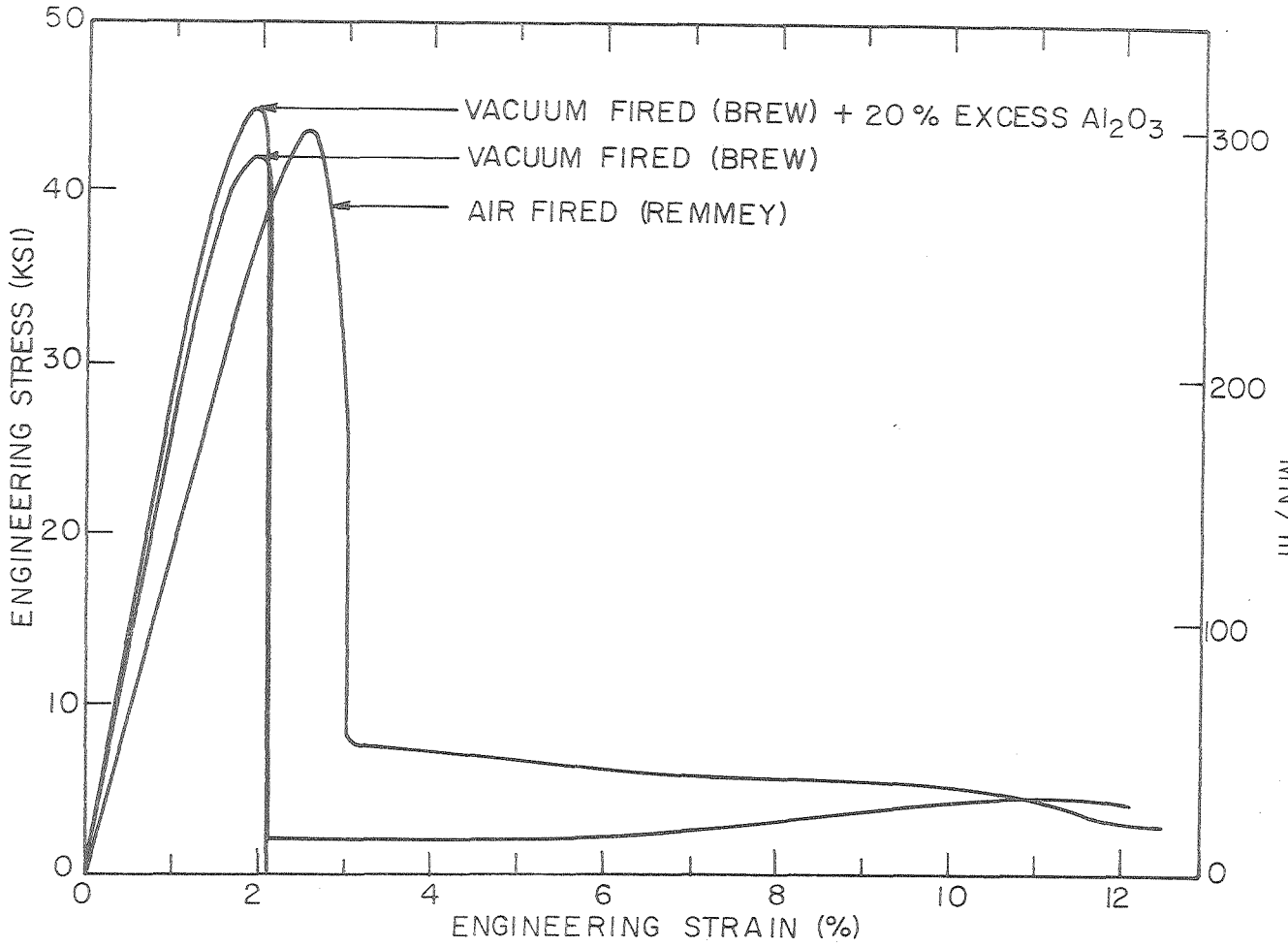

XBL7610-7623

Fig. 14. Stress-strain behavior in compression at 1200°C for kaolin/alumina compacts fired under various conditions at 1725°C. The degree of brittleness shown in the stress-strain curves is indicative of the amount of glass phase present. The sample with 20% excess Al_2O_3, with very little glass, fails catastrophically. The other samples with more glass, have viscous flow regions.

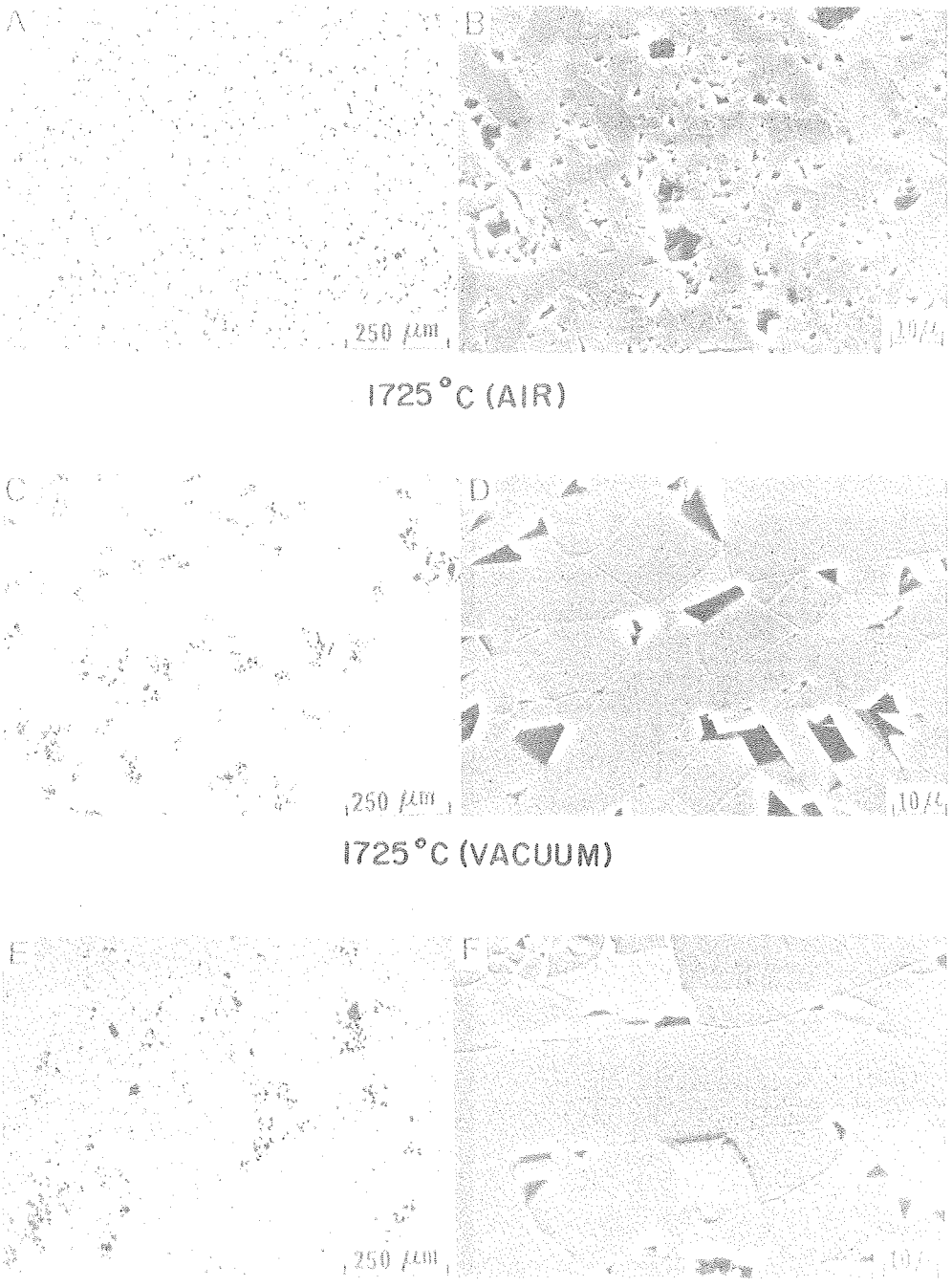

XBB760-10575

Fig. 15. Micrographs illustrating porosity (left side) and grain size (right side) effects for kaolin/alumina compacts fired under various conditions. 15D shows large areas between grains from which glass phase has been etched out (these are not the pores seen in 15C). 15F shows similar etched out areas, but they are smaller. 15B contains both pores (as seen in 15A) and small pockets between grains from which glass has been etched.

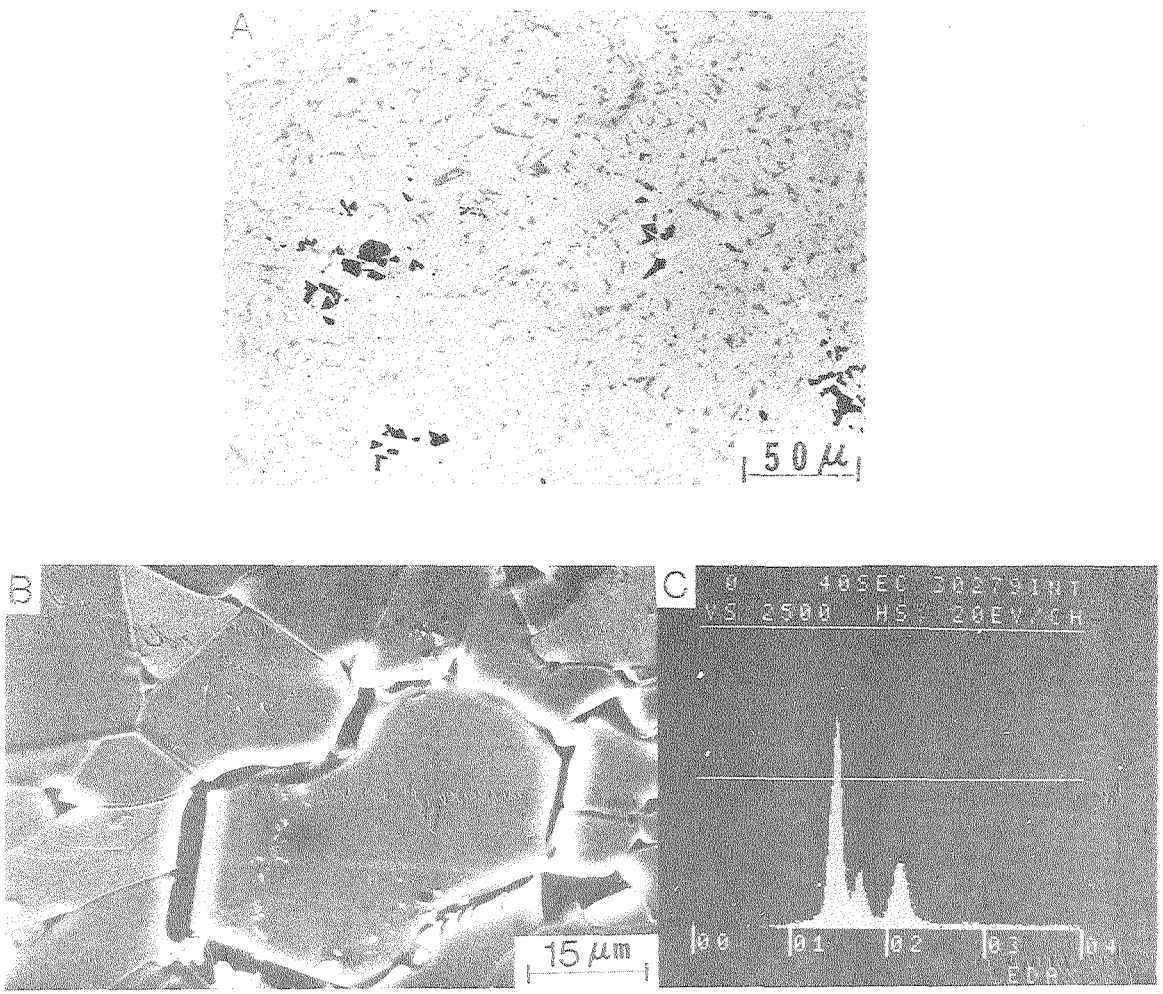

XBB760-10573

Fig. 16. A: Micrograph illustrating presence of glass phase (dark gray) due to incomplete reaction in kaolin/alumina compact of "stoichiometric" mullite composition.
B: Micrograph illustrating circumferential cracking around an alumina particle in a mullite matrix for a kaolin/alumina sample with excess alumina.
C: EDAX spectra for B; dotted spectrum is from an alumina particle; lined spectrum is from the mullite matrix.

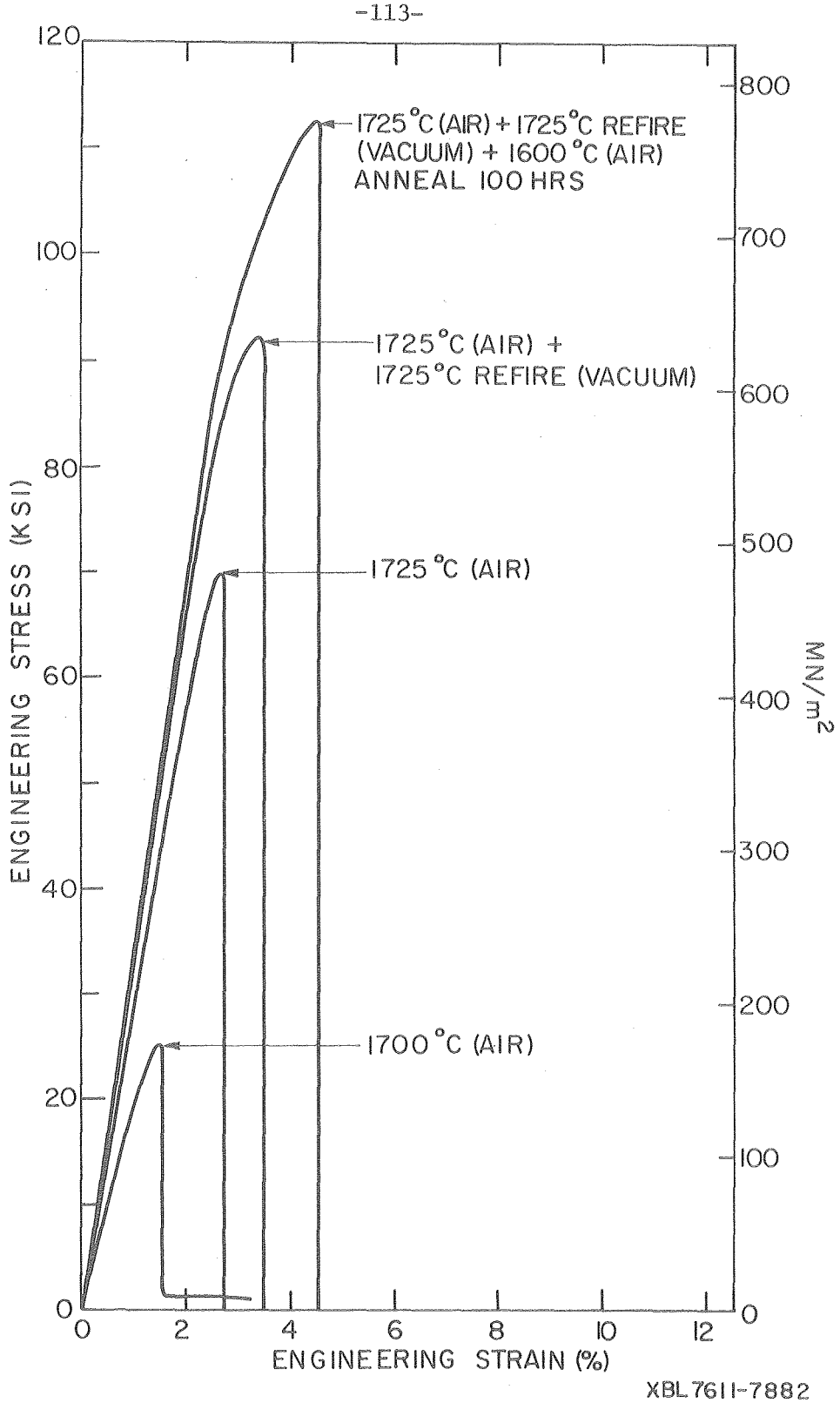

Fig. 17. Stress-strain behavior in compression at 1200°C for 71.8 wt% alumina/28.2 wt% silica compacts reaction sintered under various conditions.

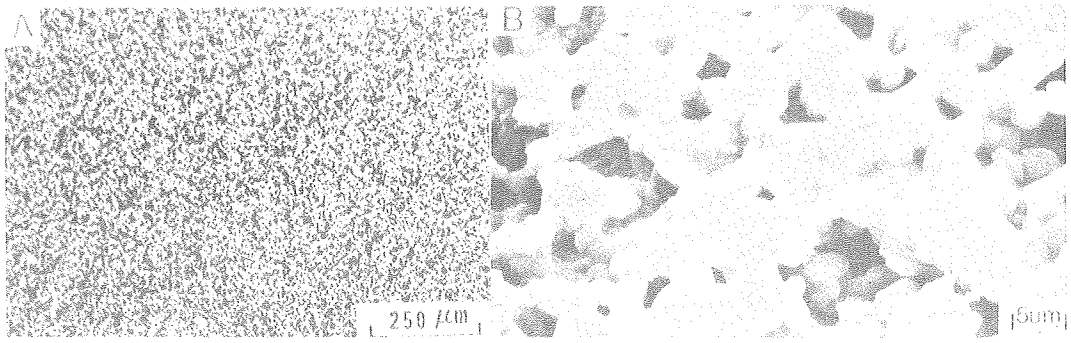

1700°C (AIR)

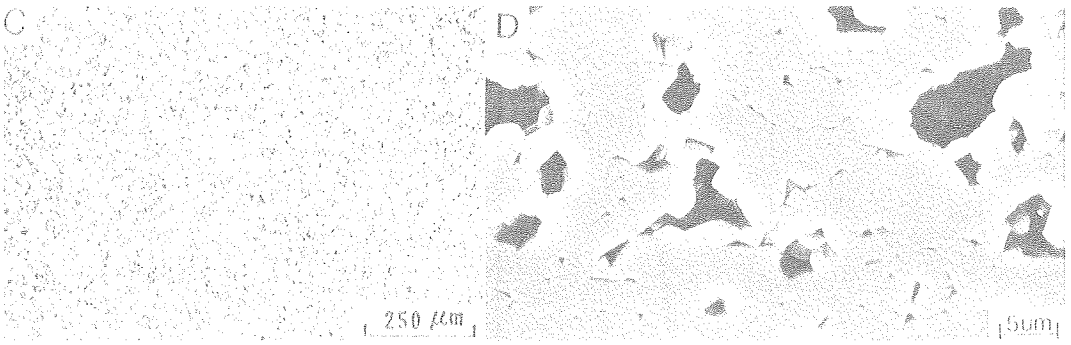

1725°C (AIR)

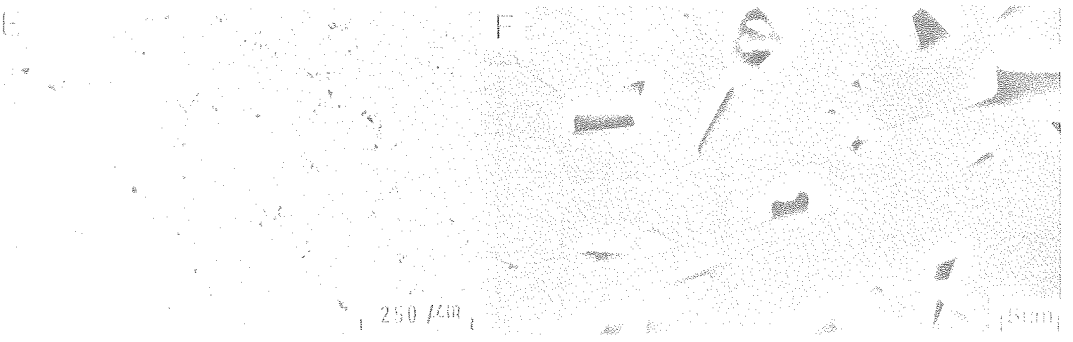

1725°C (AIR) + 1725°C (VACUUM) REFIRE

XBB760-10577

Fig. 18. Micrographs illustrating porosity (left side) and grain size and morphology (right side) effects with various sintering conditions for 71.8 wt% alumina/28.2 wt% silica samples.

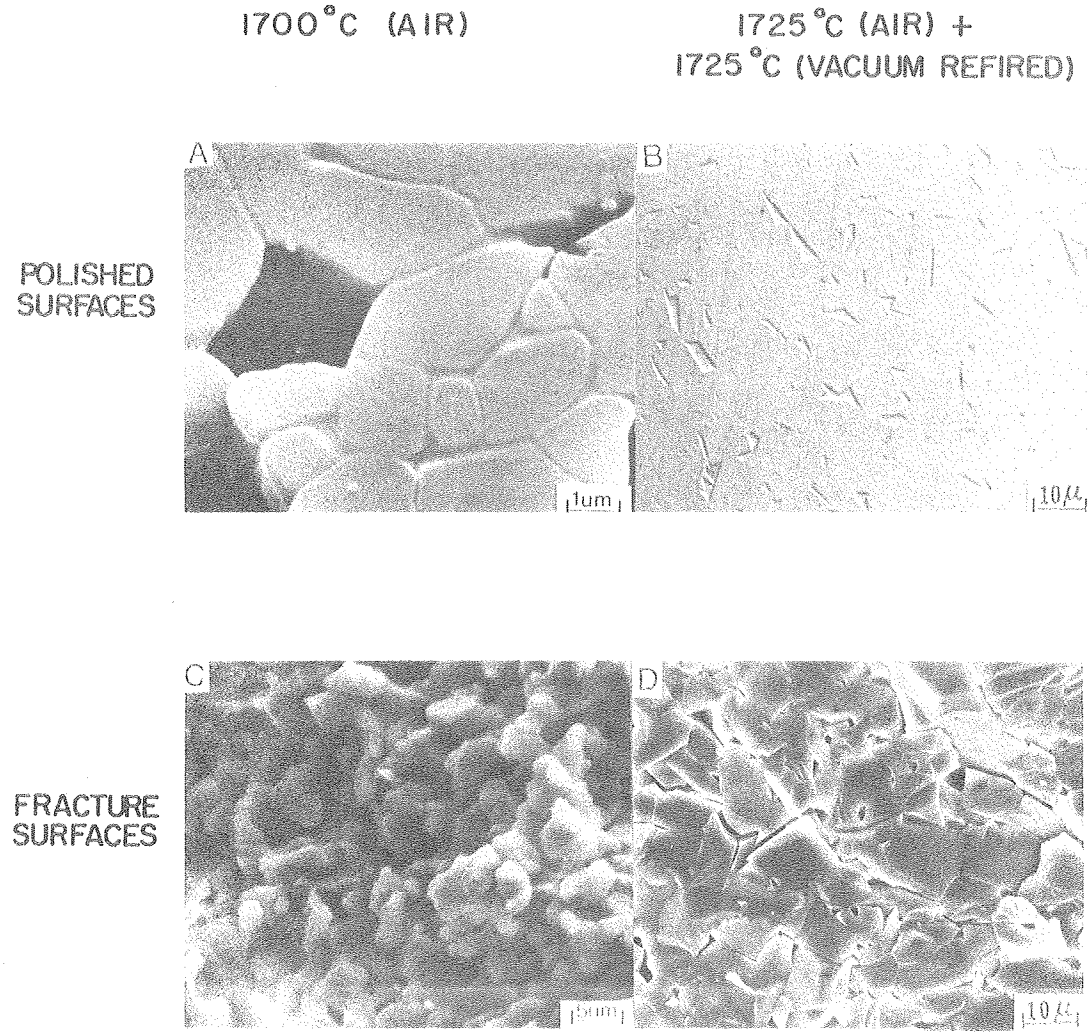

XBB771-78

Fig. 19. A: Polished surface of 71.8 wt% A-14/28.2 wt% silica flour reaction sintered (to ~1700°C in Remmey furnace) sample which shows that the glass phase is distributed almost as a continuous "film" around some of the mullite grains.

B: Polished surface of 71.8 wt% A-14/28.2 wt% silica flour reaction sintered (to ~1725°C in the Remmey furnace followed by 12 hrs at ~1725°C in the Brew furnace) sample which shows that the glass phase is isolated in angular "pockets".

C: Fracture surface of 1200°C compression tested sample A which shows intergranular fracture.

D: Fracture surface of 1200°C compression tested sample B which shows transgranular fracture.

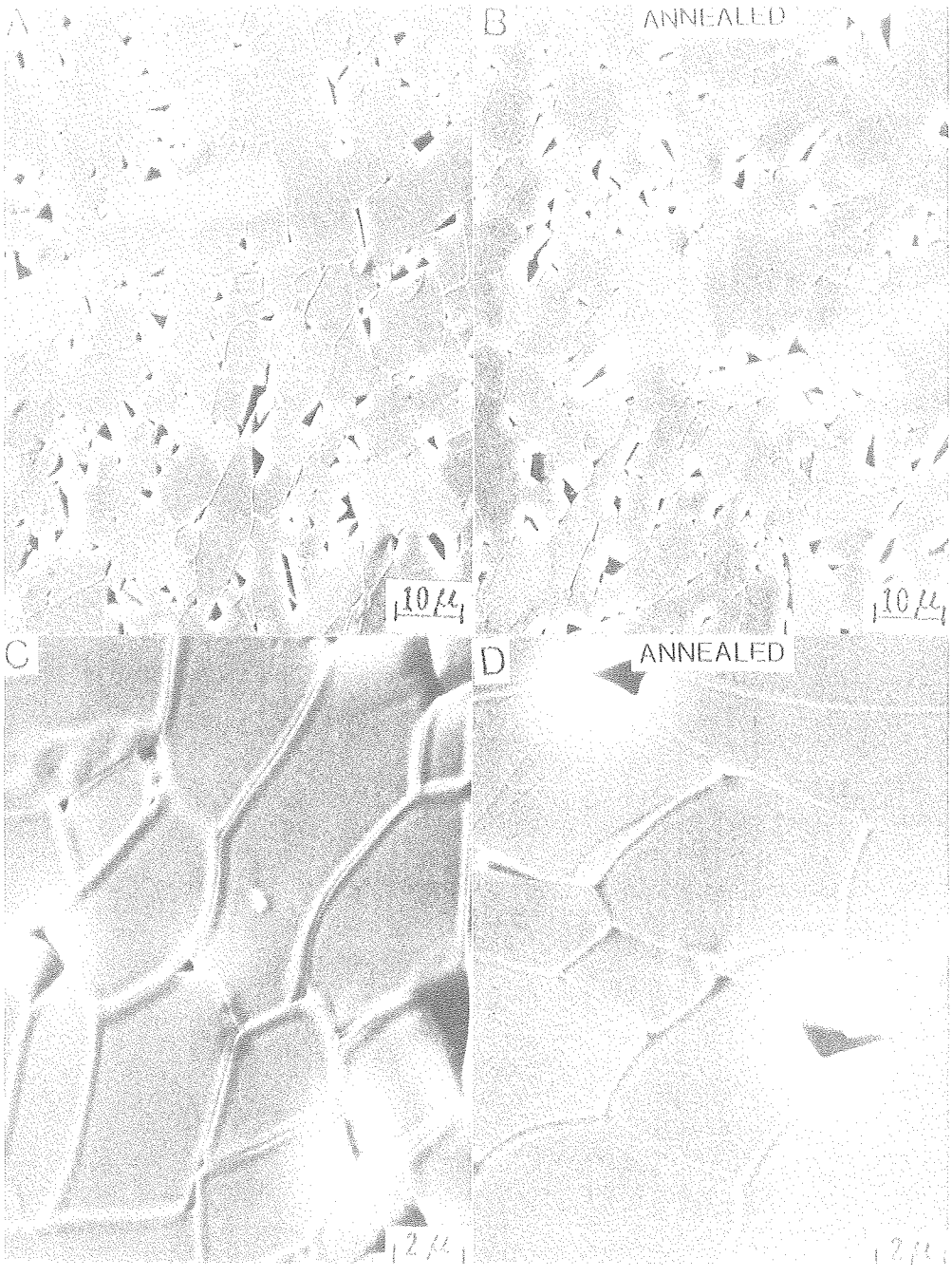

XBB771-81

Fig. 20. A: 71.8 wt% A-14/28.2 wt% silica flour compact fired to ~1725°C (Remmey), refired to ~1725°C for 12 hrs (Brew), and thermally etched in air.

B: 71.8 wt% A-14/28.2 wt% silica flour compact fired to ~1725°C (Remmey), refired to ~1725°C for 12 hrs (Brew), annealed at 1600°C for 100 hrs in air, and thermally etched in air.

C and D: Higher magnification of A and B, respectively, showing that grain boundary ridges do not occur in the annealed sample.

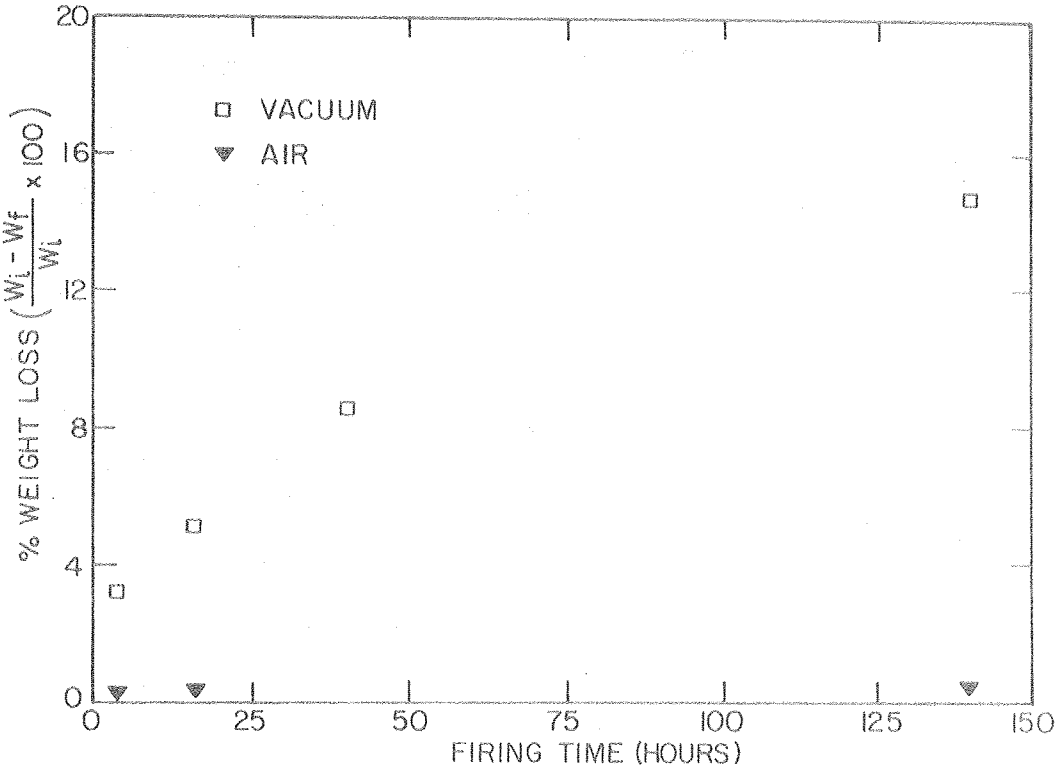

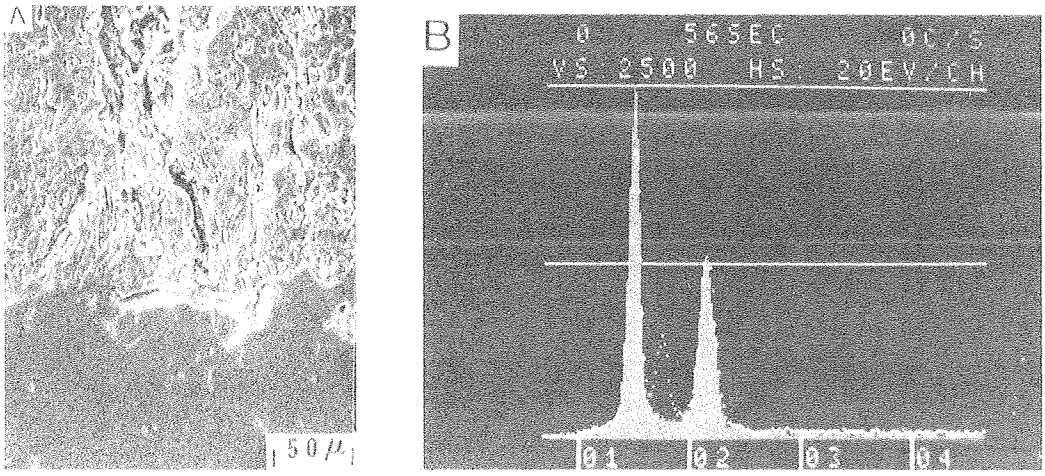

BCC760-11554

Fig. 21. Top: Correlation between % weight loss and firing time for air and vacuum fired samples at 1710°C.
Bottom: A: Microstructure of vacuum fired (1710°C) specimen illustrating the effect of mullite decomposition which results in a porous Al_2O_3 layer (top).
B: EDAX spectra for A; dotted spectrum is from the mullite matrix; lined spectra is from the porous Al_2O_3 layer.

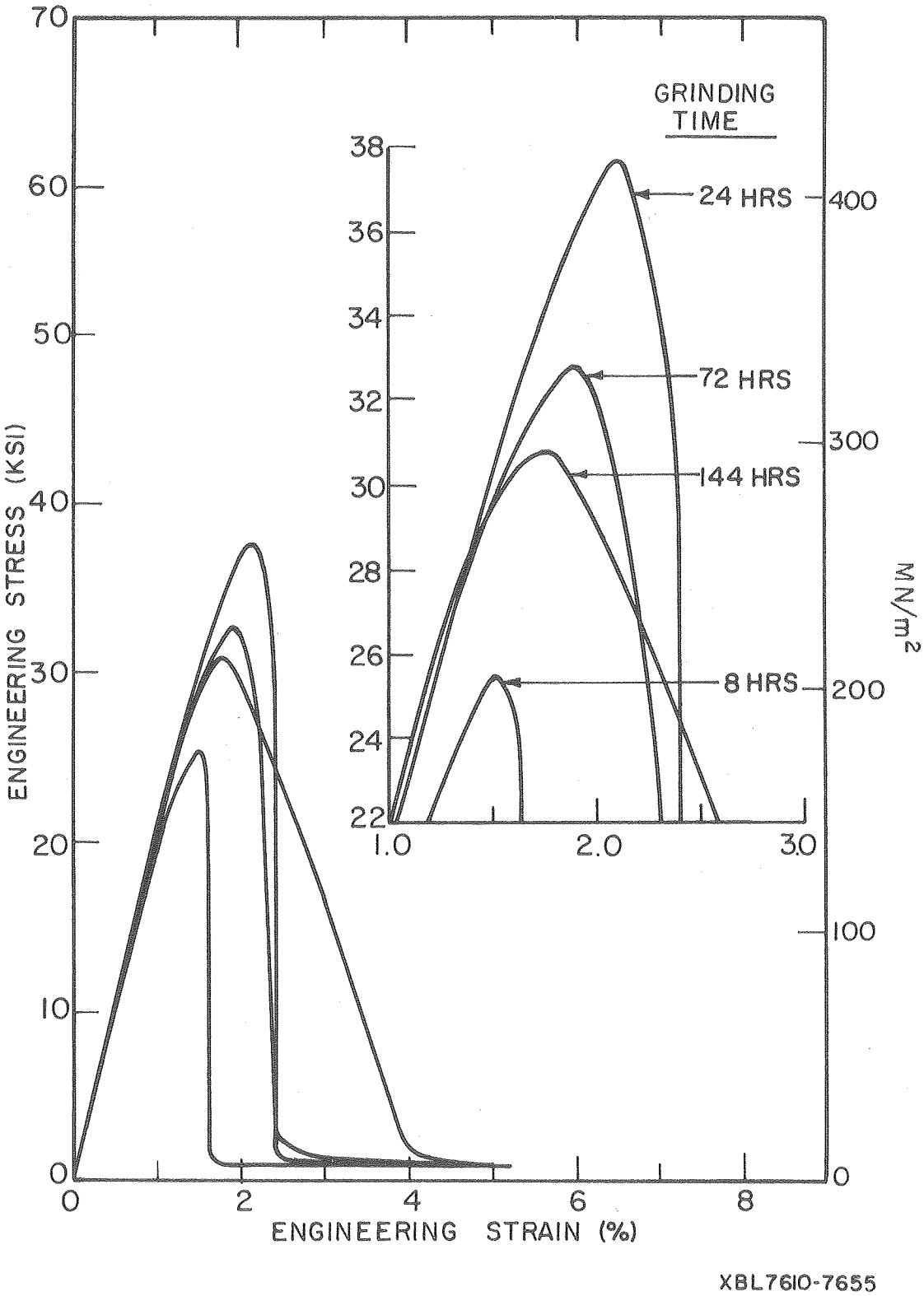

XBL7610-7655

Fig. 22. Stress-strain behavior in compression at 1200°C for compacts of mullite powder, ground for various times with alumina and flint media, sintered at ~1570°C for 24 hours in air.

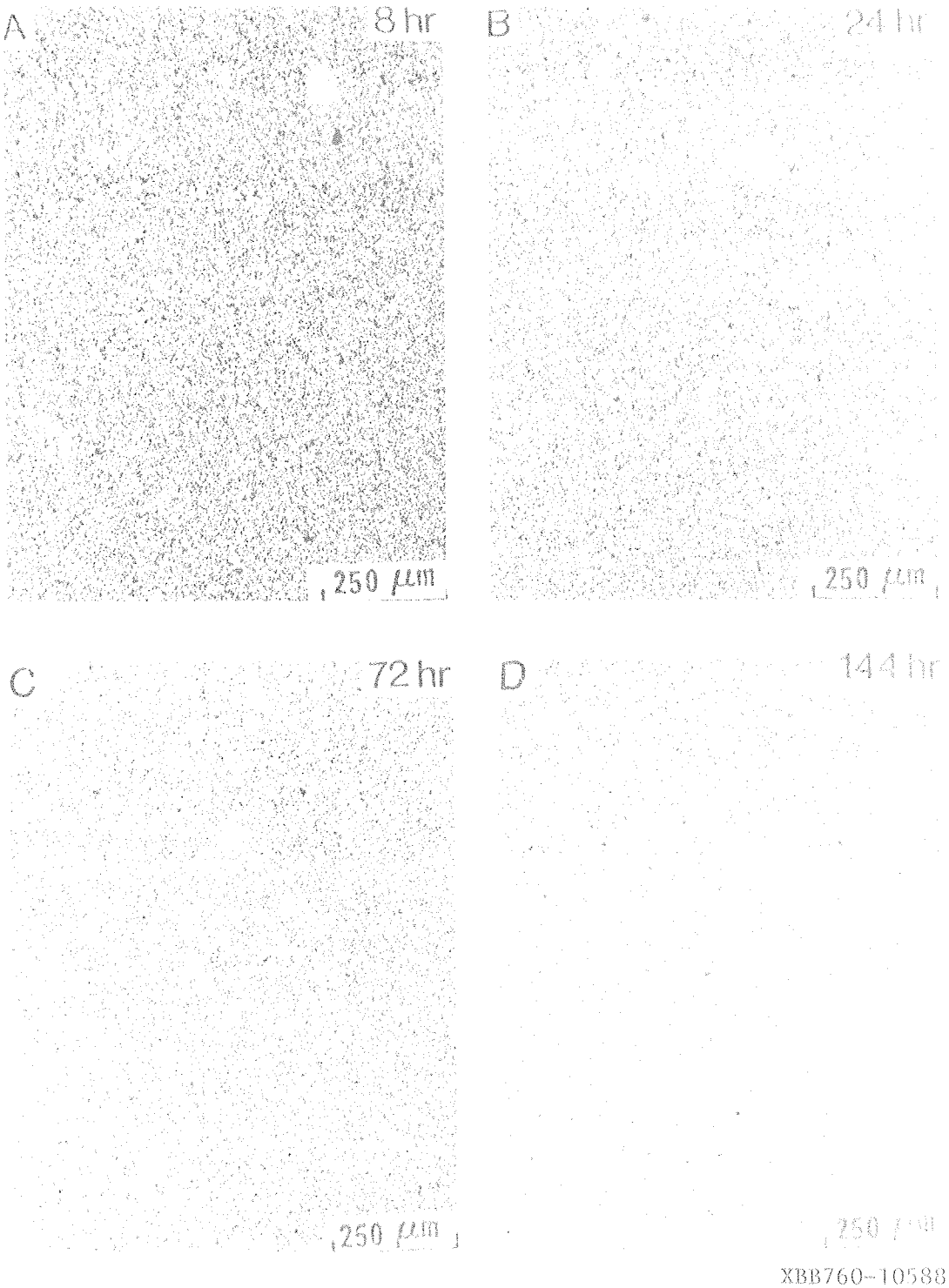

XBB760-10588

Fig. 23. Micrographs illustrating porosity effects for compacts of mullite powder, ground for various times with alumina and flint media, sintered at ~1570°C for 24 hours in air.

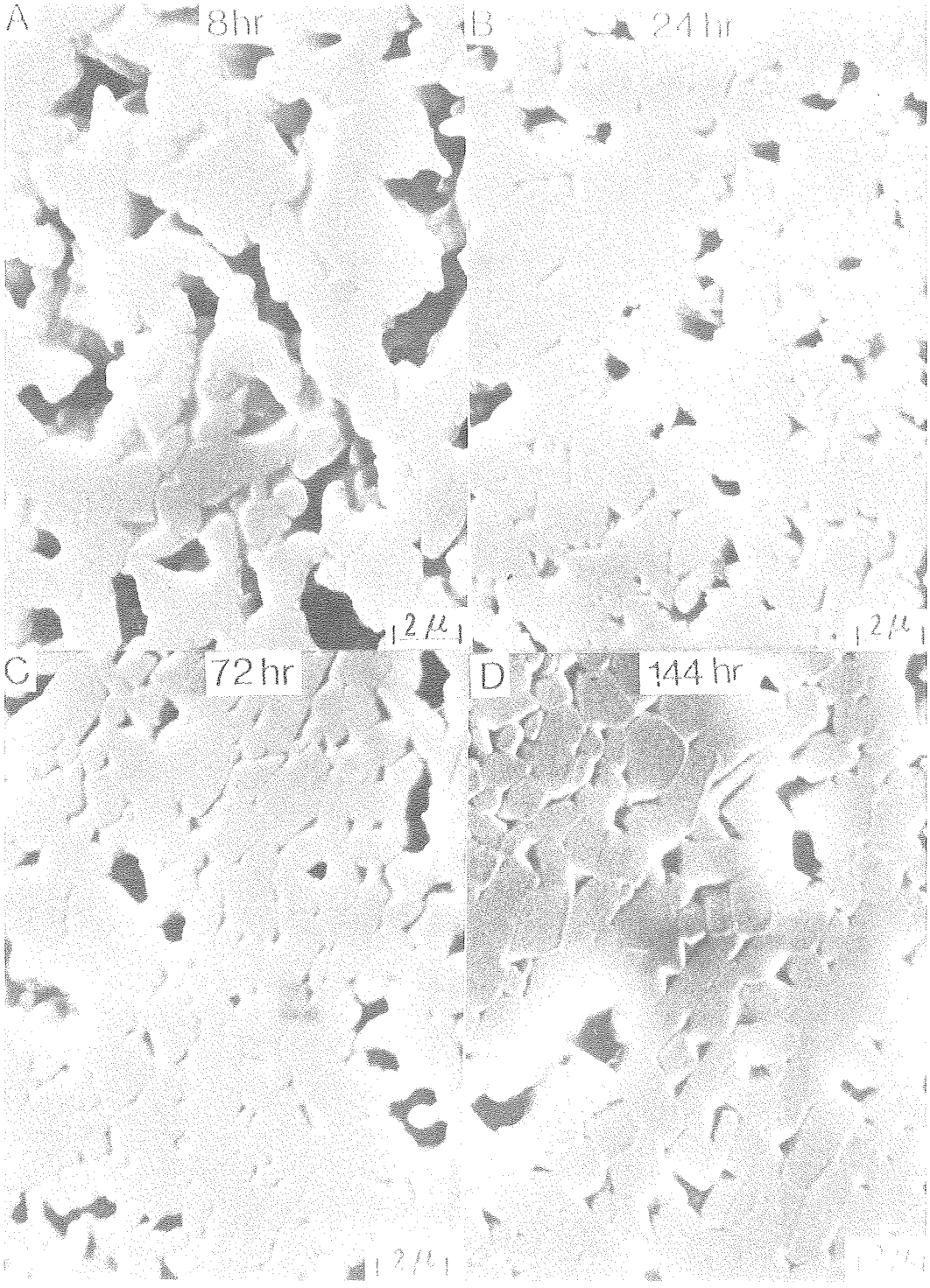

XBB760-10586

Fig. 24. Micrographs illustrating grain size effects for compacts of mullite powder, ground for various times with alumina and flint media, sintered at ~1570°C for 24 hours in air.

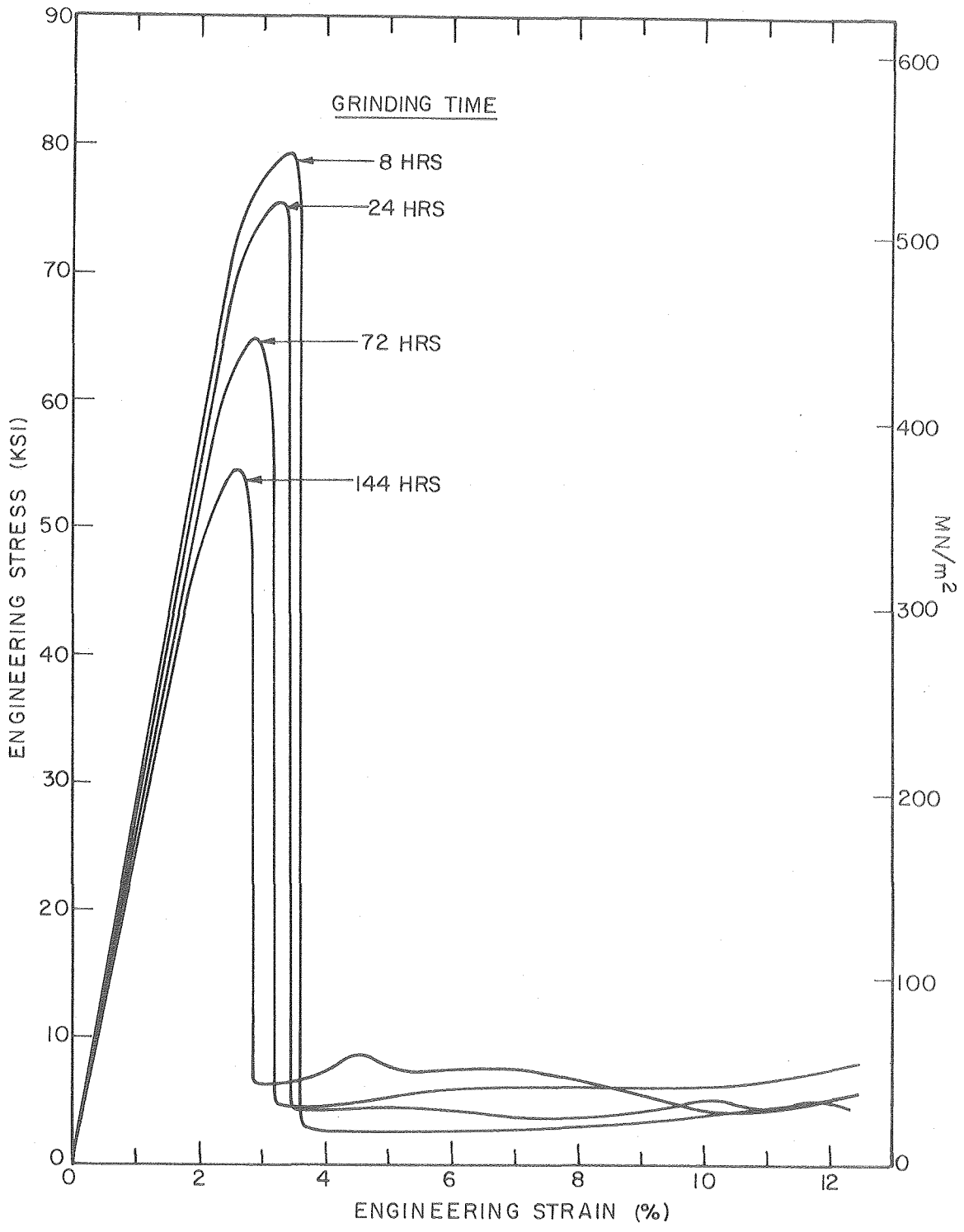

XBL 7610-7656

Fig. 25. Stress-strain behavior in compression at 1200°C for compacts of mullite powder, ground for various times with alumina and flint media, sintered to ~1725°C in air (Remmey).

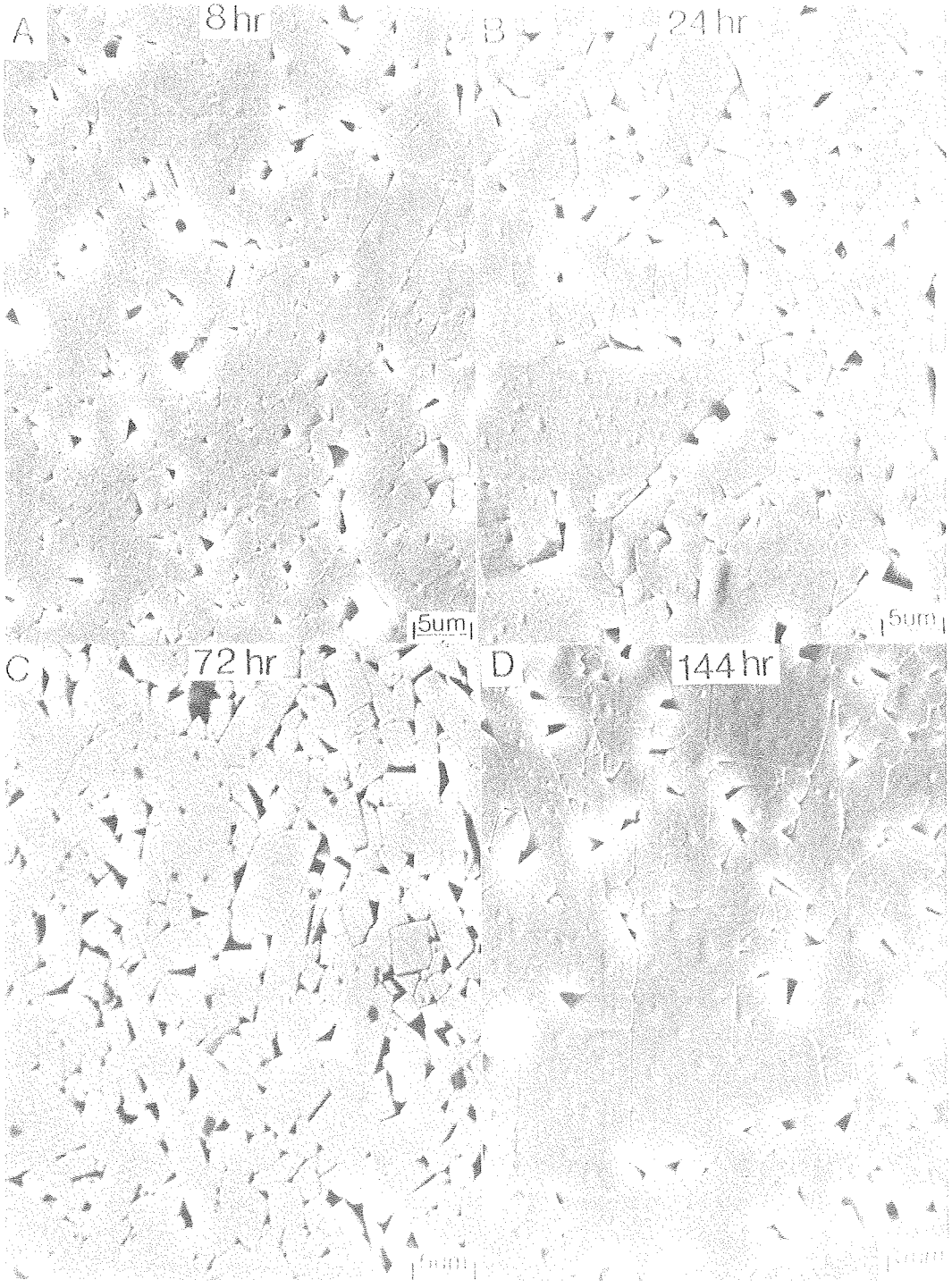

XBB760-10584

Fig. 26. Micrographs illustrating grain size effects for compacts of mullite powder, ground for various times with alumina and flint media, sintered to 1725°C in air (Remmey).

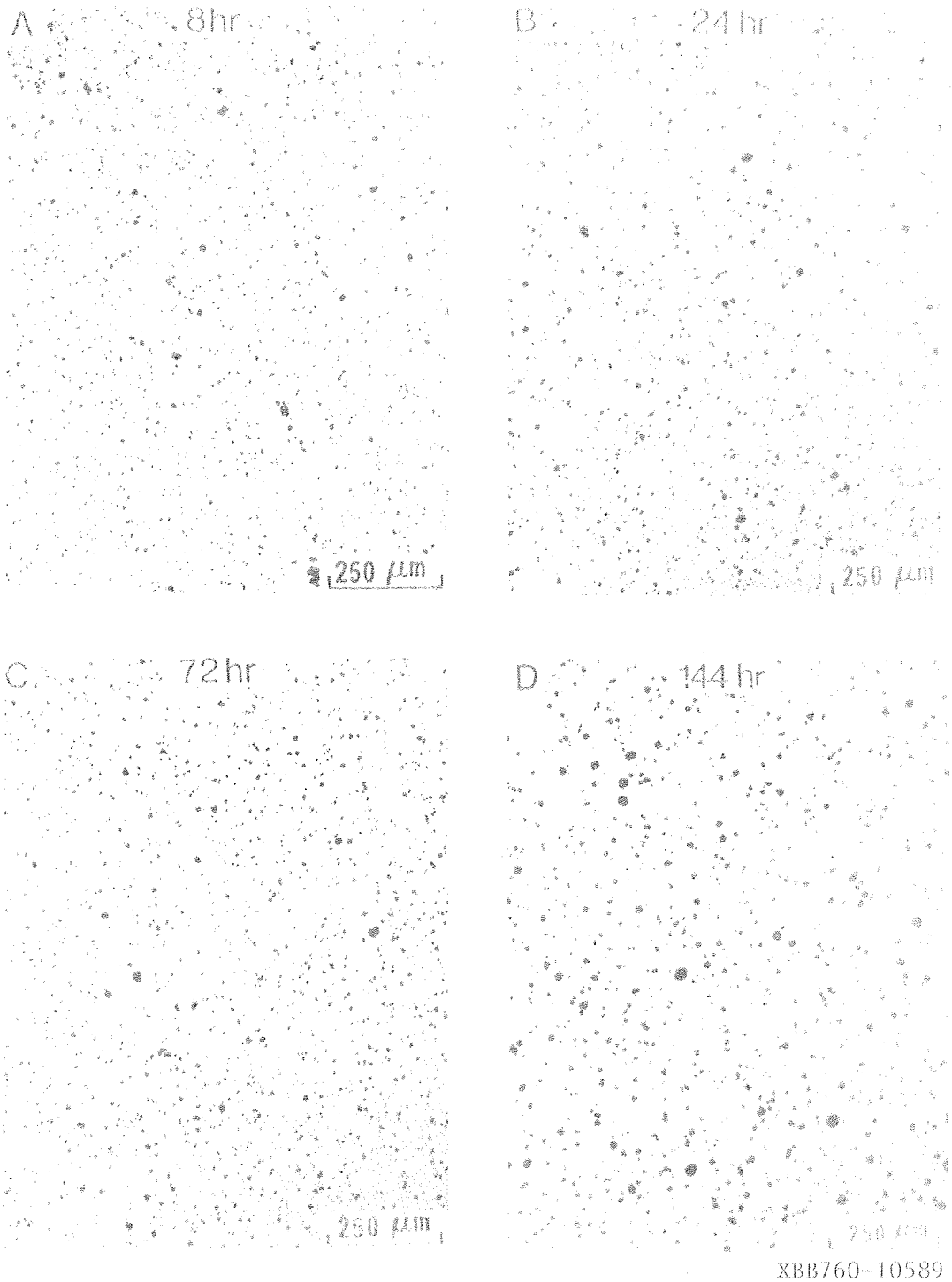

XBB760-10589

Fig. 27. Micrographs illustrating porosity effects for compacts of mullite powder, ground for various times with alumina and flint media, sintered to ~1725°C in air (Remmey).

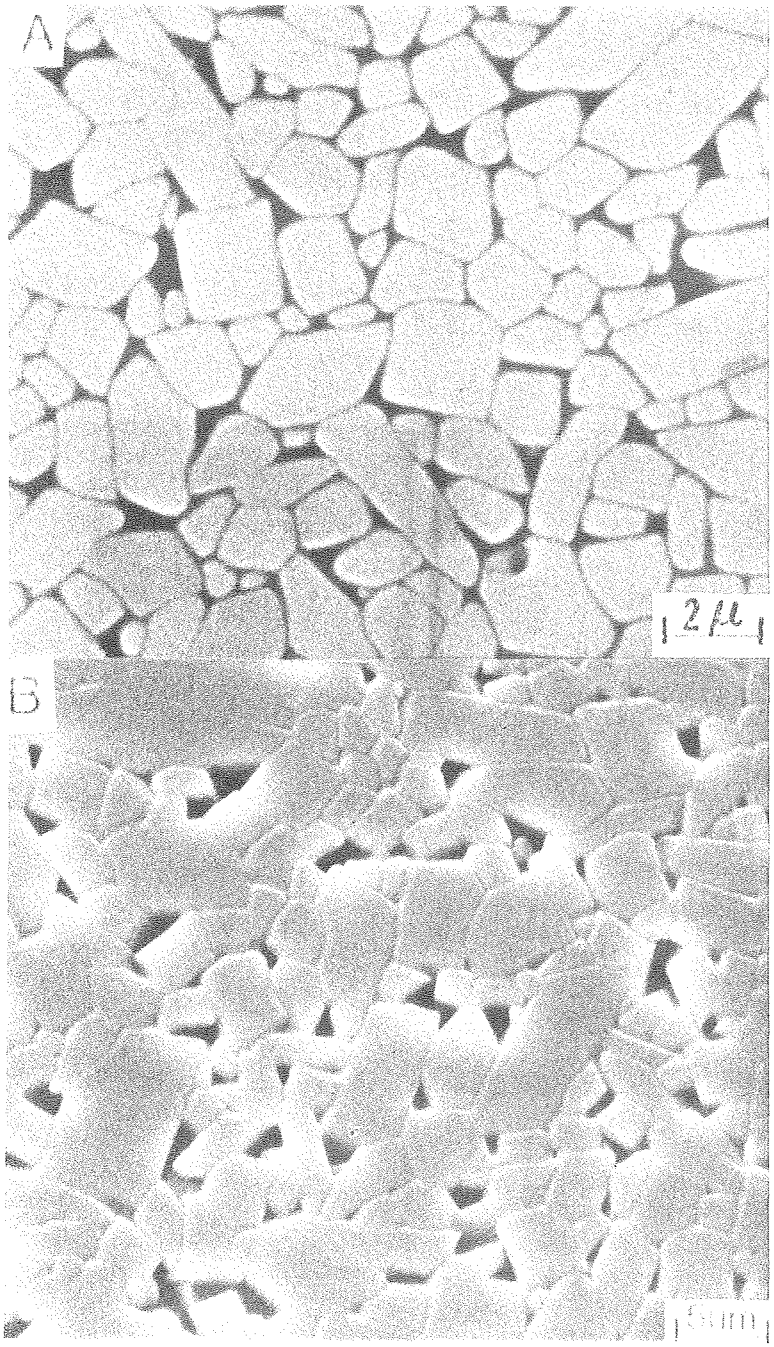

XBB771-83

Fig. 28: A: Heavily etched 144 hr.-ground (alumina and flint grinding media) mullite sample that was sintered at ~1570°C for 24 hrs in the quench furnace (air). Despite its relatively small volume fraction, the glass phase (etched out) appears to be the continuous phase.
B: Heavily etched 144 hr.-ground (alumina and flint grinding media) mullite sample that was sintered to ~1725°C in the Remmey furnace (air). The matrix is mullite; the glass phase (etched out) is restricted to "pockets", as opposed to a thin "film" around mullite crystals.

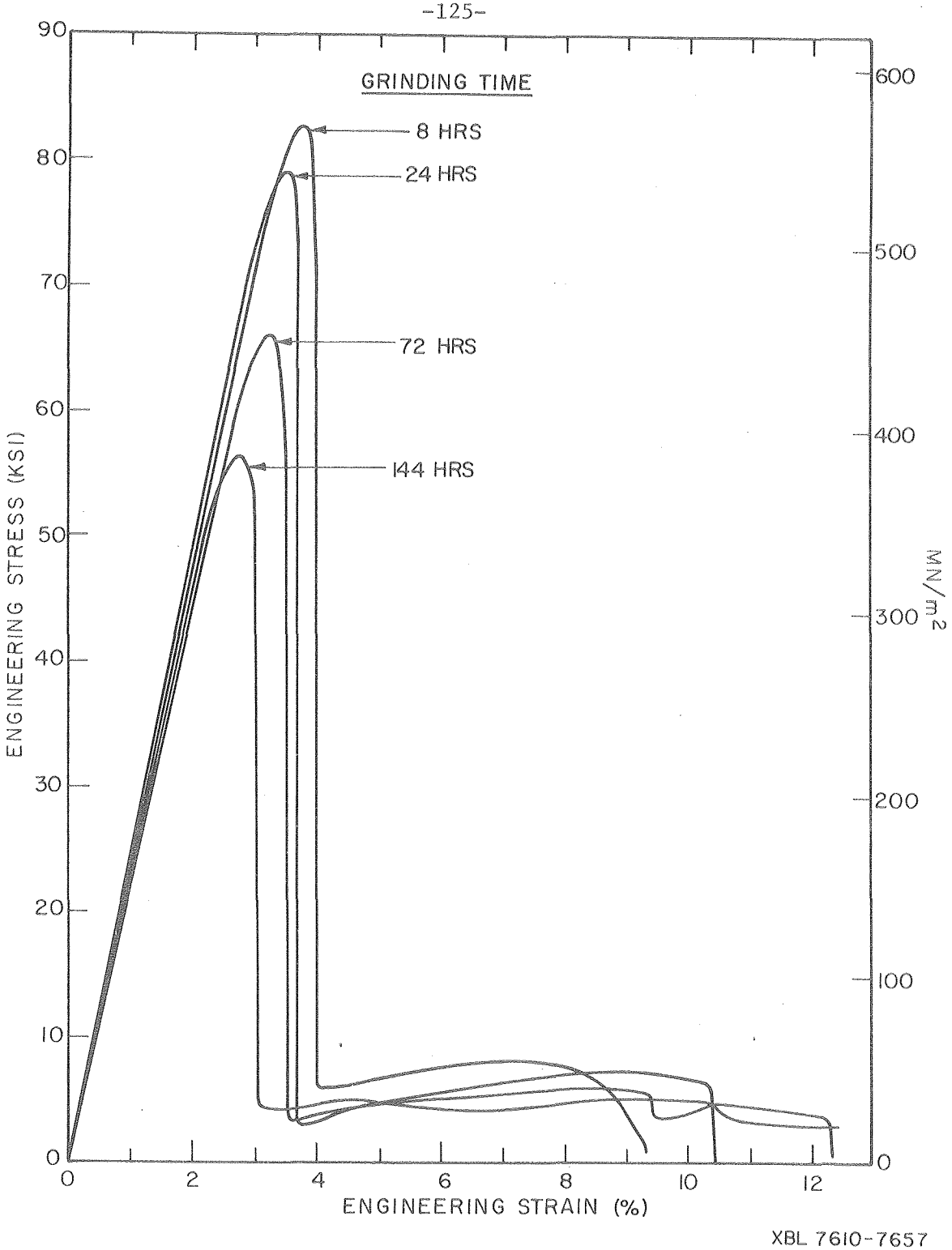

XBL 7610-7657

Fig. 29. Stress-strain behavior in compression at 1200°C for compacts of mullite powder, ground for various times with alumina and flint media, sintered at ~1725°C for 12 hrs in vacuum.

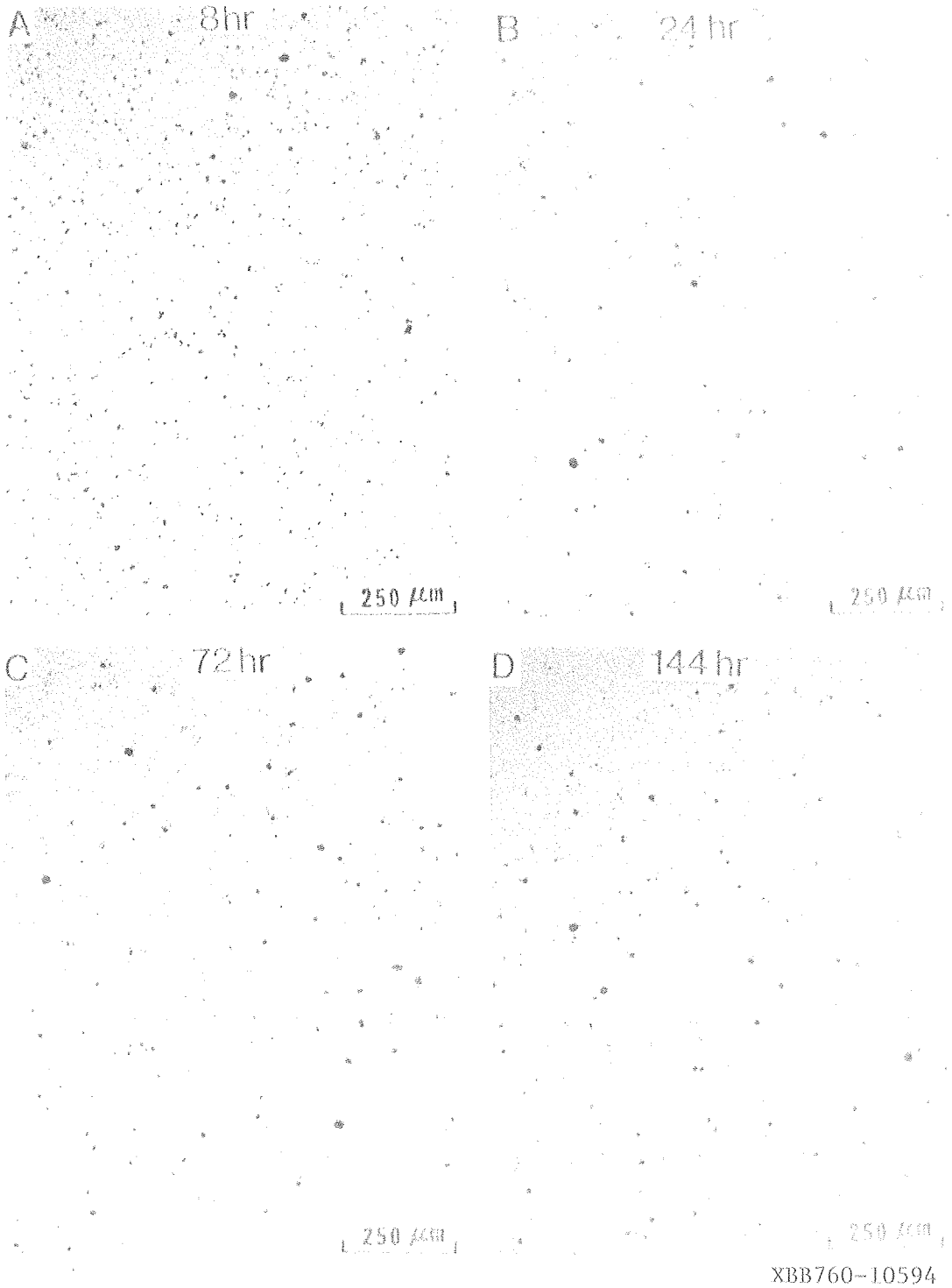

XBB760-10594

Fig. 30. Micrographs illustrating porosity effects for compacts of mullite powder, ground for various times with alumina and flint media, sintered at ~1725°C for 12 hrs in vacuum.

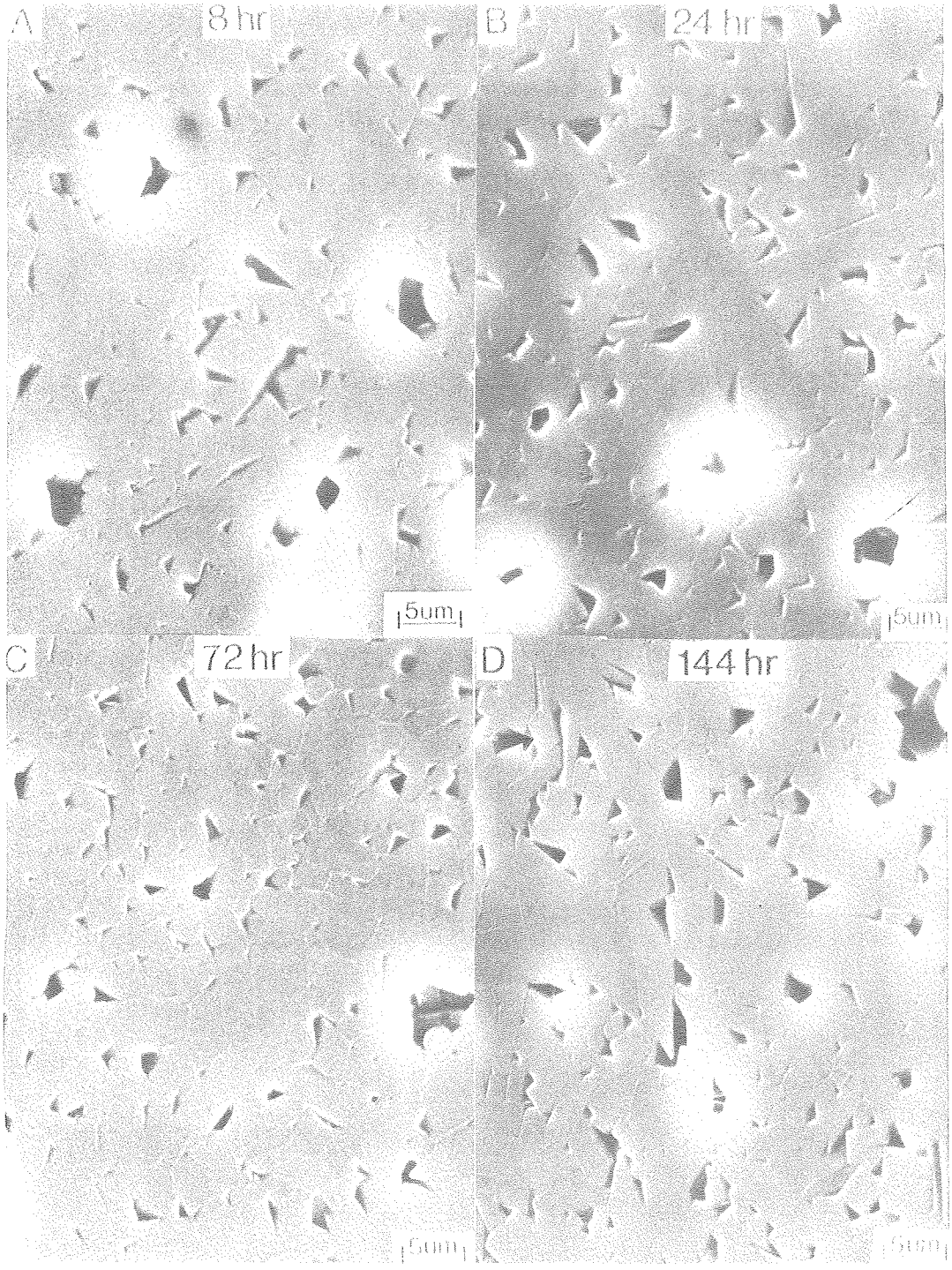

XBB760-10585

Fig. 31. Micrographs illustrating grain size effects for compacts of mullite powder, ground for various times with alumina and flint media, sintered at ~1725°C for 12 hrs in vacuum.

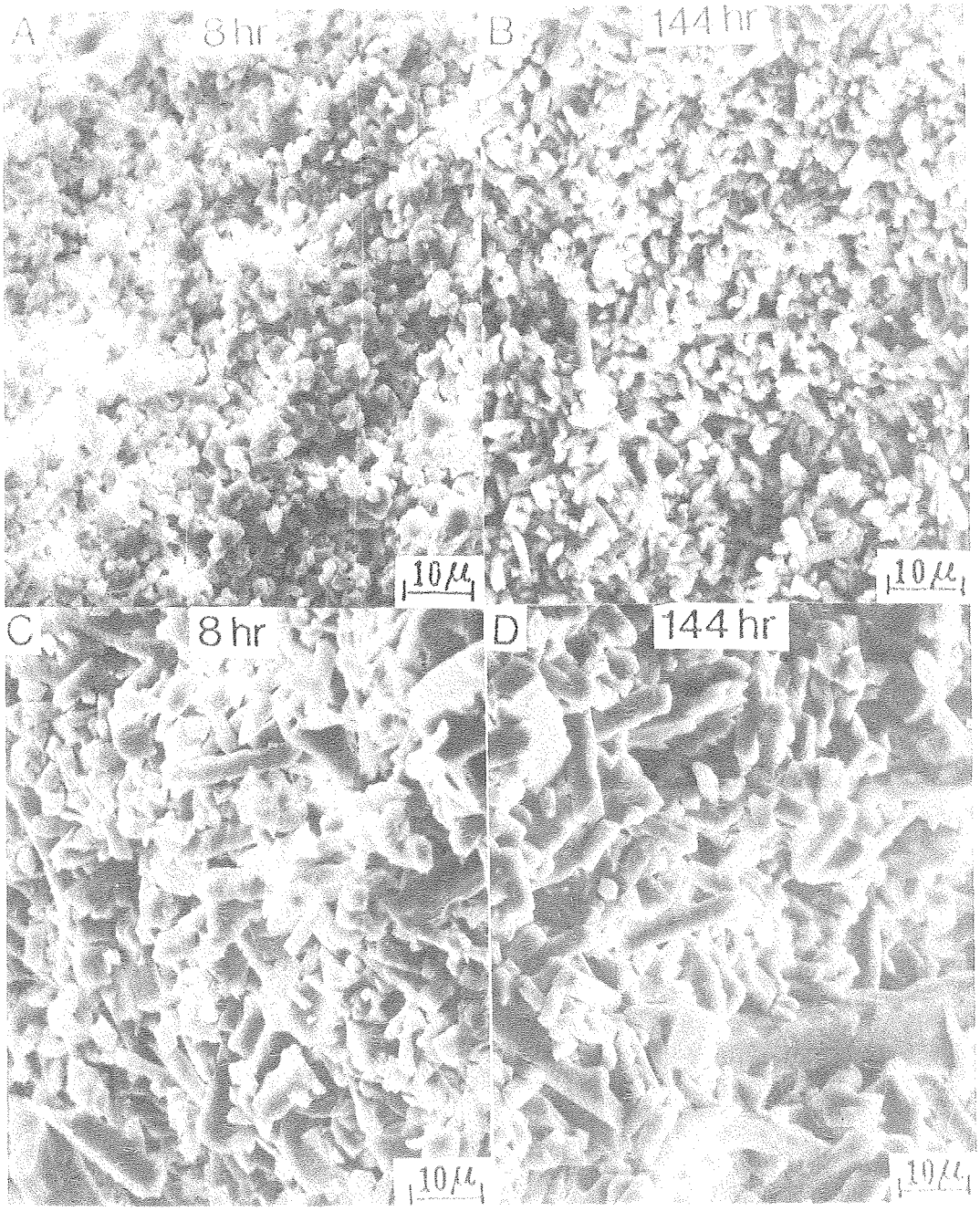

XBB771-80

Fig. 32. A and B: Fracture surfaces of 1200°C compression tested specimens made from 8 hr.-ground and 144 hr.-ground (alumina and flint grinding media) compacts fired to ~1570°C for 24 hrs. Note the development of elongated grains in B.
C and D: Fracture surfaces of 1200°C compression tested specimens made from 8 hr.-ground and 144 hr.-ground (alumina and flint grinding media) compacts fired at ~1725°C for 12 hrs (Brew).

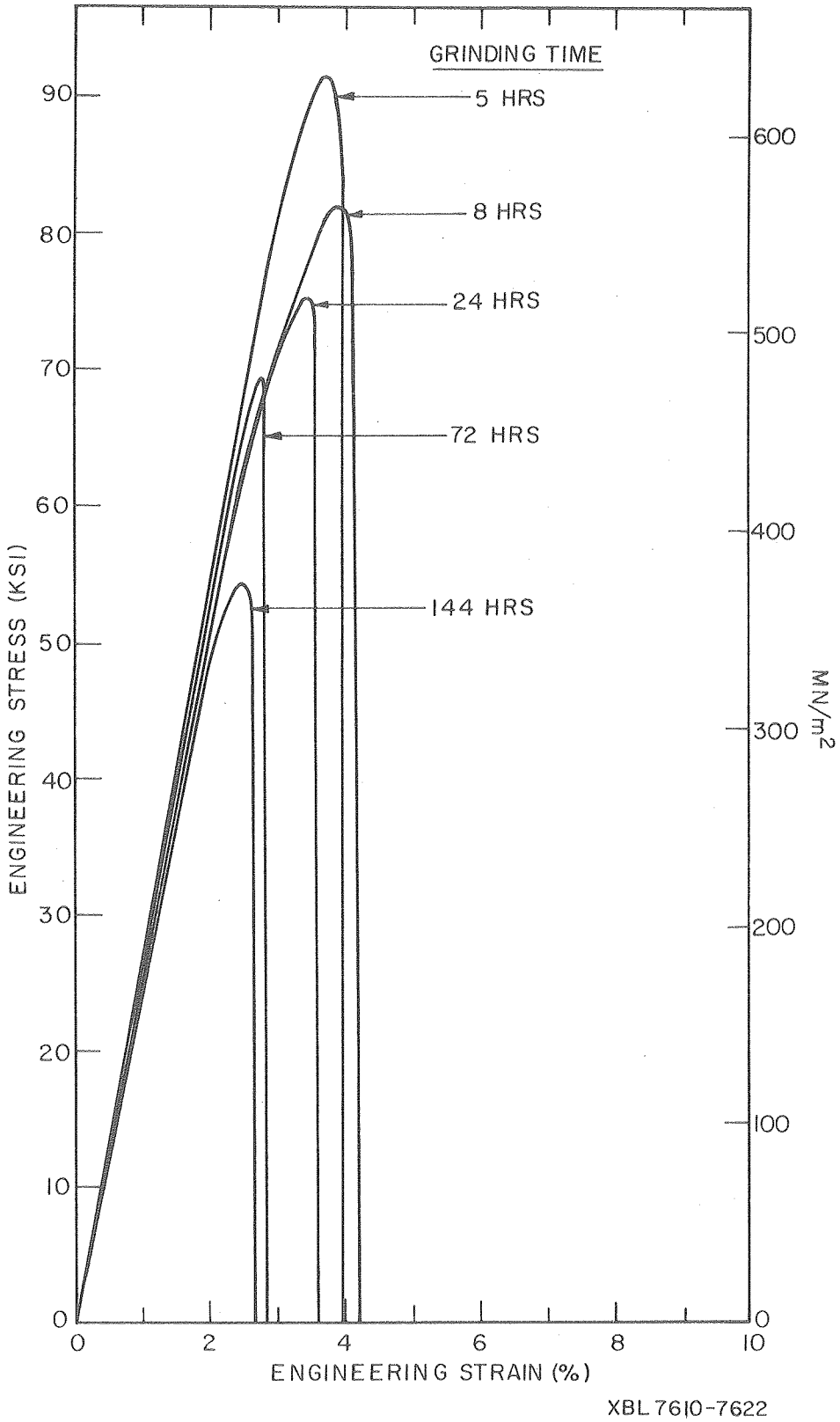

XBL 7610-7622

Fig. 33. Stress-strain behavior in compression at 1200°C for compacts of mullite powder, ground for various times with alumina media only, sintered at ~1725°C for 12 hrs in vacuum.

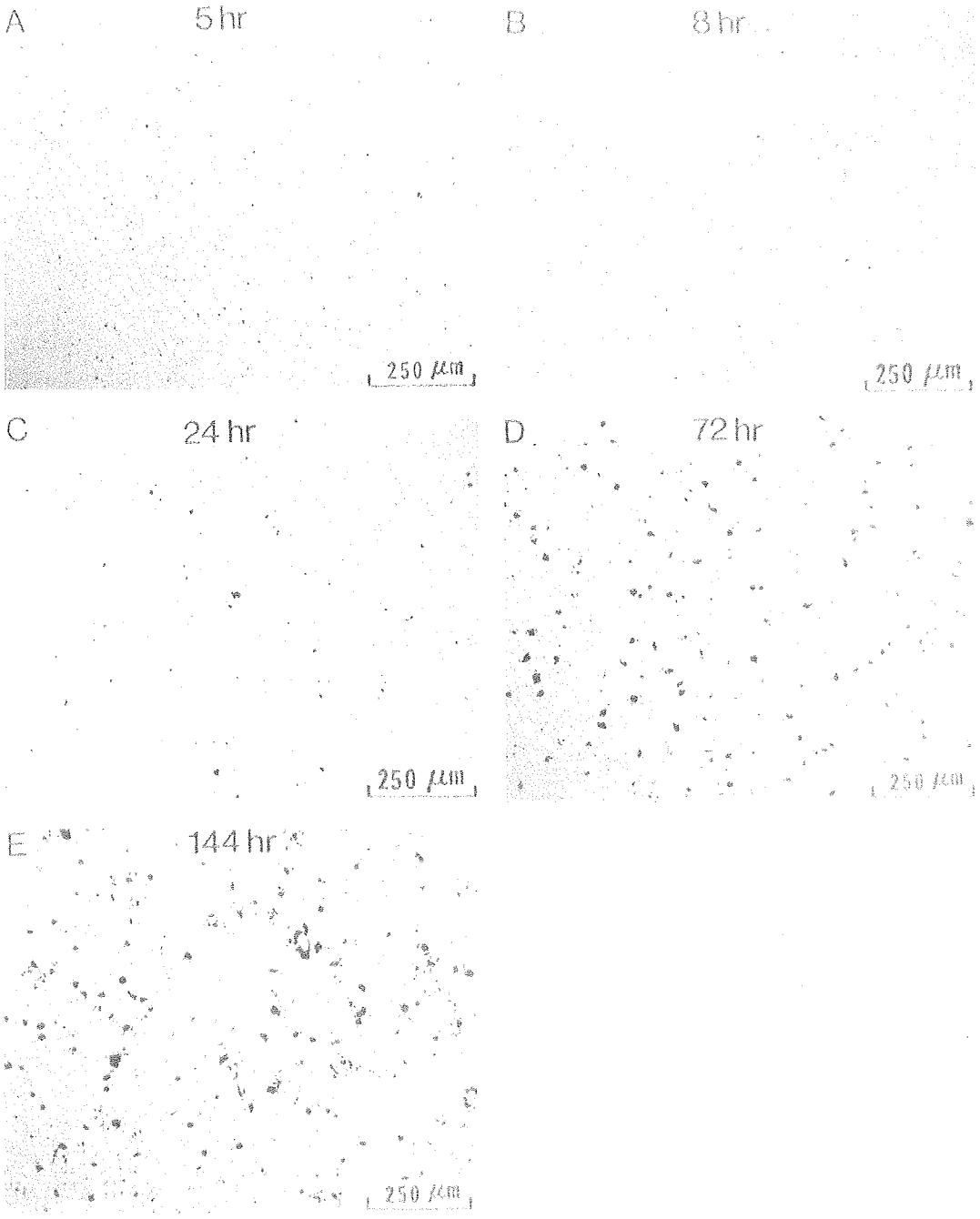

XBB760-10590

Fig. 34. Micrographs illustrating porosity effects for compacts of mullite powder, ground for various times with alumina media only, sintered at ~1725°C for 12 hrs in vacuum. Alumina particles are seen in 34E.

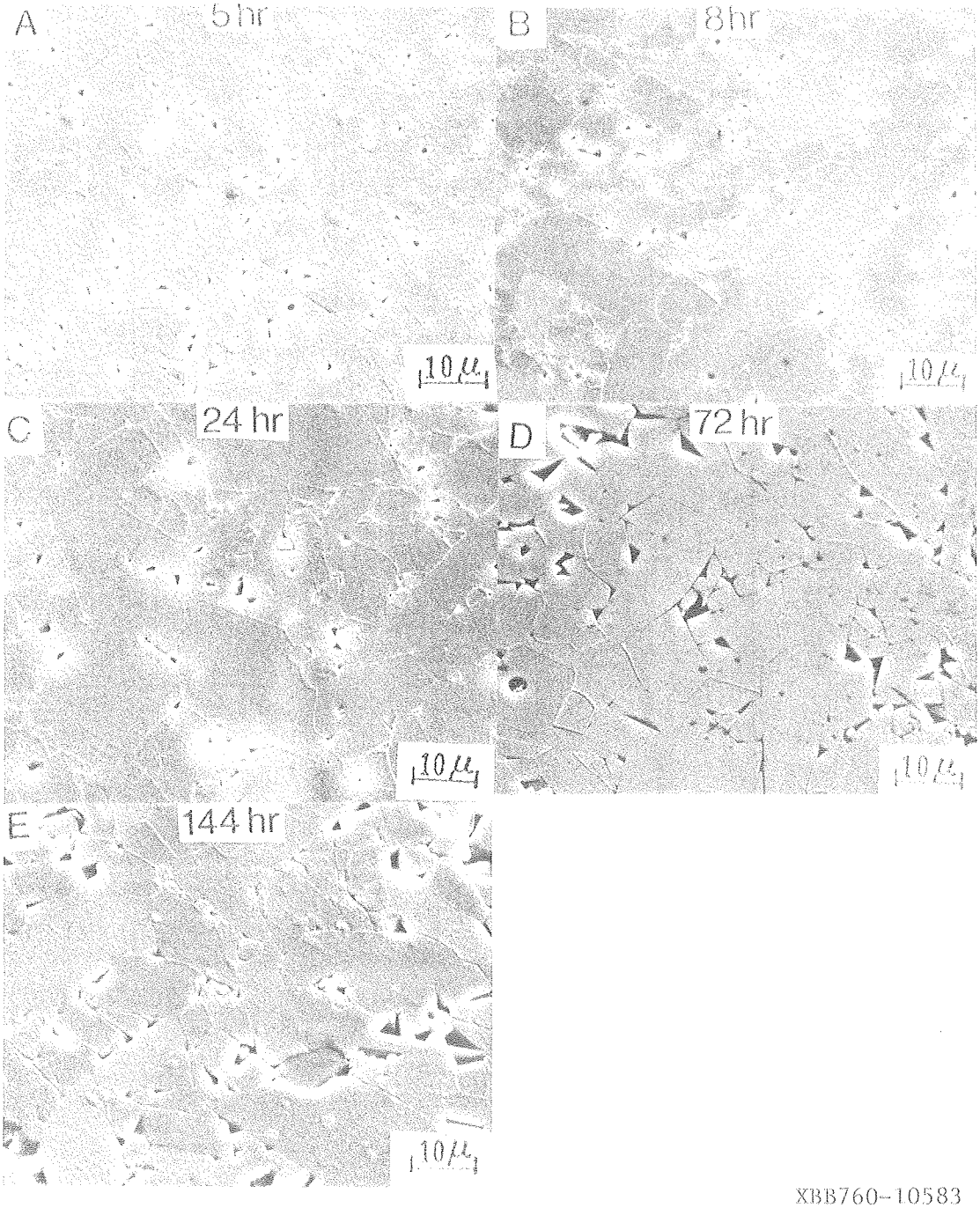

XBB760-10583

Fig. 35. Micrographs illustrating grain size effects for compacts of mullite powder, ground for various times with alumina media only, sintered at ~1725°C for 12 hrs in vacuum.

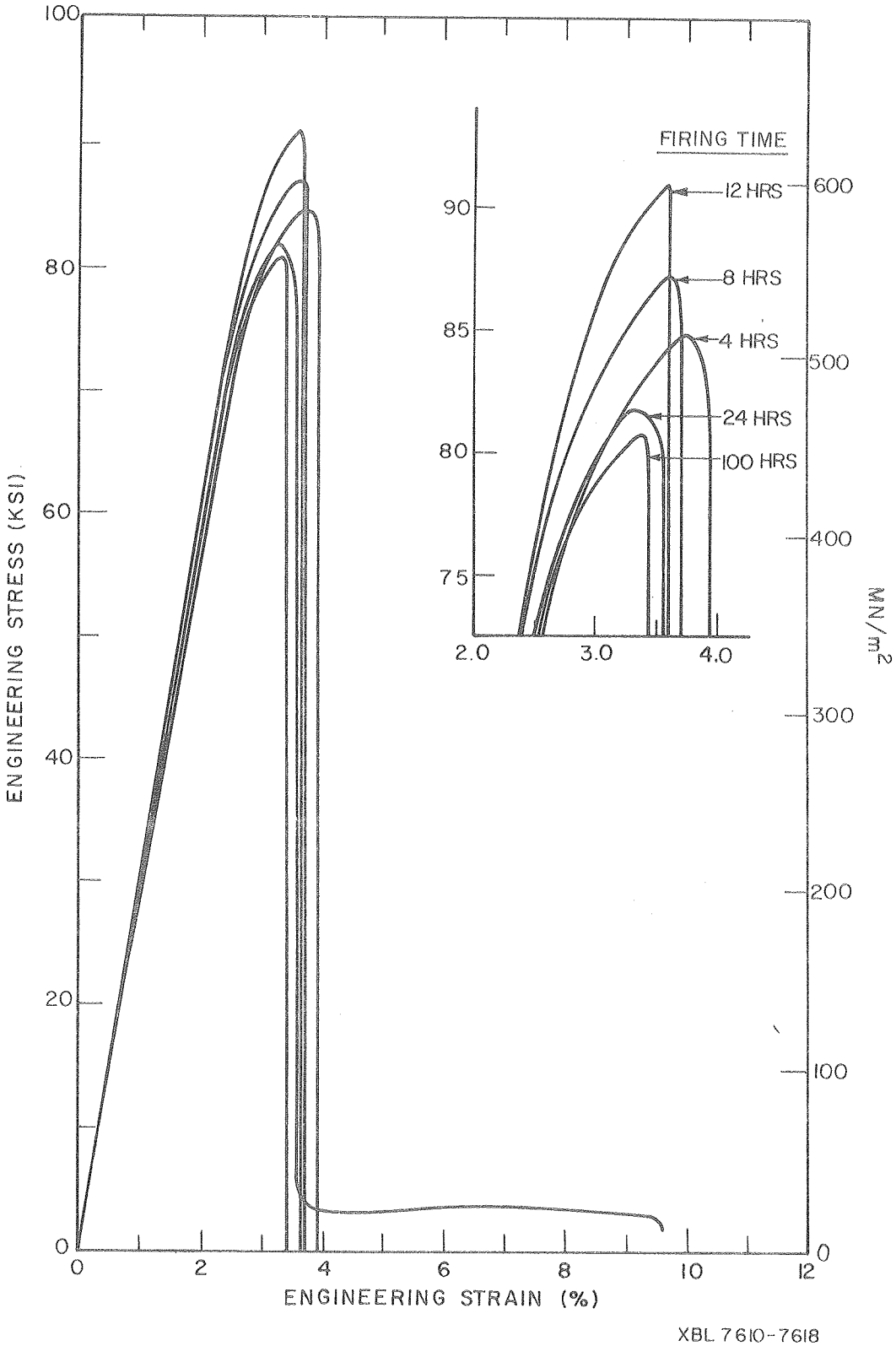

Fig. 36. Stress-strain behavior in compression at 1200°C for 5 hr.-ground samples sintered for various times in air at ~1710°C.

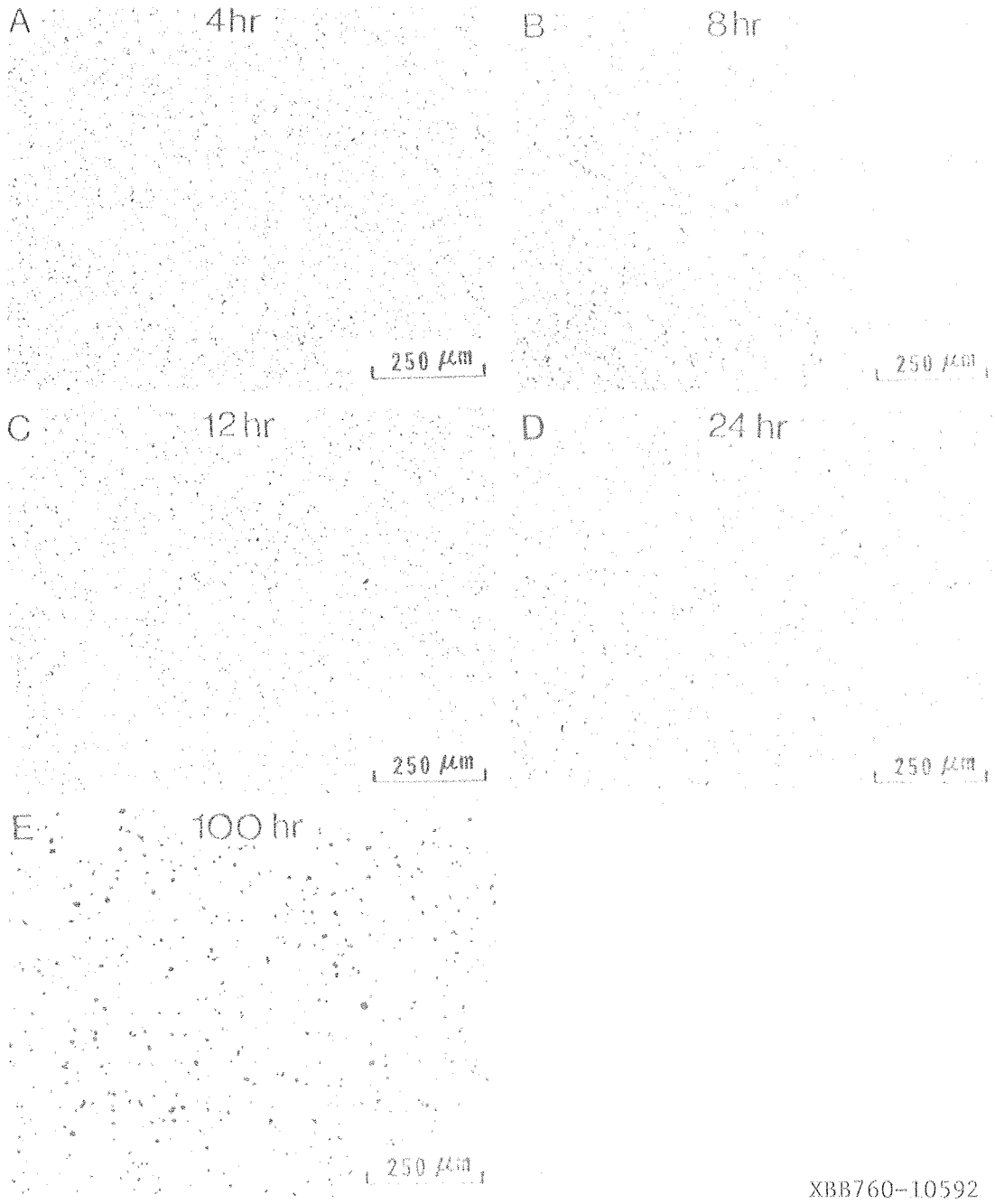

Fig. 37. Micrographs illustrating porosity changes for 5 hr.-ground mullite samples sintered for various times in air at ~1710°C.

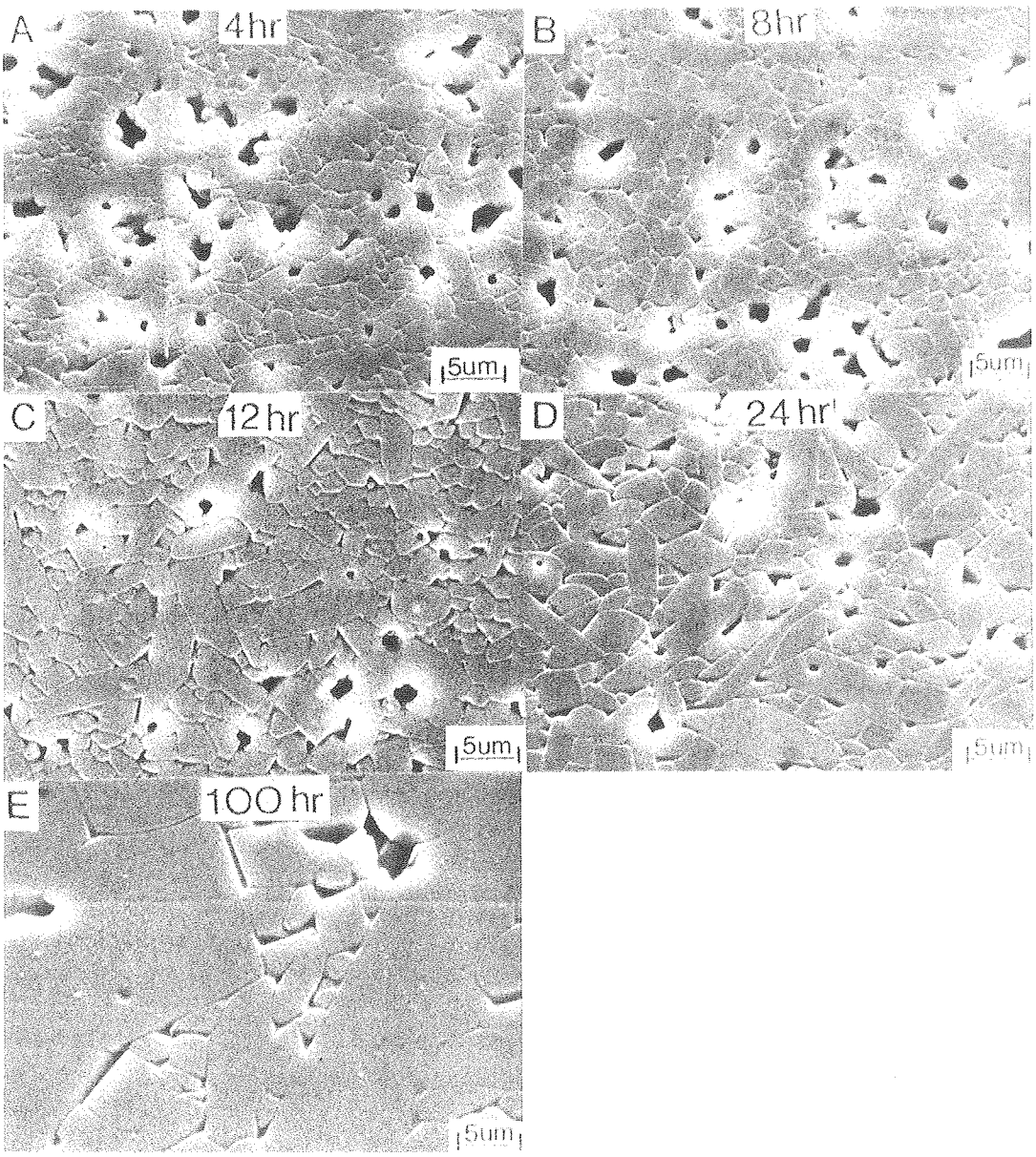

XBB760-10580

Fig. 38. Micrographs illustrating grain size and morphology changes for 5 hr.-ground mullite samples sintered for various times in air at ~1710°C.

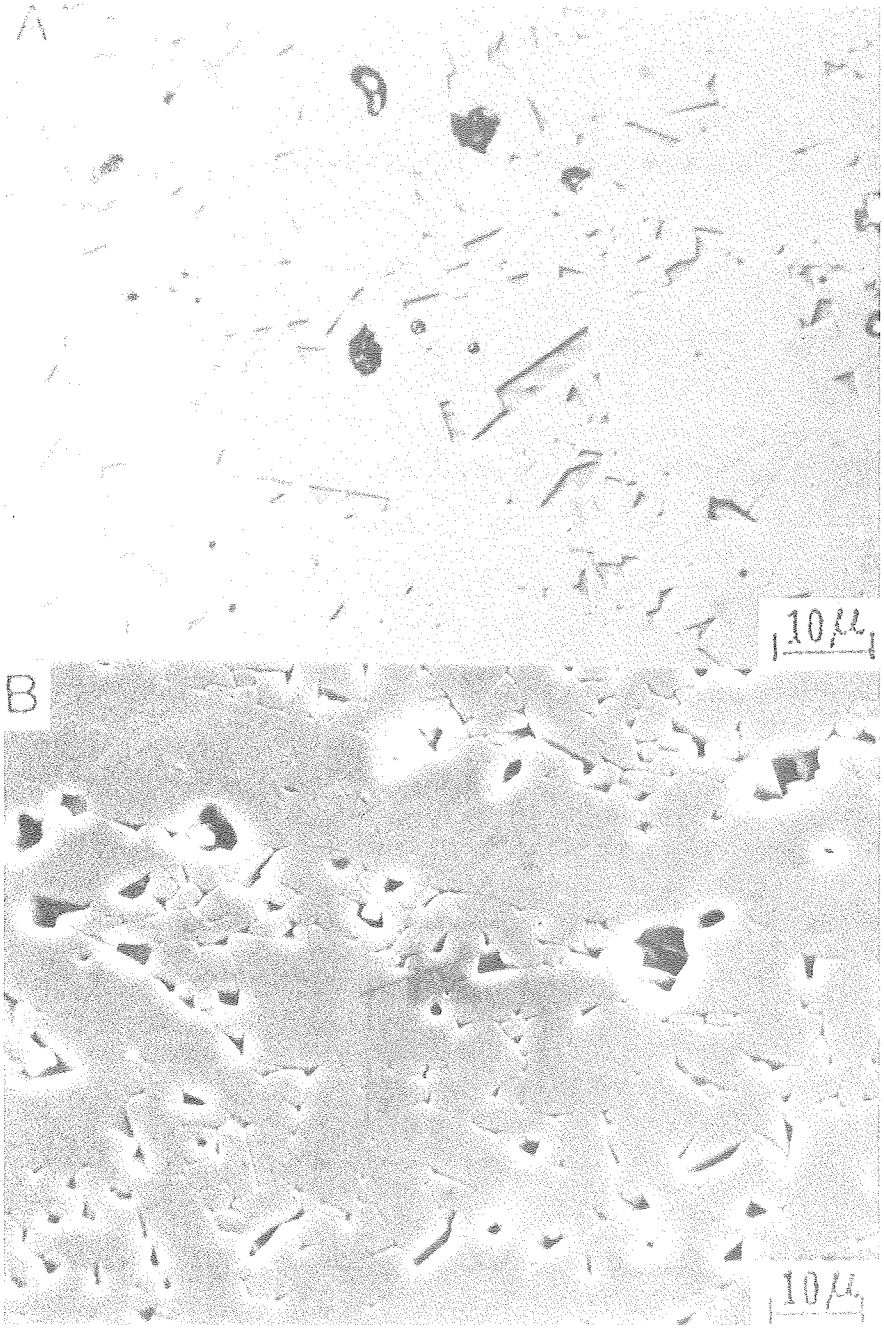

XBB771-82

Fig. 39. A: Polished surface of 5 hr.-ground mullite sample sintered at ~1710°C for 100 hrs in air which was given a very light chemical etch (~5 seconds with an ~5% HF solution) to show the glass phase isolated in angular "pockets".
B: Polished surface of 5 hr.-ground mullite sample sintered at ~1710°C for 100 hrs in air which was given a typical thermal etch (~20 minutes at ~1500°C) to bring out the grain boundaries. Glass phase has been etched out.

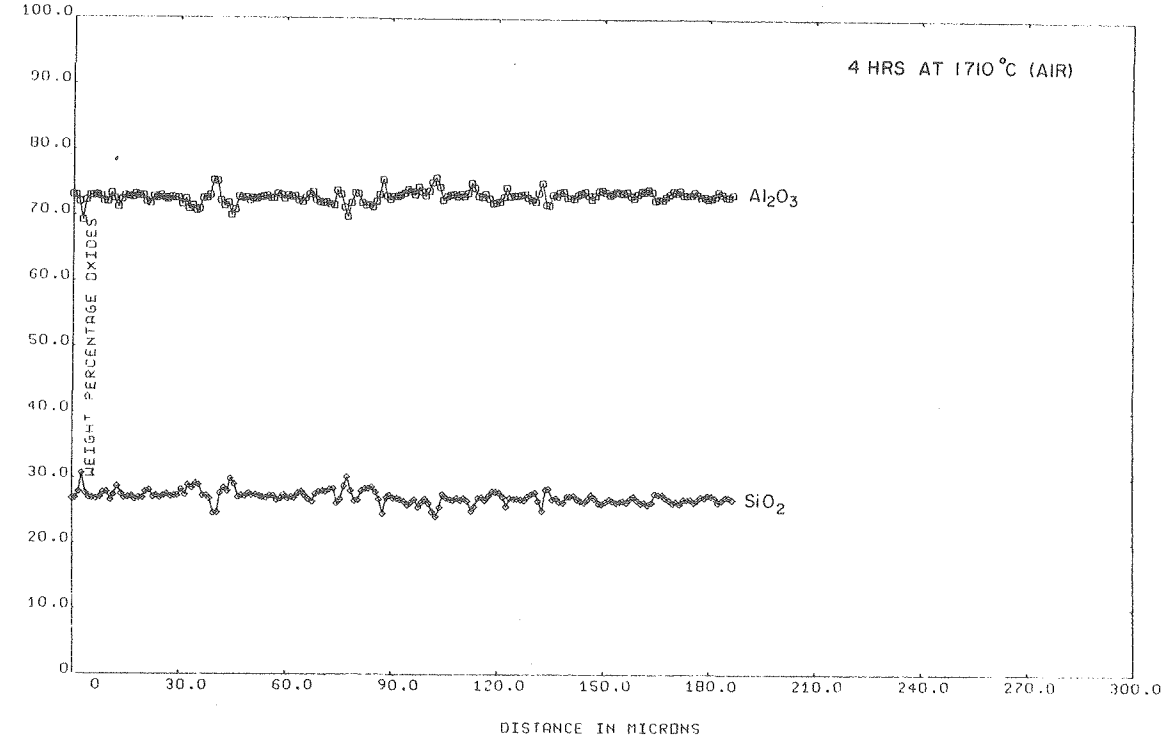

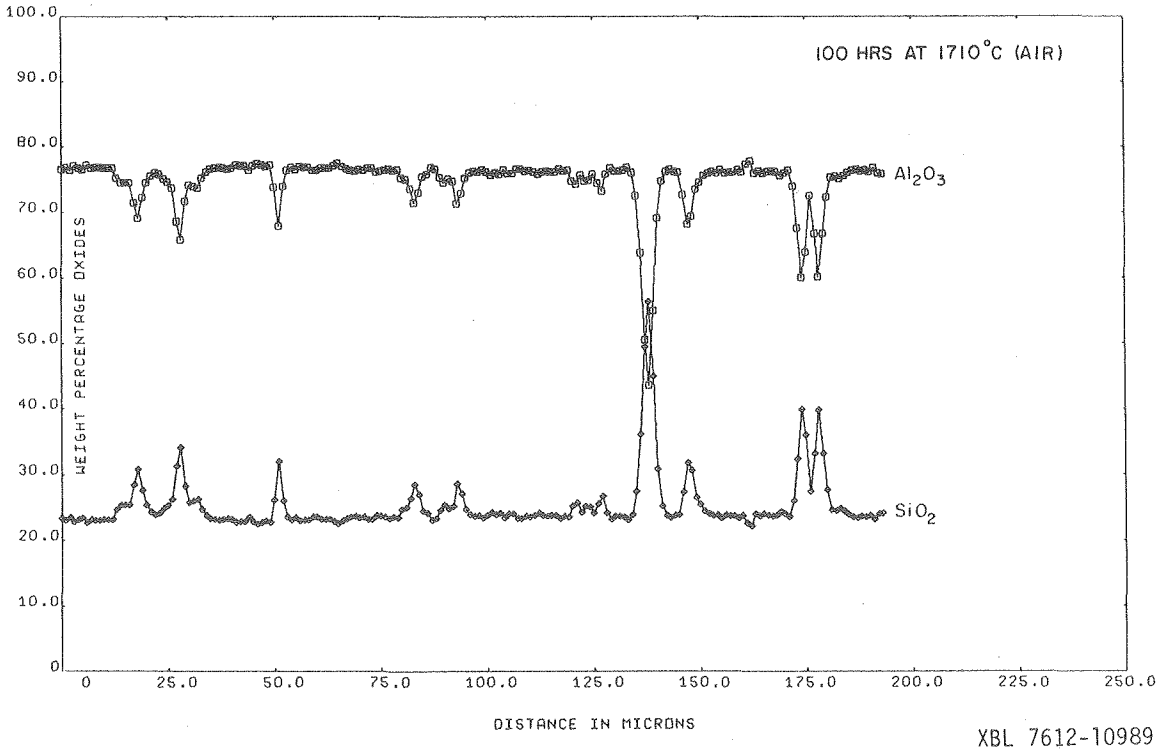

XBL 7612-10989

Fig. 40. Composition profiles obtained from electron microprobe data in which 5 hr.-ground mullite samples were scanned in one micron steps. Sharp composition shifts in the 100 hr fired sample indicate the existence of larger glass pockets.

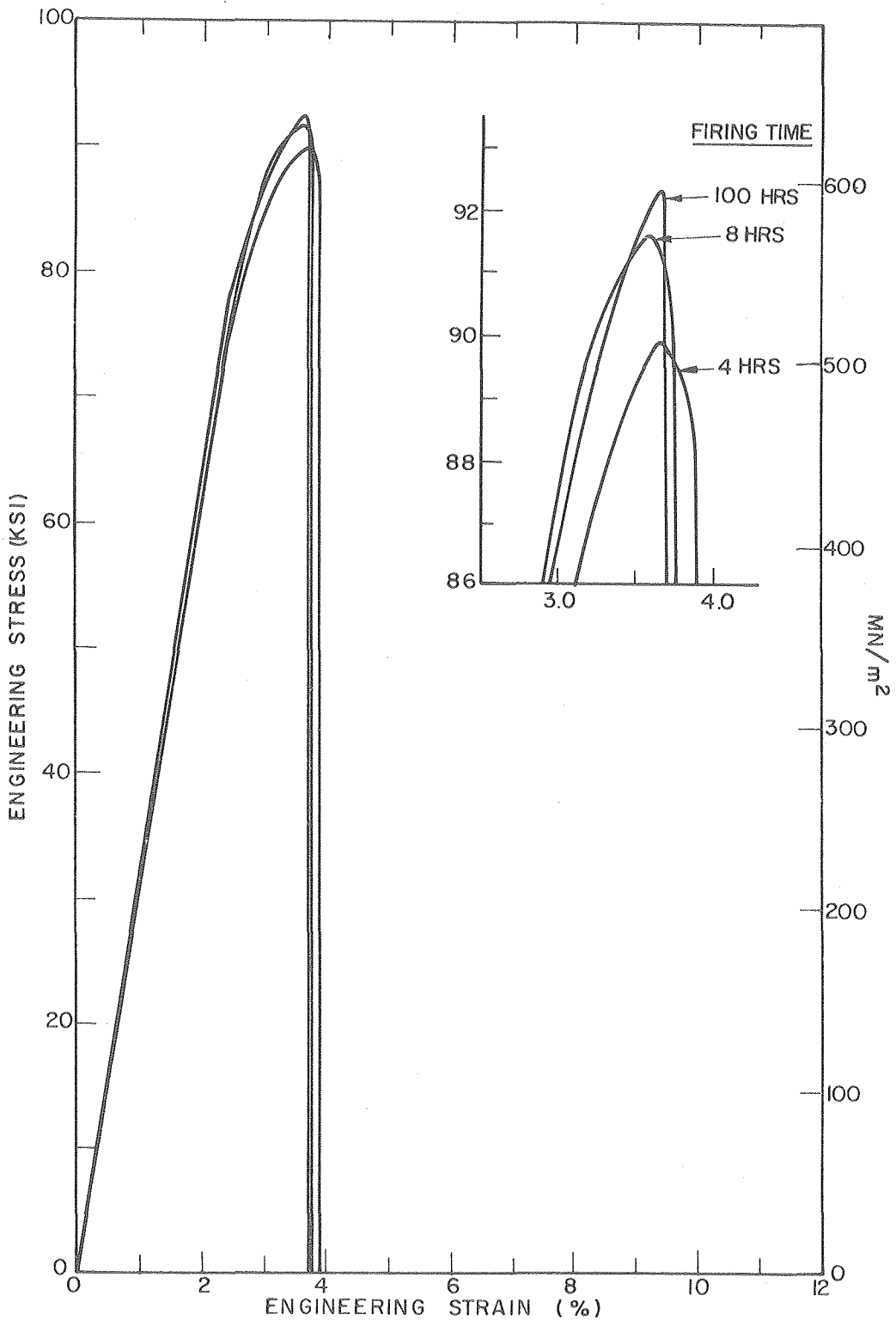

XBL 7610-7617

Fig. 41. Stress-strain behavior in compression at 1200°C for 5 hr.-ground mullite samples sintered in vacuum at ~1710°C for various times.

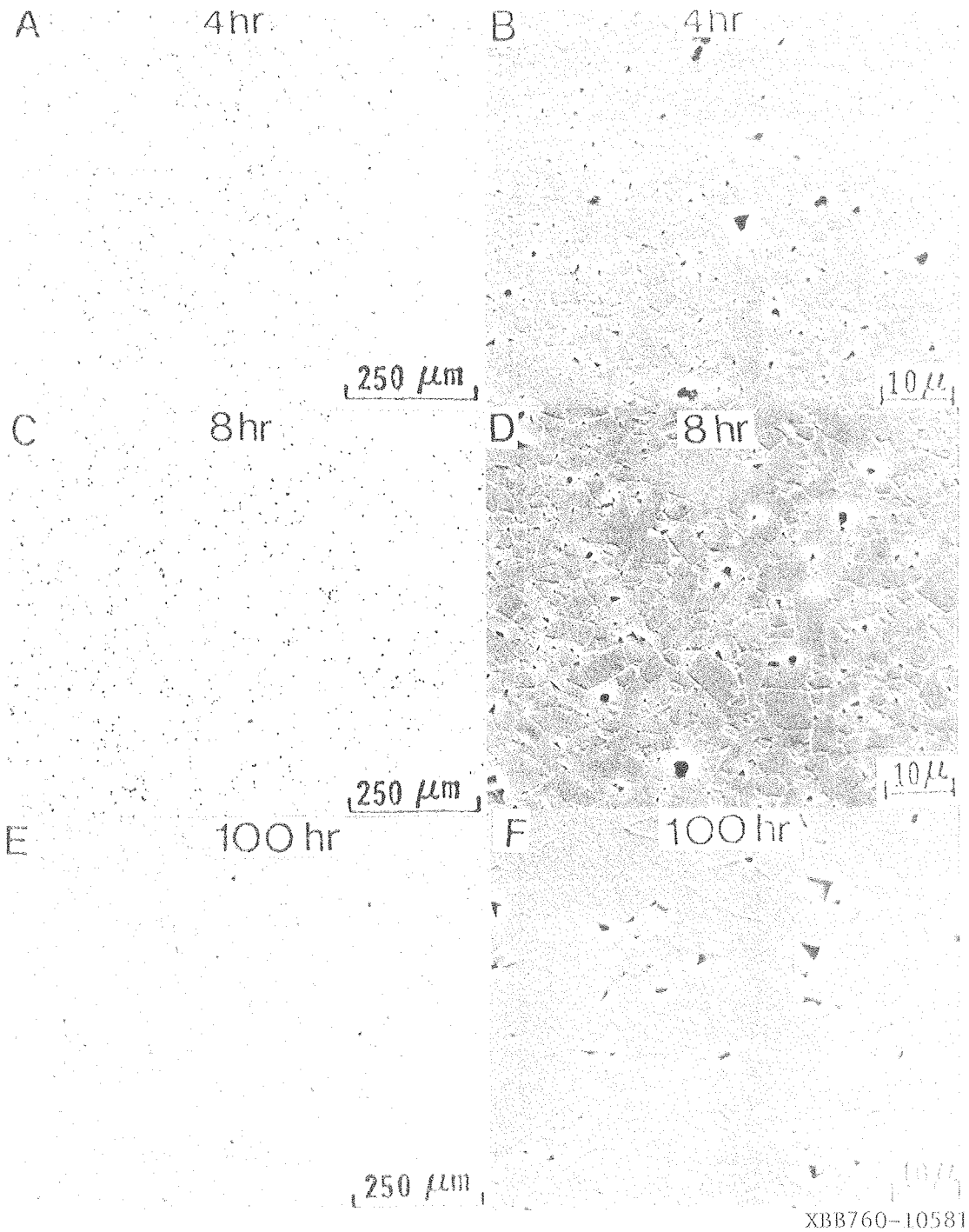

Fig. 42. Micrographs illustrating porosity (left side) and grain size (right side) changes for 5 hr.-ground mullite samples sintered in vacuum at ~1710°C for various times.

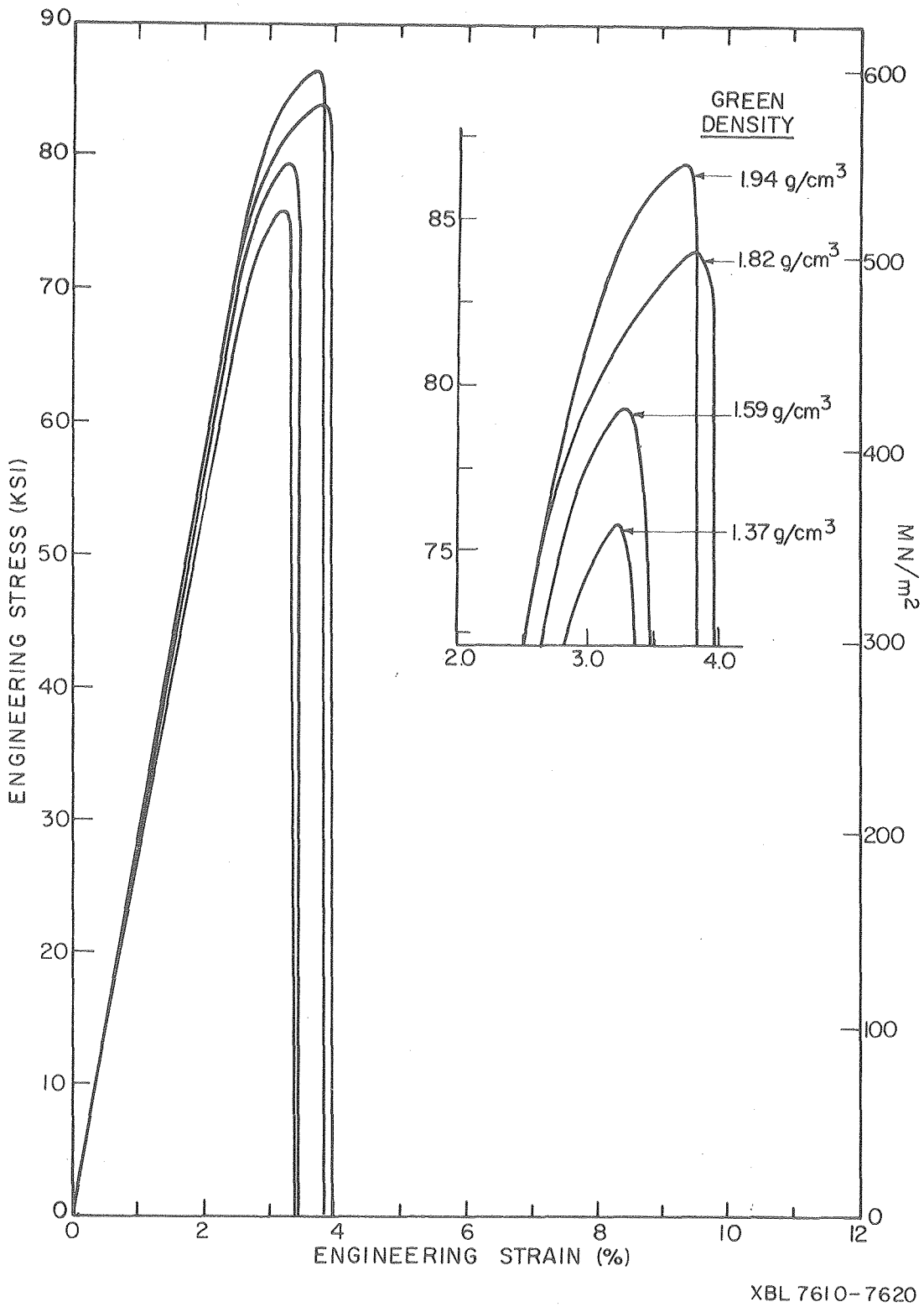

XBL 7610-7620

Fig. 43. Stress-strain behavior in compression at 1200°C for 5 hr.-ground mullite compacts of various green densities sintered at ~1710°C in air for 4 hrs.

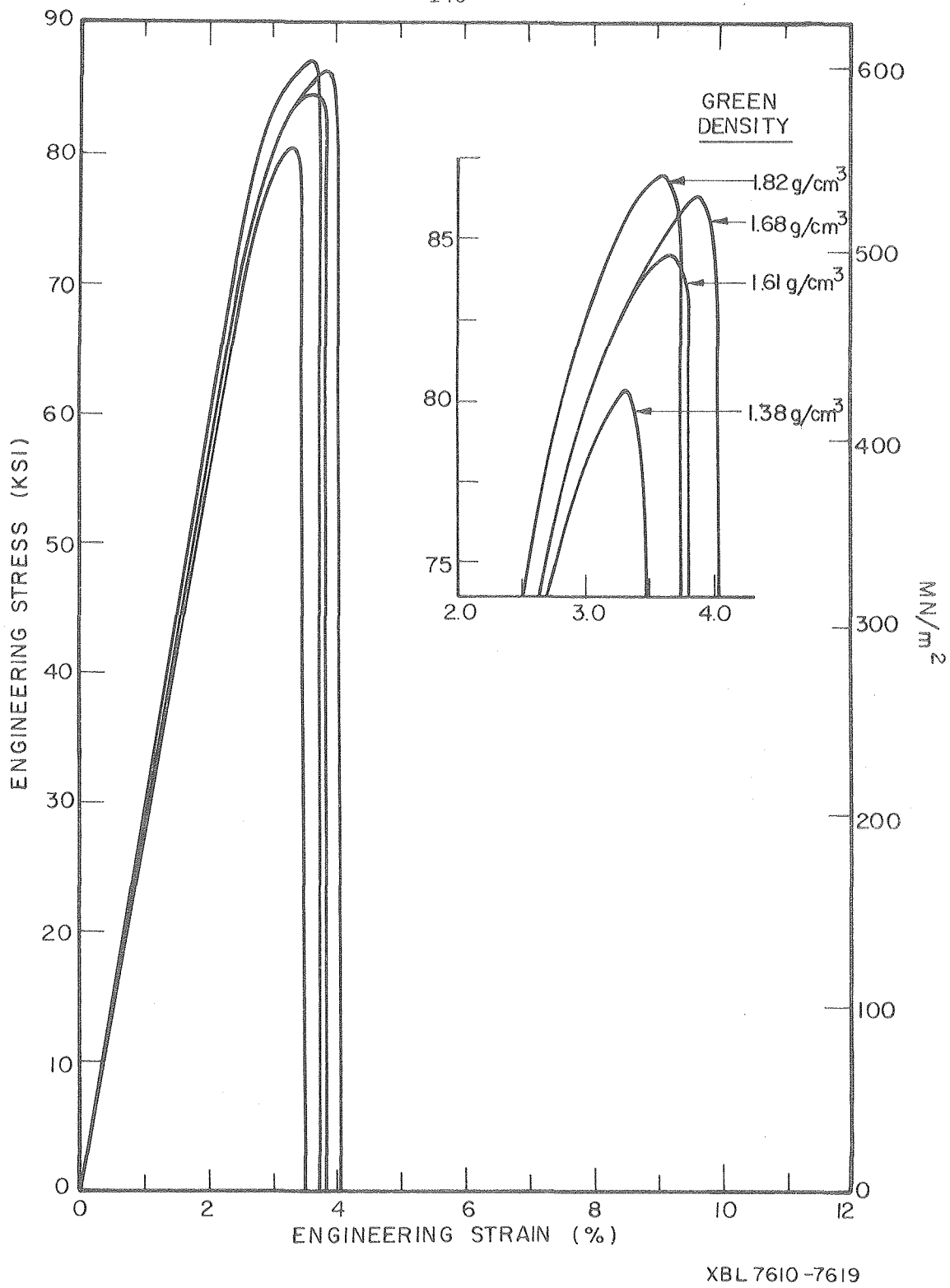

Fig. 44. Stress-strain behavior in compression at 1200°C for 5 hr.-ground mullite compacts of various green densities sintered at ~1710°C in air for 8 hrs.

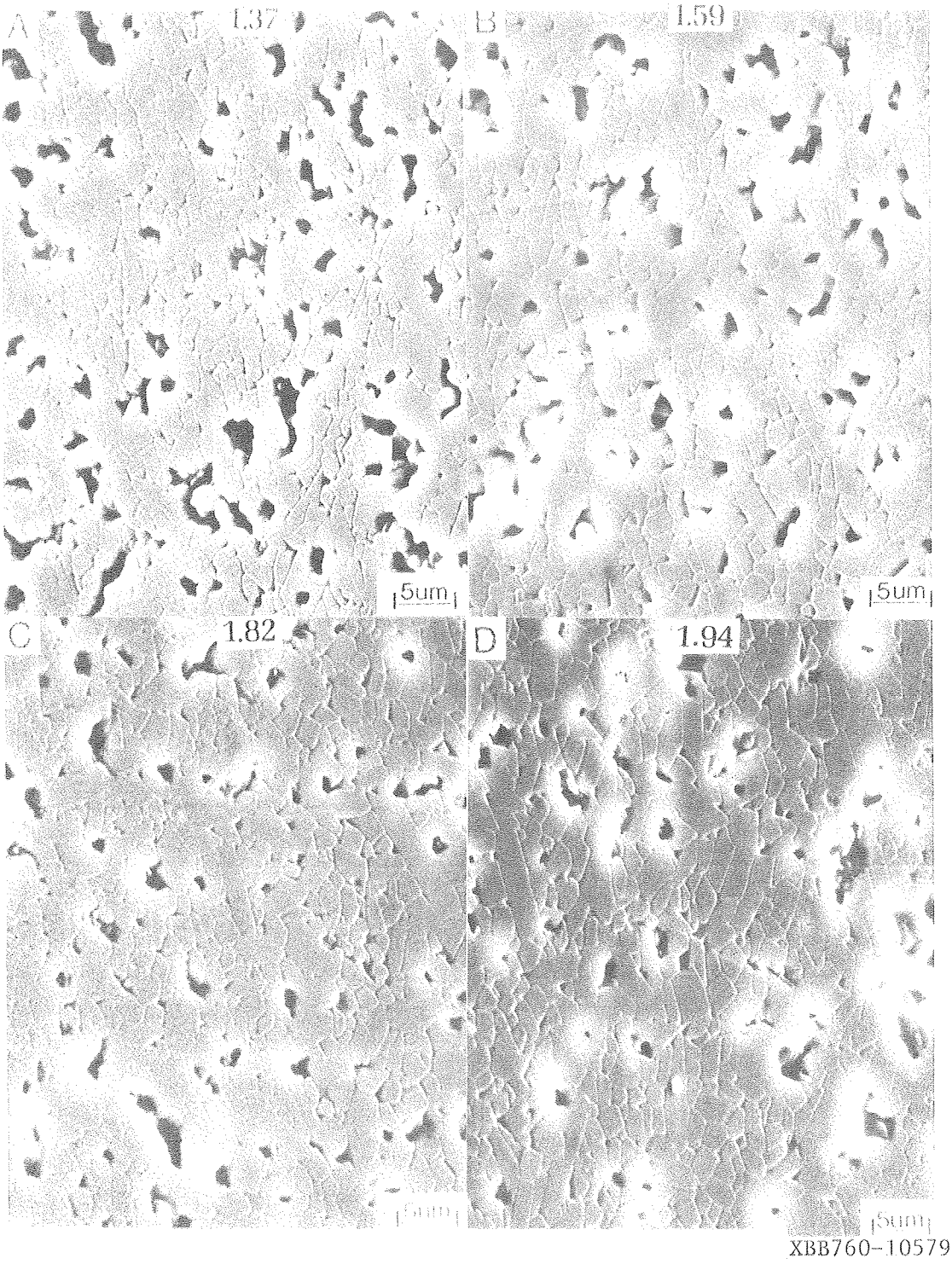

Fig. 45. Micrographs illustrating grain size effects for 5 hr.-ground mullite compacts of various green densities sintered at ~1710°C in air for 4 hrs.

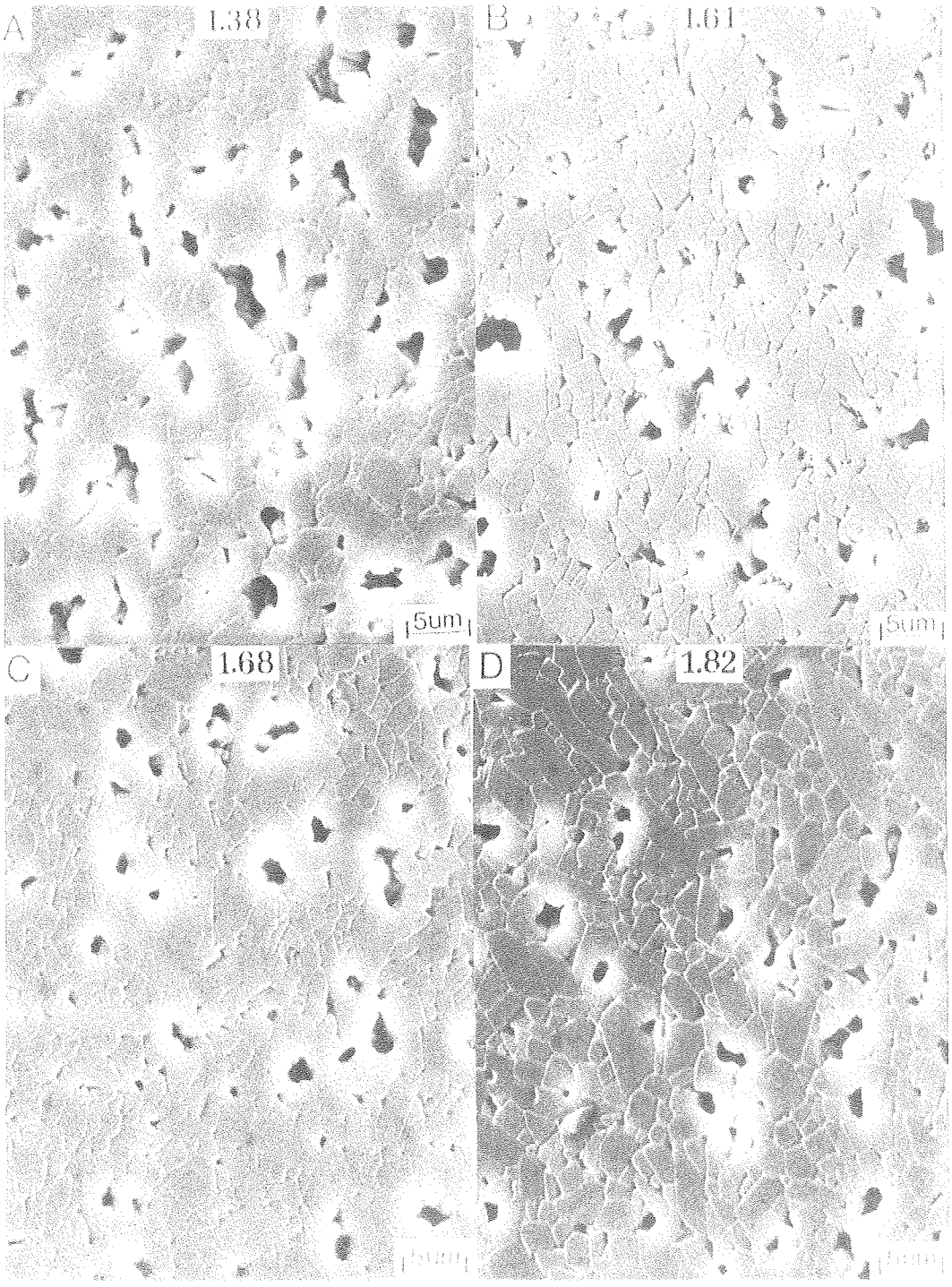

XBB760-10582

Fig. 46. Micrographs illustrating grain size effects for 5 hr.-ground mullite compacts of various green densities sintered at ~1710°C in air for 8 hrs.

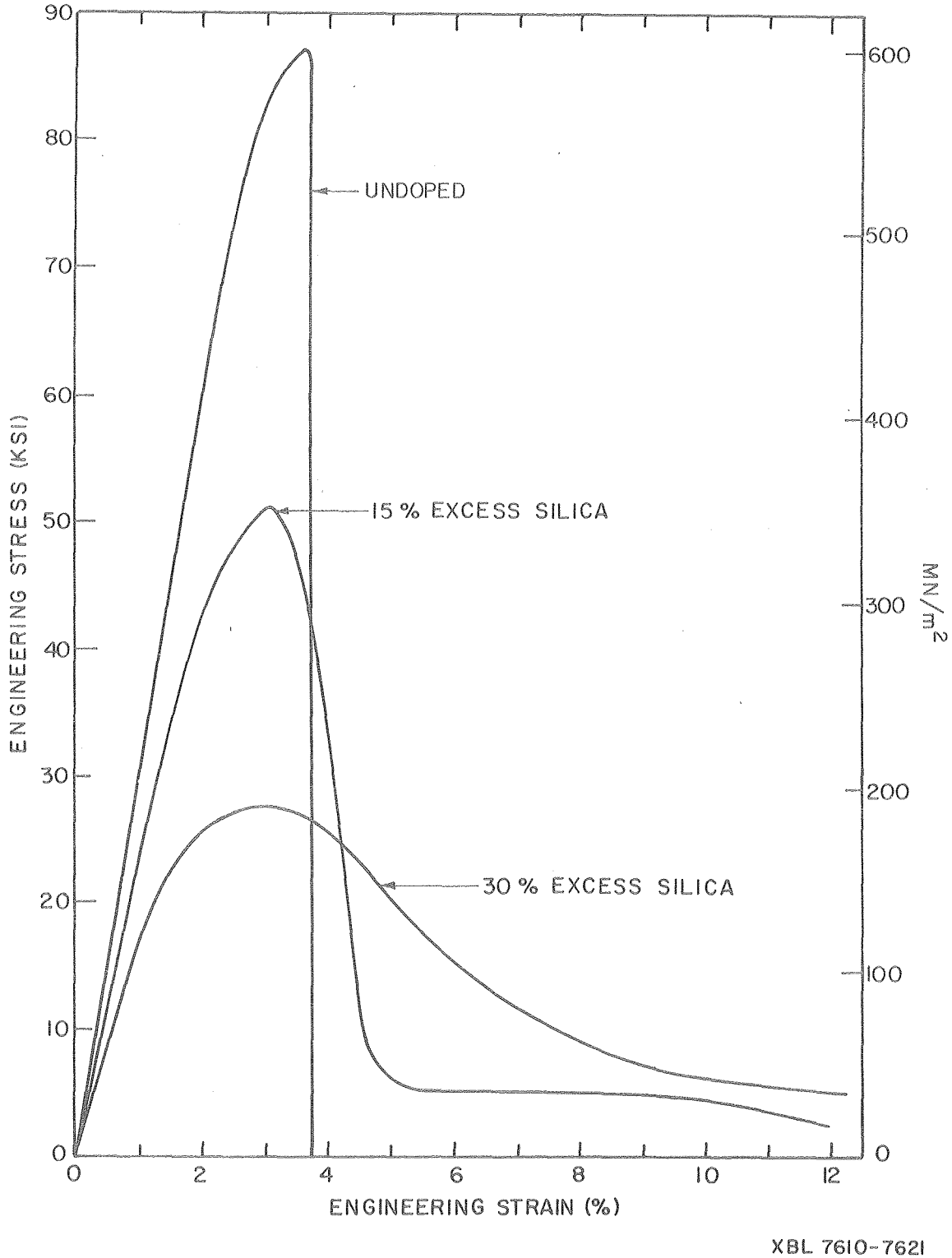

Fig. 47. Stress-strain behavior in compression at 1200°C for compacts, with various amounts of excess silica, sintered at ~1710°C for 8 hrs in air.

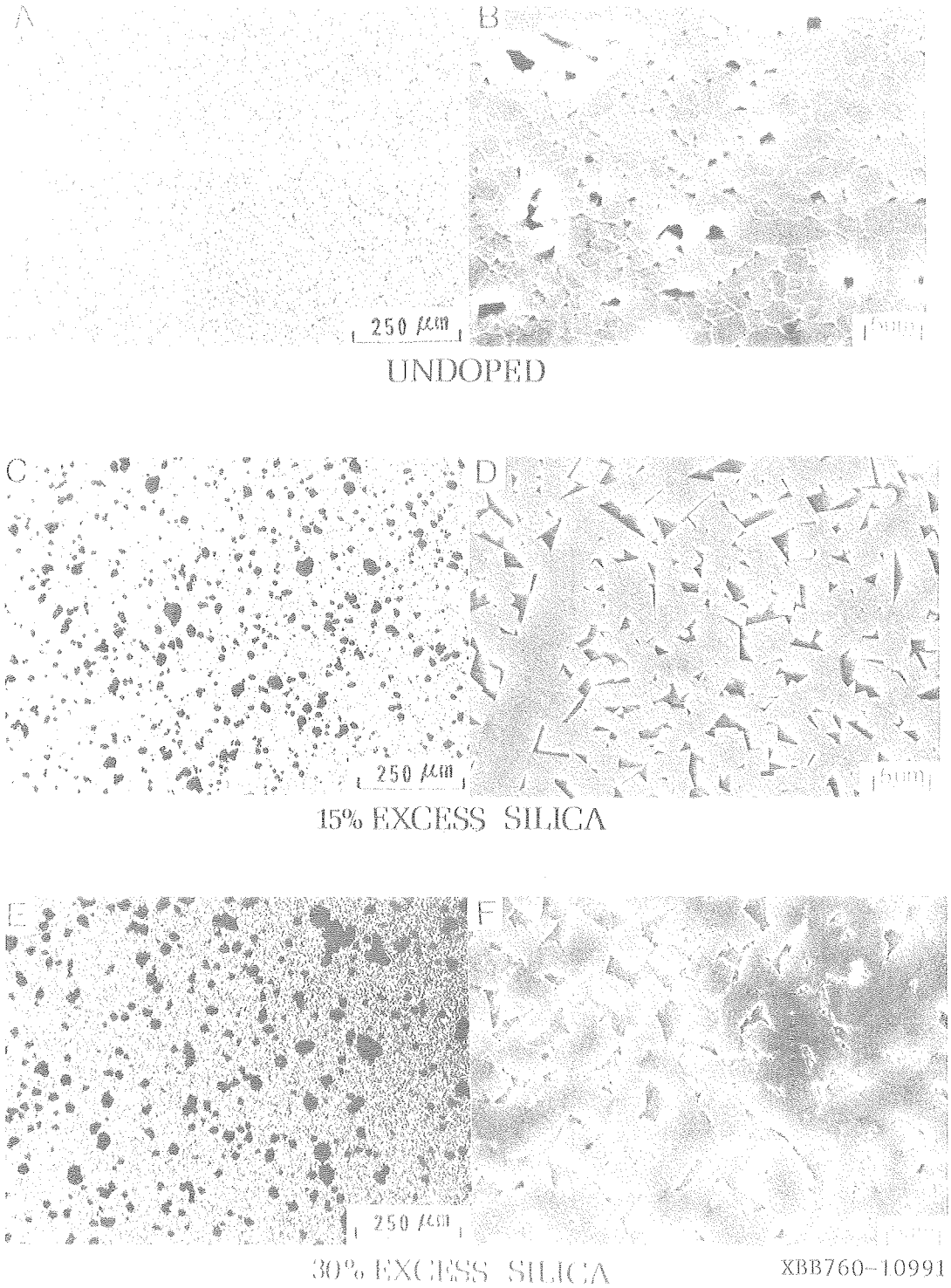

Fig. 48. Micrographs illustrating porosity (left side), grain size (right side), glass phase (right side) changes with increasing silica content for samples fired at ~1710°C for 8 hrs in air.

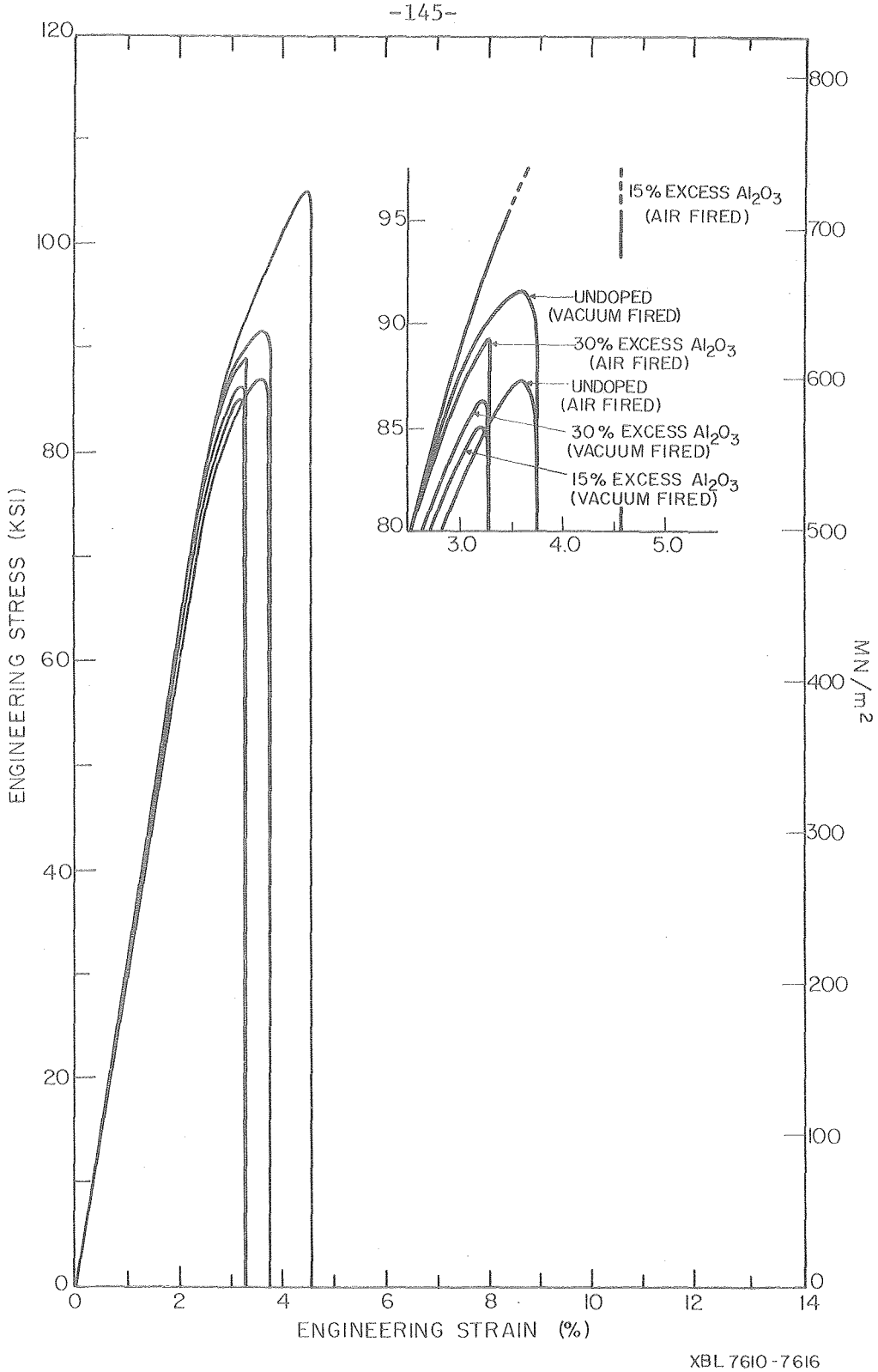

Fig. 49. Stress-strain behavior in compression at 1200°C for compacts, with various amounts of excess alumina, sintered at ~1710°C for 8 hrs in air and vacuum.

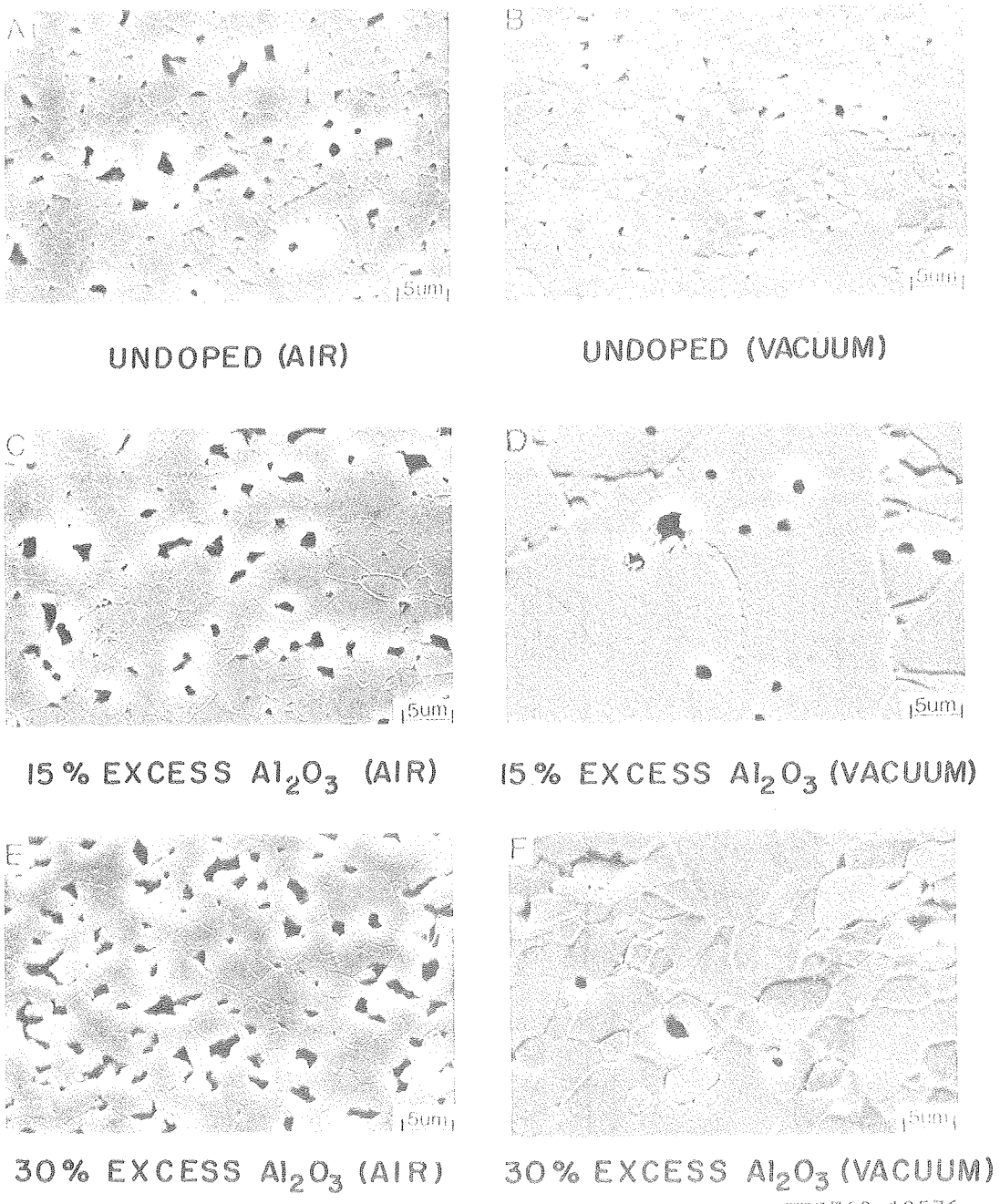

Fig. 50. Micrographs illustrating grain size changes with increasing alumina content for samples fired at ~1710°C for 8 hrs in air (left side) and vacuum (right side).

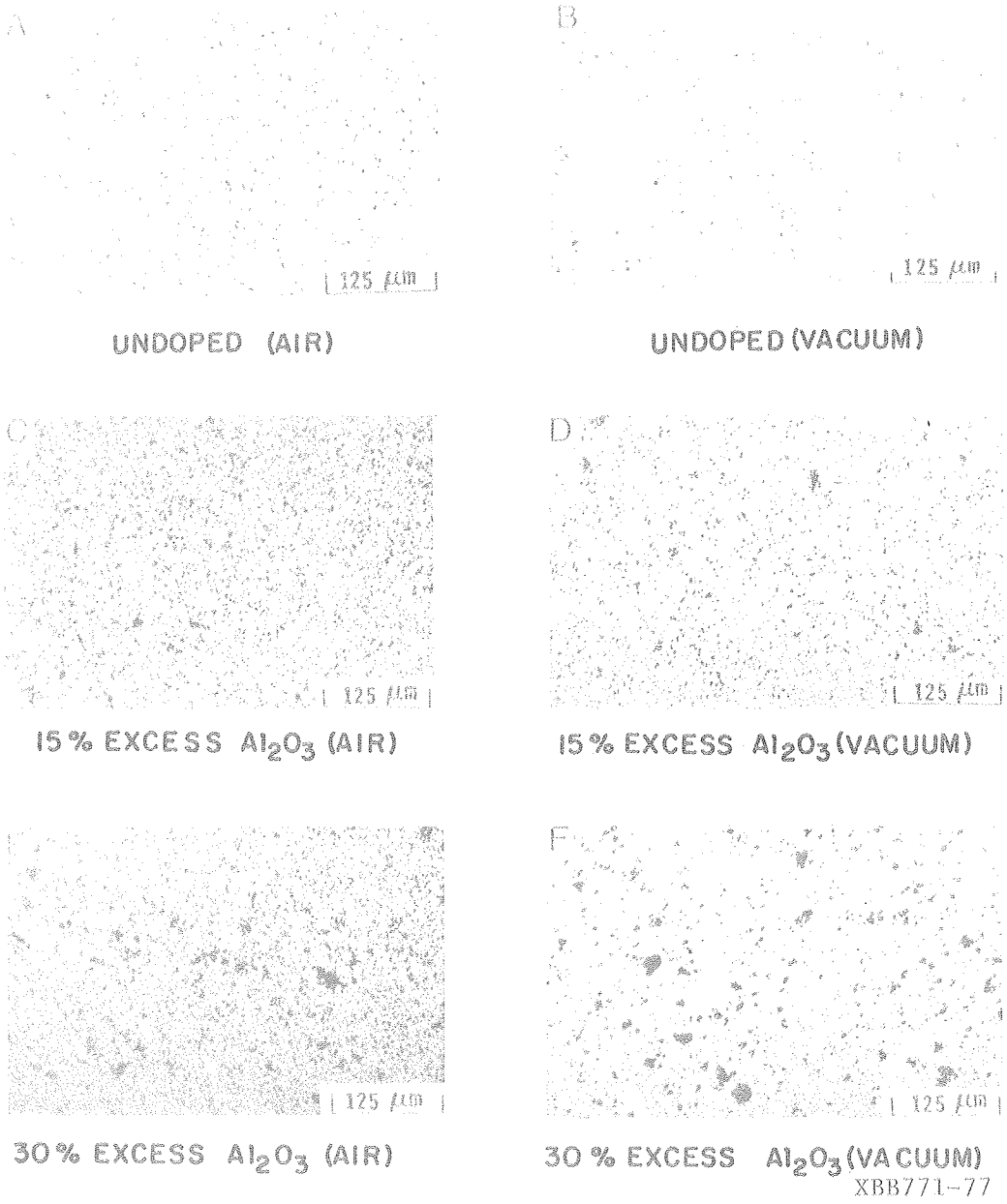

Fig. 51. Amount of porosity (black color) for sintered 5 hr.-ground mullite (undoped and with excess Al_2O_3) is shown. Specimens on the left (A, C, E) were air fired at ~1710°C for 8 hrs. Specimens on the right (B, D, F) were vacuum fired at ~1710°C for 8 hrs. White particles (C-F) are Al_2O_3.

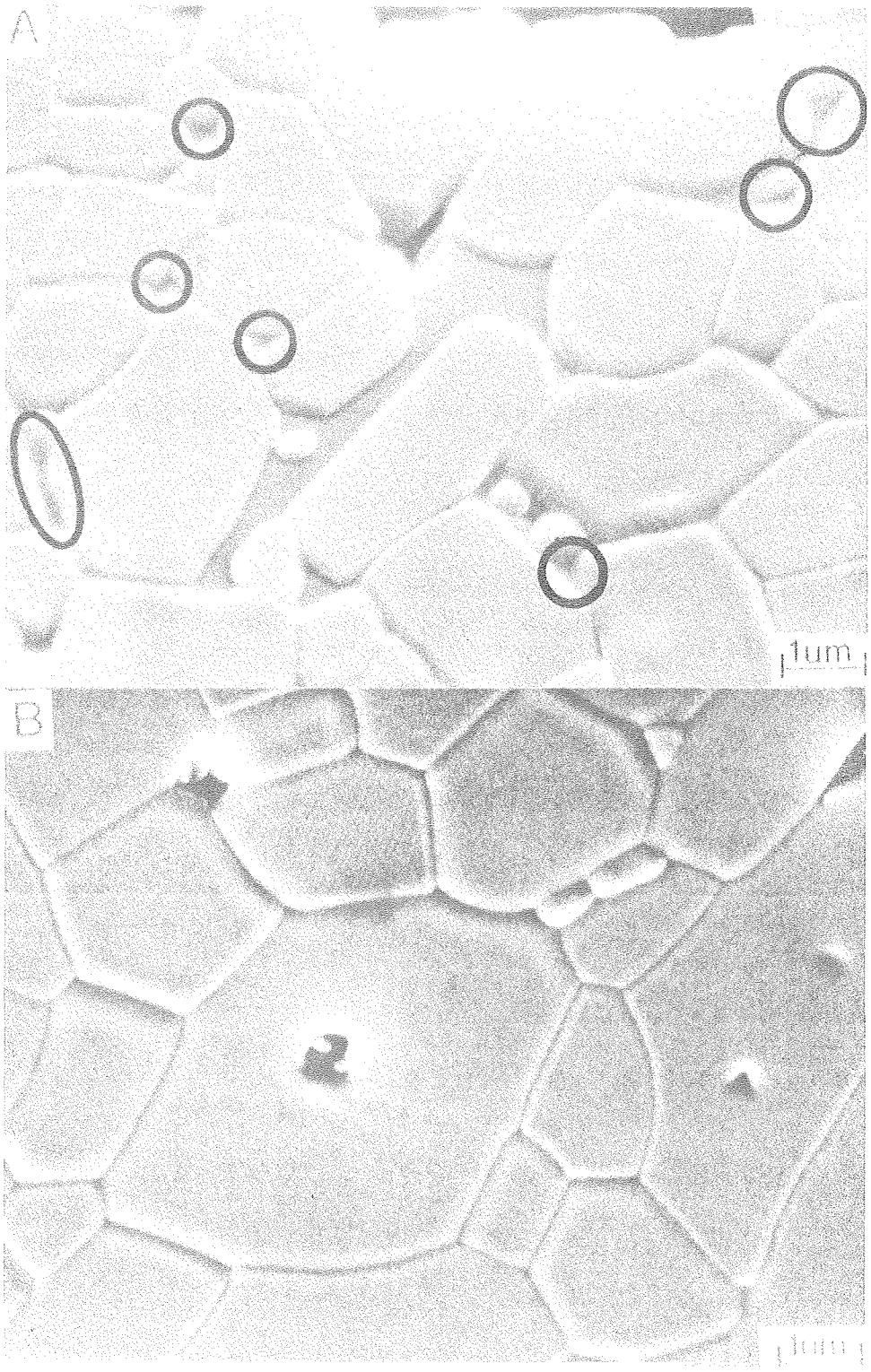

XBB760-10587

Fig. 52. A: Undoped 5 hr.-ground mullite fired at ~1710°C for 8 hrs in air illustrating suspected glass pockets (circled areas) between grains.
B: 15% excess alumina samples fired at ~1710°C for 8 hrs in air illustrating the elimination of suspected glass pockets.

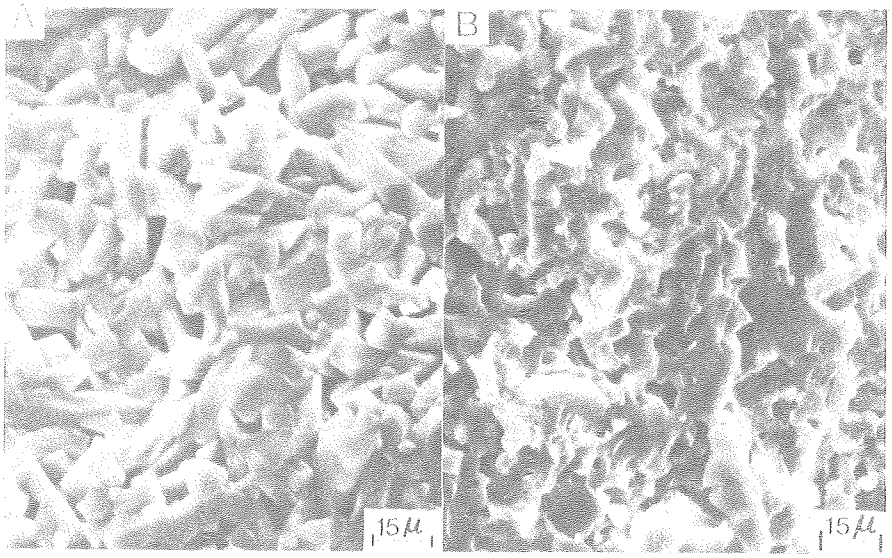

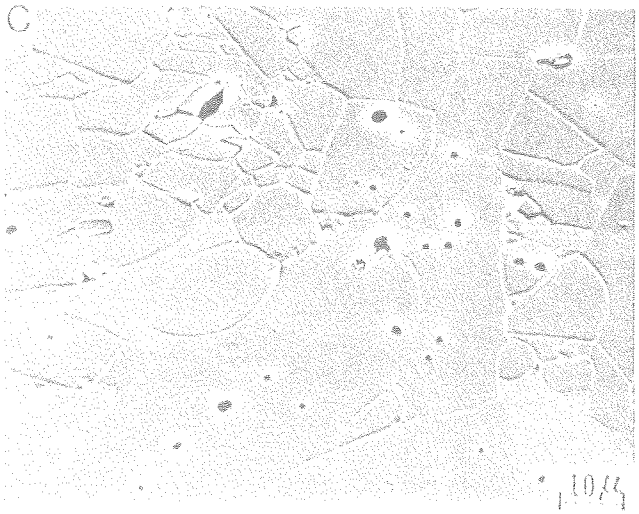

Fig. 53. A: Fracture surface of 1200°C compression tested 5 hr.-ground mullite sample which had been fired at ~1710°C for 8 hrs in air. The fracture mode is primarily intergranular.
B: Fracture surface of 1200°C compression tested 5 hr.-ground mullite with 15% excess Al_2O_3 sample which had been fired at ~1710°C for 8 hrs in air. Compared to A, the change in fracture mode (to primarily transgranular) and the increased strength are indicative of stronger grain boundaries.
C: Polished surface of a 5 hr.-ground mullite with 15% excess Al_2O_3 sample which had been fired at ~1710°C for 8 hrs in vacuum. The lack of angular "pockets" between grains indicates that the amount of glass phase present is negligible. The presence of circumferential cracking around Al_2O_3 particles is also noted.

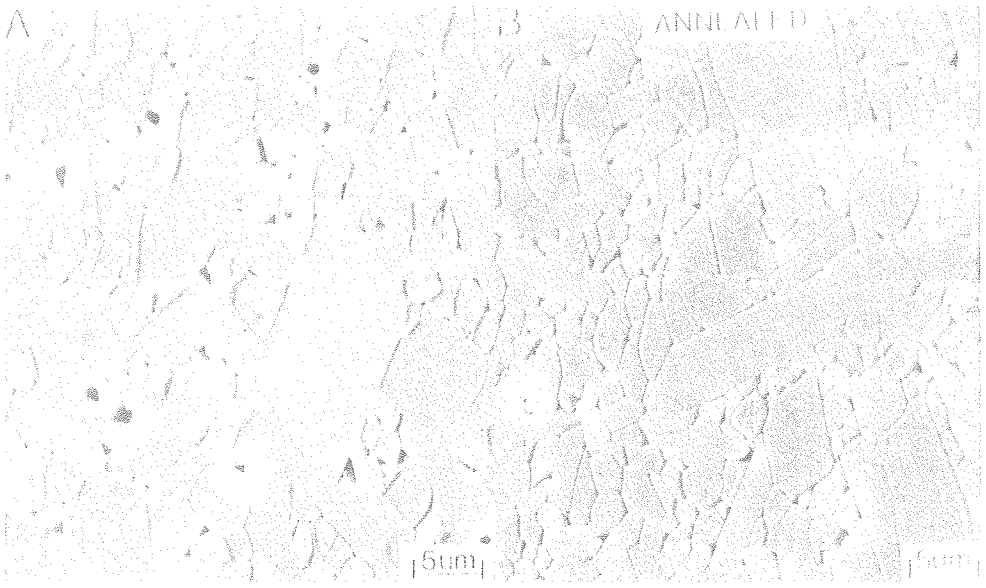

Fig. 54. A: 5 hr.-ground mullite fired at ~1710°C for 8 hrs in vacuum showing grain boundary ridges upon thermal etching.
B: 5 hr.-ground mullite fired at ~1710°C for 8 hrs in vacuum, annealed at ~1600°C for 100 hrs in air, and thermally etched. No grain size increase from A is seen and grain boundary ridges have disappeared.
C: 5 hr.-ground mullite with 30% excess alumina fired at ~1710°C for 8 hrs in air.
D: 5 hr.-ground mullite with 30% excess alumina fired at ~1710°C for 8 hrs in air and annealed at ~1600°C for 100 hrs in air.